## Title

Comparing the reactivity of capture agents and proton source for captured carbon dioxide reduction reaction. A theoretical assessment.



## Author

Kowalski, Robert Michael

## Publication Date

2024

Peer reviewed|Thesis/dissertation

UNIVERSITY OF CALIFORNIA

Los Angeles

# Comparing the reactivity of capture agents and proton source for captured carbon dioxide reduction reaction. A theoretical assessment.

A thesis submitted in partial satisfaction

of the requirements for the degree Master of Science

in Chemical Engineering

by

Robert Michael Kowalski

2024

ABSTRACT OF THE THESIS

Comparing the reactivity of capture agents and proton source for captured carbon dioxide reduction reaction. A theoretical assessment.

by

Robert Michael Kowalski

Master of Science in Chemical Engineering

University of California, Los Angeles, 2024

Professor Philippe Sautet, Chair

Since the industrial revolution, the concentration of atmospheric $CO_2$ has drastically risen. Currently, the $CO_2$ reduction reaction ($CO_2RR$) has been extensively studied to convert $CO_2$ into higher values products like CO, formic acid, methane, etc. Industrially, the first step of the $CO_2RR$ is to capture the $CO_2$ using some capture agent, typically an amine. However, as these chemicals bind $CO_2$ quite strongly a large amount of thermal energy is required to liberate the $CO_2$. Thus, it has been proposed to directly reduce the capture agent in the general captured $CO_2$ reduction reaction (c-$CO_2RR$). This work is a prospective on Ag that considers different capture agents, proton source effects, and facets. We show that the proton source chosen has a large effect on the reactivity, we show that methanol is predicted to be a competitive capture agent compared to $NH_3$, and we show that steps and kinks sites hinder or do not improve the c-$CO_2RR$. However, overall, we determine that on Ag the HER dominates and therefore, further catalyst development is necessary.

The thesis of Robert Michael Kowalski is approved.

Carlos G. Morales Guio

Yuzhang Li

Philippe Sautet, Committee Chair

University of California, Los Angeles

2024

**Table of Contents**

**List of Figures – Main Text**

**List of Figures – Appendix**

**Equations**

**Acknowledgements**

Firstly, I want to thank God for all His blessings on my academic journey leading to this point. In 1 Thessalonians 5:16-18 we are told to always rejoice, pray and give thanks under any circumstance. Thank you Lord for helping me to strive towards this during my PhD thus far.

I want to thank my parents and my brother Joey as well. Their support has been unwavering in my entire academic journey, and I would not be at this point without them.

I want to thank my advisor Dr. Philippe Sautet. His mentorship has been invaluable and has helped me to understand and complete this work as well as continue with my PhD.

I want to thank the members of the Sautet lab and especially (in alphabetical order): Celine Tesvara, Dr. Hio Tong Ngan, Jasmine Dinari, Dr. Simran Kumari, and Zahra Almisbaa. Thank you guys for all of the memories we made in the lab.

Finally, I would like to thank the University of California Office of the President and the National Laboratory Research Fees Program for award L22CR4468, which supports the Center for Direct Conversion of Captured $CO_2$ into Chemicals and Fuels. Computational calculations were run on the UCLA Institute for Digital Research and Education's Research Technology Group's cluster Hoffman2 and Advanced Cyberinfrastructure Coordination Ecosystem: Services & Support's (ACCESS) clusters Expanse and Bridges2 through the allocation CHE170060 at the San Diego Supercomputing Center through ACCESS. All figures and computational data taken in this work is reproduced from:

**Robert Michael Kowalski,** † Avishek Banerjee, † Chudi Yue, Sara Gracia, Dongfang Cheng, Carlos G. Morales-Guio,* and Philippe Sautet*. Electroreduction of Captured $CO_2$ on Silver Catalysts: Influence of Capture Agent and Proton Source, *J. Am. Chem. Soc.*, **2024** (submitted).

# Chapter 1: Introduction

## 1.1 Motivation

Since the industrial revolution the concentration of atmospheric $CO_2$ has been increasing.[1] It was shown that from 1959 to 2010 the cumulative emissions of carbon had increased by 350 PgC. It was found that about 45% of that carbon had been released into the atmosphere and the rest was captured by the land and seas. Additionally, it was determined that during those 5 decades the rate at which carbon was being released was increasing.[2]

From an atmospheric perspective, additional $CO_2$ causes challenges as it is a greenhouse gas. The greenhouse effect is defined as the mechanism in which certain chemicals, such as $CO_2$ and $H_2O$, in the atmosphere can absorbed thermal infrared (IR) radiation that is emitted by the Earth's surface and atmosphere. This causes the temperature of the atmosphere to warm, which in turn leads it to release some thermal IR radiation. This thermal radiation can be used to warm the air near the Earth's surface. In fact, it has been reported that the temperature of the Earth is about 30$^o$C with the greenhouse effect than without.[3] Thus, the greenhouse effect is required for life to function on Earth. However, although necessary for life, there is a tipping point. As the concentration of greenhouse gases in the atmosphere increases, there are more greenhouse gas molecules that can absorb and release more thermal IR radiation. Thus, as the concentration of greenhouse gases increases the temperature of the Earth's surface rises.

However, the $CO_2$ can also be absorbed by the ocean. $CO_2$ reacts with water to form carbonic acid by equation 1:

$$CO_2 + H_2O \leftrightarrow H_2CO_3 \quad \text{(Eq 1)}$$

Carbonic acid has 2 acidic Hs and has the $pK_a$ values of 3.49,[4] for the first dissociation, and 10.3 for the second dissociation,[5] shown by equations 2 and 3:

$$H_2CO_3 \leftrightarrow H^+ + HCO_3^- \quad \text{(Eq 2)}$$

$$HCO_3^- \leftrightarrow H^+ + CO_3^{2-} \quad \text{(Eq 3)}$$

Thus, as the concentration of $CO_2$ increases, the pH of the ocean water decreases. This has been reported to negatively affect certain marine life's survival, growth, and reproduction. This effect was typically worse in organisms that calcify.[6] Thus, as the concentration of $CO_2$ increases certain marine life suffers from the acidification of the oceans. It is important to note that the solubility of $CO_2$ in $H_2O$ is a function of temperature. As the temperature increases the solubility of $CO_2$ decreases. Thus, as the surface of the Earth is warmed less $CO_2$ can be adsorbed by the oceans.[7] However, this does not necessarily help, as this means that more $CO_2$ will enter the atmosphere and make the warming effect worse.

It has been reported that manufacturing plants can release up to 15 vol% $CO_2$.[8] Therefore, efforts to mitigate this rise in $CO_2$ concentration have included carbon capture and utilization (CCU). In this method carbon is taken from a point source and converted into higher value products.[9] Classically, this first involves the capture of $CO_2$ using some capture agent, typically an amine.[10] Industrially, the $CO_2$ is typically flowed into an absorber unit that contains an amine-containing aqueous solution.[8] The captured $CO_2$ is then concentrated and released from the capture agent where the $CO_2$ can get converted into higher value products thought the $CO_2$ reduction reaction ($CO_2$RR).[10] Reports have shown that the captured $CO_2$ complex must be raised to temperatures between 120°C – 150°C to releases the $CO_2$.[11] Thus, it has been proposed to directly electroreduce the captured $CO_2$ instead of first thermally releasing the $CO_2$ from the capture agent and then running the $CO_2$RR. This new process, which we have termed the captured $CO_2$ reduction reaction (c-$CO_2$RR) extends upon the $CO_2$RR. However, to fully motivate the c-$CO_2$RR it is first necessary to look at the success of $CO_2$RR first, as the c-$CO_2$RR is inherently a more challenging

reaction. Thus, if the pure $CO_2$RR is impossible then it is highly illogical that the c-$CO_2$RR would be reasonable.

## 1.2 Success of the $CO_2$RR

Significant work has already been conducted on reducing $CO_2$ both thermochemically and electrochemically.[12–17] A myriad of products are possible from the $CO_2$RR, though the most common are CO and HCOOH (formic acid).[18–20] Equations 4 and 5 show the overall balanced equation for these reactions when done electrochemically:[21]

$$CO_2 + 2(H^+ + e^-) \rightarrow CO + H_2O \quad \text{(Eq 4)}$$

$$CO_2 + 2(H^+ + e^-) \rightarrow HCOOH \quad \text{(Eq 5)}$$

Starting from pure $CO_2$, two coupled proton electron transfer (PCET) steps occur to either reduce the $CO_2$ into CO and $H_2O$ or formic acid. The mechanism is quite different[18,22] and the identity of the catalyst has been observed to determine the identity of the products produced.[19] Typically what is reported that to produce either of these compounds $CO_2$ must first chemisorb to the catalyst. At this point a PCET occurs to produce either *COOH or *OCHO. Typically, if *COOH is produced then usually CO will form via a second PCET, and if *OCHO is produced then usually formic acid will form via the second PCET.[18,23] However, there have been reports of formic acid being produced when the *COOH intermediate is formed.[22] If formic acid is produced that is typically the end of the reduction process. However, if CO is produced then it is possible for additional products such as methane, methanol, or even larger C chain molecules like ethanol and acetone to form.[18]

A common method to measure activity of a set of catalysts is through the usage of a volcano plot. To construct a volcano plot a descriptor or set of descriptors are chosen to represent a reaction.

Then the descriptors are plotted against some measure of activity, such as onset potential. In the $CO_2$RR, the binding strength of *CO and of *OH have been reported as descriptors for some of the various products possible from the $CO_2$RR.[24,25] If the chosen descriptor is good at describing the system, then an optimum will occur. This happens because of the different potential limiting steps that occur for different catalysts. Thus, when two of these potential limiting steps cross an optimum occurs. When multiple potential limiting steps occur then the crossing that produces the least favorable onset potential is taken.[25]

For the $CO_2$RR, Ag, Au, and Cu all appears within the vicinity of the peak of the volcano.[24,25] For Ag and Au, typically the PCET from $CO_2$ → COOH* is found to be the potential limiting step. However, as Cu is able to produce products beyond CO and formic acid its potential limiting step is found to be the PCET converting CO* → CHO*.[25] Although they are known to produce different products this volcano plot provides interesting evidence on the effectiveness of these catalysts for the $CO_2$RR. Experimentally, faradaic efficiencies (F.E.) of CO of about 99% have been observed on Ag under optimized conditions,[26] thus validating Ag as a good $CO_2$RR catalyst.

## 1.3 Challenges with the HER

As the captured $CO_2$ reduction reaction (c-$CO_2$RR) and the $CO_2$RR are run in solution under reductive conditions, a possible side reaction occurs with the hydrogen evolution reaction (HER). This reaction is unwanted because 1) it used an active site that could be occupied by $CO_2$ or the capture $CO_2$ complex and 2) it uses a proton source. In the $CO_2$RR there are 2 required protonations and in the c-$CO_2$RR there are 3 as shown in equation 6.

$$KRCO_2 + 3XH + 2e^- \rightarrow CO + H_2O + RH + KX + 2X^- \quad \text{(Eq 6)}$$

In equation 6, RH is the capture agent, XH is the proton source used, and KX is the corresponding salt formed. The specific capture agents and proton sources used in this work will be discussed in Chapter 3. However, equations 1-3 show that if the proton is reduced into $H_2$ then it is essentially wasted. Therefore, it is imperative to choose a catalyst that hinders the HER.

In this work Ag is chosen as that catalyst because it has been observed to not bind hydrogen strongly.[27] In the HER, the H adsorption is seen as a descriptor of a catalyst's activity.[27] This is because the HER is essentially 2 PCETs with the H* as the middle intermediate.[28] Thus, if the H does not bind well onto the catalyst at reasonable potentials, then it will require large overpotentials to force the H to adsorb, allowing the HER to run. Likewise, if the catalyst binds H very strongly then it will adsorb but getting it to react is very challenging. In those cases, the overpotential must be made very negative to allow for the second PCET to be reasonable. From HER volcano plots it is observed the Pt sits near the peak and a H adsorption energy of about -0.4 eV.[27] Coinage metals tend to bind H weakly, while early group transition metal oxides tend to bind H strongly.[29] Thus, there exists two families of catalysts that could potentially supply c-$CO_2$RR catalysts. In this work Ag is chosen for 4 reasons. One is that Ag has been reported in the literature to provide high faradic efficiencies (FE) for CO.[30] Additionally, choosing a catalyst the binds H weakly provides computational advantages. When a catalyst binds H strongly it is important to properly model that. This greatly increases computational cost as well as the additional challenges that come from accurately modeling metal oxides under realistic reaction conditions.[31] Third, on a HER volcano plot Au and Cu are in a similar position, but Ag is significantly below both of those metals.[32] Finally, previous work has shown that Ag may provide some c-$CO_2$RR activity.[8,11] Therefore, as Ag is known to be a poor catalyst for HER, and the worst for the coinage metals, a known good

$CO_2$RR catalyst, and some promising results for the c-$CO_2$RR, it was chosen as the catalyst for this study.

## 1.4 Why Alcohols are Important

Commonly, amines are used to capture $CO_2$.[33] However, amines bind $CO_2$ strongly, so releasing $CO_2$ from them to conduct the $CO_2$RR is energy intensive.[34] Moreover, although not explicitly tested on the N-C bond between amines and $CO_2$, it has been reported that strong bonds that need to be broken leads to larger overpotentials.[35] Therefore, alternatives to amines were considered.

Alcohols were chosen as a possible alternative for multiple reasons. When using amines for $CO_2$ capture 2 amines are required for each $CO_2$. This is because in the capture process, first the amine and the $CO_2$ form a zwitterion. Then another amine is used to remove the positive charge leaving just the negatively charged carbamate.[34] This raises a couple of issues. As the ammonium cation produced has a relatively low $pK_a$ it is a good proton donor.[36] This in theory should improve reactivity of the $CO_2$RR and c-$CO_2$RR thermodynamically speaking. However, this will also improve the reactivity of the HER. Work was published that shows that the presence of these ammonium cations in the c-$CO_2$RR reaction network improved the HER much greater than the c-$CO_2$RR and essentially killed the activity for c-$CO_2$RR.[5,37] Additionally, amines have a high $pK_a$.[38] Typically, the c-$CO_2$RR is run in aqueous environments.[8,11] Therefore, there is a risk of reprotonating the capture agent and prematurely releasing the $CO_2$.

Therefore, alcohols were a reasonable alternative. Alcohols can bind the $CO_2$ in a 1:1 ratio as an alkoxide.[38] This also means that the formation of the ammonium cation is no longer an issue. For the case of methanol as a capture agent, in methanol solvent the only proton source available

is methanol. The $pK_a$ of methanol is 15.5,[39] higher than that of $H_2O$, bicarbonate, and $NH_4^+$ (all of the proton sources present in an ammonium carbamate c-$CO_2$RR reaction network).[5,36,40] Therefore, it theoretically should suppress the HER. However, this means it will also suppress the c-$CO_2$RR. However, alcohols bind $CO_2$ weaker than amines do.[38] Therefore, this means that there should be a smaller overpotential associated with reducing a carbonate rather than a carbamate.[35] This does mean that at equilibrium less $CO_2$ will be captured by the alcohol as compared to the amine. However, because alcohol-based c-$CO_2$RR can be run in an alcohol solvent this means the risk of reprotonating the capture agent either no longer exists or is much smaller as the alcohols using in capturing the $CO_2$ and used as the solvent will either be identical or have similar $pK_a$s. Therefore, it is of interest to consider alcohol capture agents.

# Chapter 2: Computational Methods

## 2.1 VASP

All calculations used density function theory (DFT) interfaced via the Vienna *ab-initio* Simulation Package (VASP).[41,42] The electron ion interactions were modeled via the projected augmented wave (PAW). The Perdew-Burke-Ernzerhof (PBE)[42] functional with D3[43] corrections to account for the van der Waal interactions was taken to model the exchange correlation interactions. All the energetics in this work are free energies, as we are considering a grand canonical model. To run VASP, the Atomic Simulation Environment (ASE) was used throughout this work.[44]

For the Ag(111) slab a Γ-centered k-point mesh of 4 x 4 x 1 was used to integrate the Brillouin-zone (BZ). The valence electronic states in the plane-wave basis set were set by a planewave cutoff energy of 400 eV.[43] During relaxations an ionic step was considered complete

when the energy difference between consecutive electronic steps was less than $10^{-6}$, and an optimization was considered completed when the max force was less than 0.02 eV/Å. For all calculations, as the catalyst was Ag, the smearing used a Methfessel-Paxton method of order 2. The width of this smearing was set to 0.2. The solution algorithm used a combination of the blocked-Davidson and RMM-DIIS methods. In this work calculations were typically not spin polarized.[41,42] As Ag is non-magnetic it is safe to assume that calculations would not have a magnetic moment.[45] Some spin-polarized calculations were run to test this claim and a magnetic moment of 0 was always found. Figure A1 shows an example of the typical VASP INCAR using in all optimizations.

For the Ag(211) and the $KCO_2$* a slightly different method was used. For the Ag(211) the system was quite large as there were 102 Ag atoms per units cell. Therefore, to speed up the calculations process it was assumed that optimizing the system asymmetrically at potential of zero charge (PZC) gave a reasonable approximation of the necessary geometry. As explained in the surface charging section getting the geometry as close to global minimum as possible was crucial for determining realistic energetics. Therefore, what was tested was to first completely optimized the Ag(211) symmetrically. This process was quite slow. Then the same intermediate was made and optimized asymmetrically. Then the results of this asymmetric calculations were symmetrized, and surface charging methods were used to obtain the energetics as a function of potential. The results of this test is shown in Figure 1.

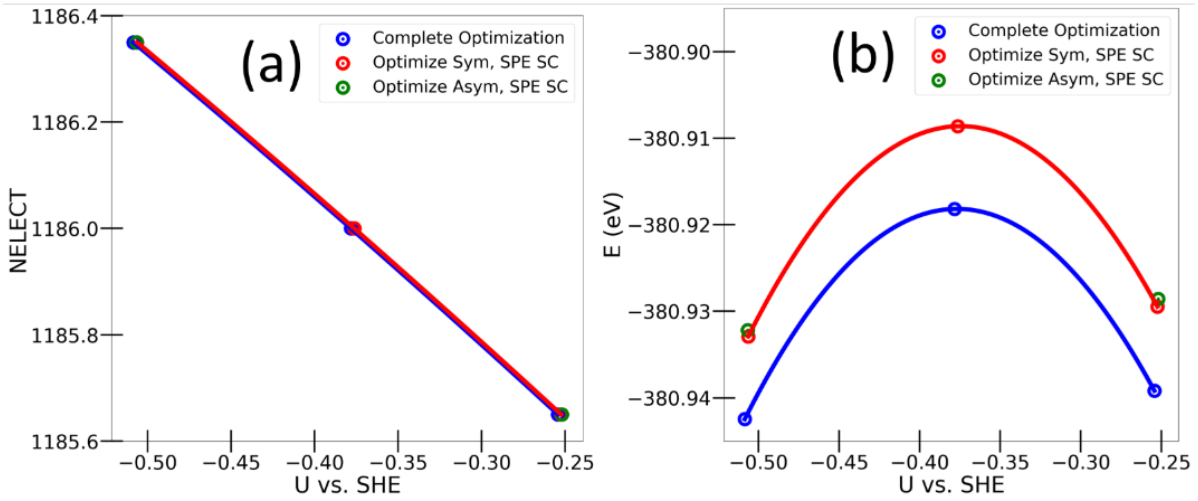


**Figure 1:** Benchmarking the usage of asymmetrical optimization followed by single point surface charge (green) against symmetrical optimization followed by single point surface charging (red) or followed by optimized surface charging (blue). (a) the number of electrons and (b) electronic energy are plotted as a function of potential.

From Figure 1 it is clear that the complete symmetrical surface charging is not necessary. When considering the potential as a function of the injected charge in Figure 1a there is no noticeable difference between optimizing the system symmetrically for each potential, (blue) optimizing the geometry symmetrically and then using single point surface charging (red) and optimizing asymmetrically and using single point symmetrical surface charging (green). From Figure 1b there is a slight difference between the methods when comparing the energetics as a function of potential. The fully symmetrical model is slightly more stable than the other 2 methods. However, the difference in energy is less than 10 meV. Thus, it was safe to assume that these methods provided similar enough results. Interestingly, optimizing symmetrical seemed to provide no additional benefit to the energetics. Figure 1b clearly shows the red and green points have almost identical energetics. However, the red method required a complete optimization using a

symmetrical slab. Therefore, to reduce computational cost, the method of first optimizing the slab asymmetrically and then running single point surface charging was adopted.

The $KCO_2$* intermediate has a similar method of optimization. However, on the Ag(111) the unit cell was small enough that a complete symmetrical optimization followed by single point surface charging was possible. It was necessary to do this as the $CO_2$ changes from its stable linear mode to an unstable bent mode to adsorb. Therefore, quite negative potentials are necessary to generate this structure. If the potential is not made negative enough the system will optimize into its physiosorbed mode which is not interesting in this work. Therefore, what is done is to optimize symmetrically at a negative potential (~+1 e above PZC) and then run single point surface charging to obtain the energy was a function of potential. This was documented as a legitimate method of obtaining chemisorbed $CO_2$ energetics in previous work.[46] For more negative potentials it was possible to fully relax the $KCO_2$* intermediate without the physiosorbed mode appearing. In these cases, the system was fully relaxed.

Interestingly, this method was not necessary when the $K^+$ was not present. The $K^+$ cation acts to stabilize the $CO_2$ which leads to smaller adsorption energies.[47] It accomplishes this by injecting its charge into the surface, so PZC more negative. However, when this $K^+$ cation is not present this charge injection is also not present. Therefore, the PZC is at a much weaker negative potential. Therefore, to reach the interesting potentials of $CO_2$RR and c-$CO_2$RR (~ -1 to -2 V vs. SHE) it is necessary to inject significant charge into the electrode. Therefore, at the interesting potentials the $CO_2$* can be fully relaxed without the threat of the system optimizing into the physiosorbed mode.

This does not mean however, that the results predict that the $K^+$ cation does not assist in the $CO_2$ adsorption. As Figure 2 shows the opposite trend was observed.

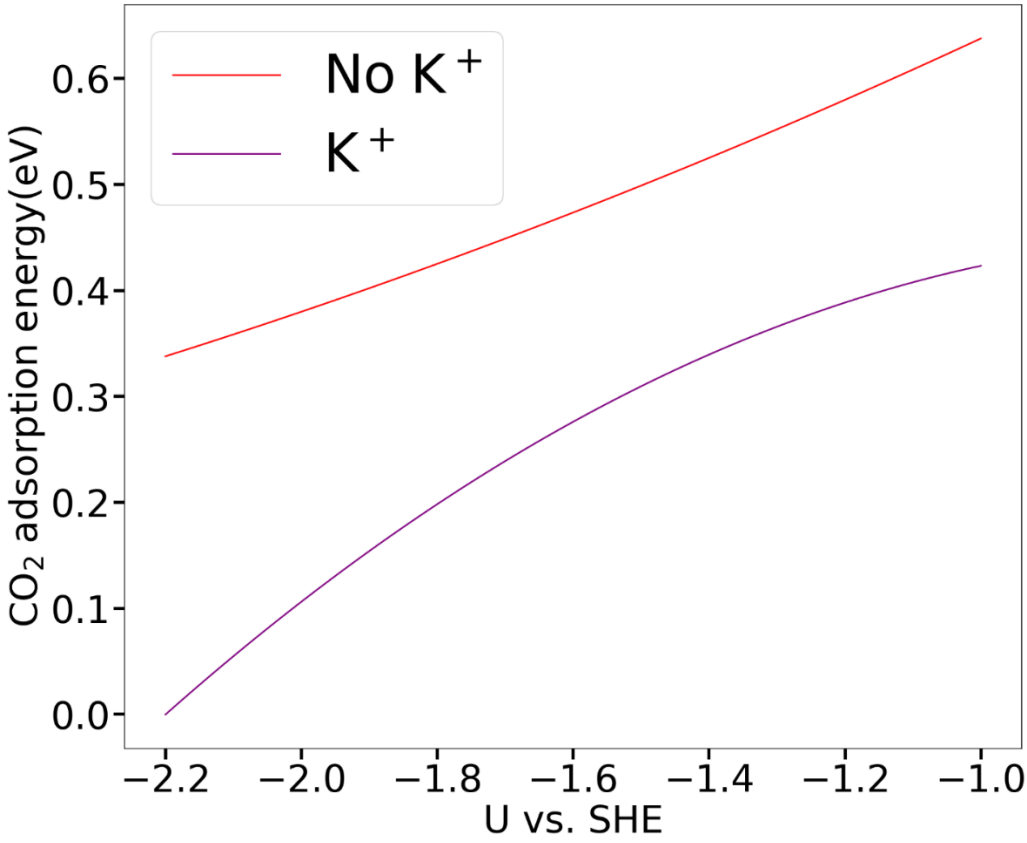


**Figure 2:** Adsorption of $CO_2$ with (purple line) and without (red line) the presence of $K^+$.

This is important as it gives confidence and experimental validation to the model. Therefore, in this work all the $CO_2$ was done in the presence of a $K^+$ cation.

For convergence parameters the Ag(211) used identical parameters to the Ag(111) except that the BZ integration was done with 3 x 4 x 1 Γ-centered k-point mesh as the unit cell was extended in the x direction.

## 2.2 VASPSol

Solvation and charging in this work were treated implicitly by the VASPSol package.[48,49] In this method the implicit solvent can be modeled with a handful of parameters. The solvent is modeled as a continuum and the only required parameter needed to differentiate between different

solvents is the dielectric constant.[49] VASPSol assumes that the dielectric constant is truly constant throughout the entire media. However, the dielectric constant is truly a function of position and time.[50]

All explicit models are treated as solute in the VASPSol framework.[48,49] Thus, to place them inside the model a cavity must be made in the solvent. This cavity is described by 3 parameters: the surface tension (tau)[49], the electron density present when the cavity forms (nc_k), and the width of the dielectric cavity (sigma_k).[48]

Work was done that shows that setting the surface tension to 0 provided similar results to non-zero surface tension values.[51] Therefore in this work the surface tension will be set to 0. The default values of nc_k and sigma_k are 0.0025 $Å^{-1}$ and 0.6, respectively.[49] Thus, these are the values taken in this work.

### 2.2.1 Surface Charging

In this work, the influence of potential is important, so a charging is applied. To account for this additional charge the solvent continuum contains a density of counter charge. Physically, this would be the electrolyte. This counter charge is modeled as a solution to the linearized Poisson-Boltzmann equation (LPBE) which requires the Debye screening length. The Debye screening length can be calculated via the dielectric constant of the medium, the temperature, and the concentration of electrolyte.[49]

To calculate the energetics as a function of potential the method of surface charging (SC) was used. In this method the system can be modeled as a capacitor. Therefore, given the potential of zero charge (PZC), the energy can be given by equation 7.[52]

$$E = E_0 + C(\Phi - \Phi_0)\Phi_0 + \frac{C(\Phi - \Phi_0)^2}{2} \quad \text{(Eq 7)}$$

$E_0$ is the electronic energy at PZC, $\Phi_0$ is the work function at PZC, C is the capacitance of the system, and E and Φ are the electronic energy and work function at the potential of interest. This assumes that the capacitance of this capacitor is constant. This is typically, true but as the charge is brought away from PZC, the capacitor becomes more non-linear. In this work it was assumed that the capacitance was kept constant and thus, the energy can be modeled parabolically as a function of work function, which can be converted to potential.[52]

Classically, electrochemical reactions were treated using the computational hydrogen electrode (CHE) model developed by Nørskov *et al*. In this method the chemical potential of a coupled proton and electron can be determined by equation 8 when the potential is given in the Standard Hydrogen Electrode (SHE) reference:[53]

$$G_{H^+ + e^-} = \frac{1}{2} G_{H_2(g)} - eU - ln(10) * k_B * T * pH \quad \text{(Eq 8)}$$

In this U is the potential in SHE, e is the amount of charged transferred in the PCET, $G_{H2}$ is the free energy of $H_2$ gas. Thus, it is possible model the reaction energy as a function of potential following this framework. However, this means that each proton coupled electron transfer (PCET) will be potential dependent, and all adsorption and chemical steps will be potential independent.[54] As will be explained in this work later, this framework will cause severe errors in the context of c-$CO_2$RR. However, even before this work it was noted various times that there were deviations between the CHE model and surface charging model.[55] This is because the CHE method assumes that the potential has no effect on the internal energy, while the SC method explicitly changes the internal energy as a function of potential.[54] Therefore, to avoid this issue the SC method was used.

To use the surface charging method the electronic energy is calculated via VASPSol.[48,49] This calculation is done at multiple number of injected charges to get a range of potential. However, as the work function is changed this slightly alters the geometry of the adsorbates.

Typically, for a narrow range of potential the geometry is closer enough that a parabola can be fit to equation 4 to get the energy as a function of potential. However, if the geometry is made different enough then the capacitance term will change, and this leads to completely different parabolas. Figure 5 shows an example of method happening with 2 $KCH_3OCO_2$* binding modes.

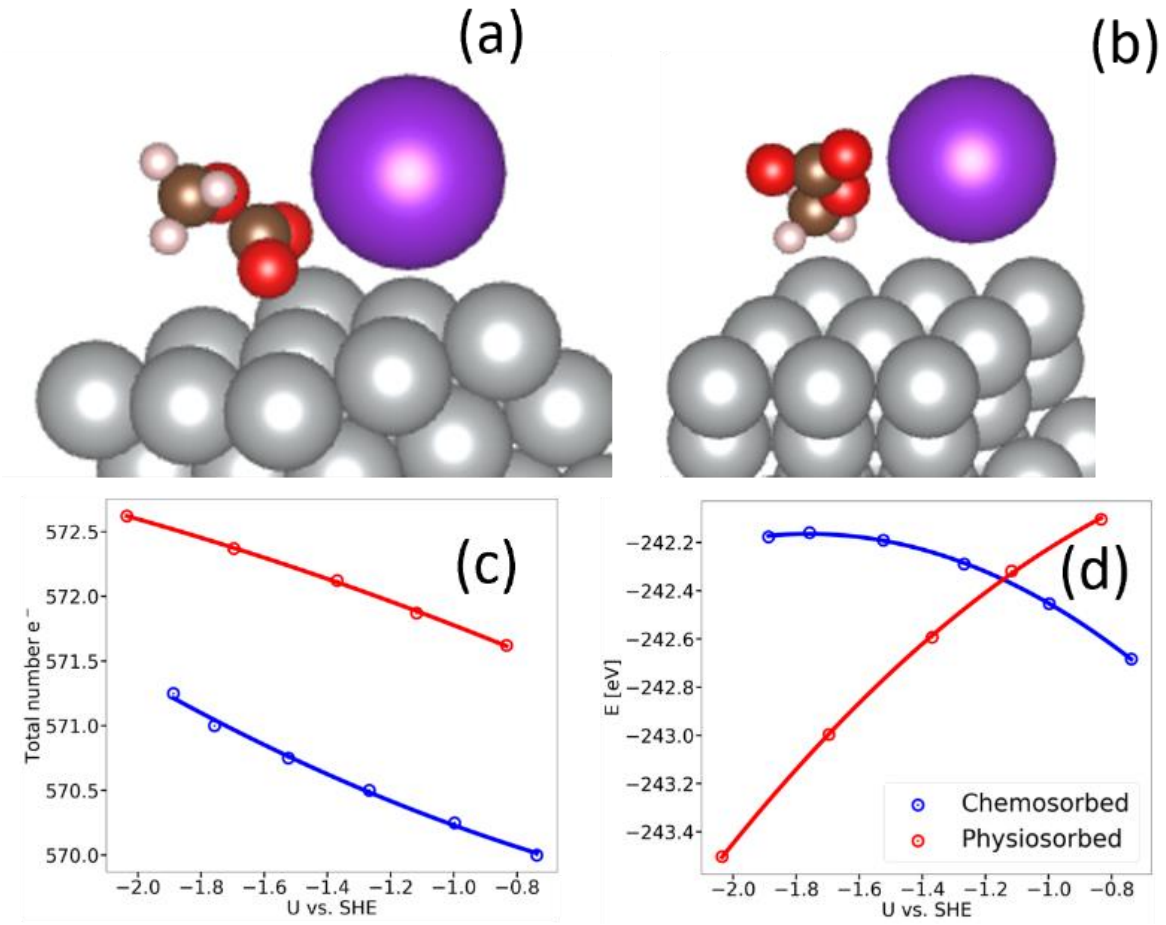


**Figure 3:** Different binding modes of $KCH_3OCO_2$* on Ag(111). (a) is chemosorbed and (b) is physiosorbed. (c) Plot of the number of electrons and (d) electronic energy as a function of potential. Blue line is chemosorbed (structure in (a)) and red line is physiosorbed (structure in (b)).

In Figure 3 there are clearly the modes of adsorption, the chemosorbed (Figure 3a and the blue line in Figures 3c and 3d) and the physiosorbed (Figure 3b and the red line in Figures 3c and 3d). Clearly from Figures 3c and 3d the surface charging parabolas are quite different. Thus, it is

important to consider both methods of adsorption in the work, but to only include the most stable mode of adsorption at a given potential.

When using the surface charging method there are 2 additional assumptions. The first is that the Poisson Boltzmann equation can be perfectly linearized. This assumption breaks down in the limit of highly negative potentials. The other assumption is that there is a constant distribution of electrolyte. Similar to the dielectric constant, the distribution of electrolyte is a function of position and time.[50]

In this work, 2 solvents were used, a mixture of 30/70 wt% MEA/water and methanol. The dielectric constant of methanol was taken as 32.42 from literature.[56] These conditions were used to match experimental conditions. This work is based off the previous works of Sargent *et al*. and Shen *et al*. These works used a 30/70 wt% MEA/water solvent, so this was done here as well.[8,11] The dielectric constant of the MEA/water solvent was taken as a molar weighted average of the dielectric constants of the pure components. The pure dielectric constant of water is 78.4,[57] and for MEA is about 32.[58] Therefore, when the molar average is applied this leaves a dielectric constant of 73.4 for the system.

In Sargent's paper they used a 2M KCl electrolyte.[11] Therefore, this concentration was also taken for our electrolyte. Therefore, for the MEA/water solvent it had a Debye screening length of 2.09 Å, and the methanol solvent has a Debye screening length of 1.382 Å.

## 2.3 Atomic Model

In this work all models are symmetric. This is to eliminate the known dipole that would occur in asymmetric models.[54,55,59] Figures 4 and A2-A17 show the models used in this work:

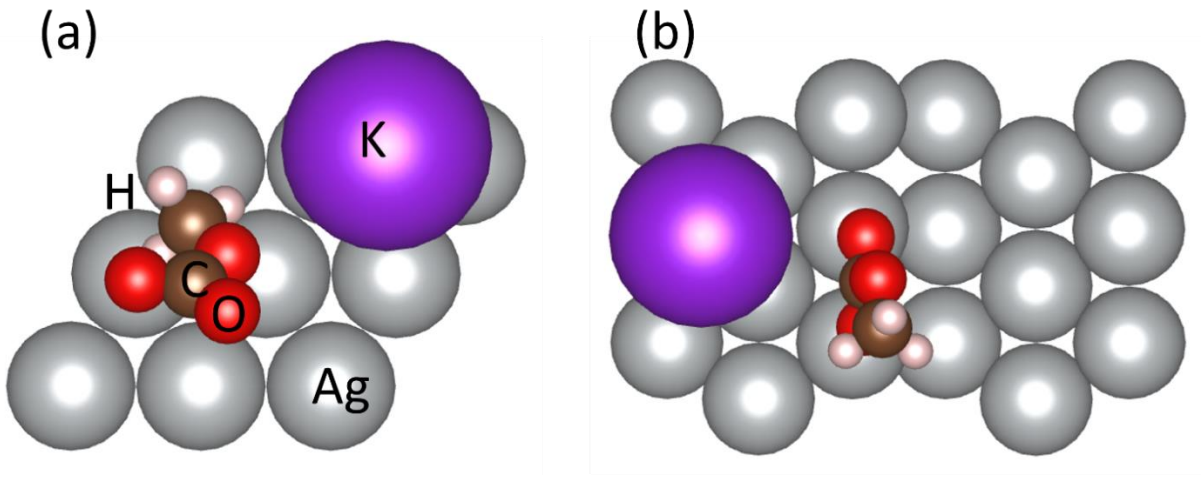


**Figure 4:** Top down view of the $KCH_3OCO_2$* intermediate on the (a) Ag(111) and (b) Ag(211).

For the (111) a 1/9 ML coverage of both the $K^+$ cation and the captured $CO_2$ complex was used. We tested 2/9 ML coverage of the $K^+$ to allow for the surface to always contain the cation double layer and allow for the complex to be in its neutral form as it adsorbs to the surface. However, it was determined that the adsorption energy of the complex with and without this additional $K^+$ was similar. In literature a coverage of about 1/9 ML or smaller is common.[60–62] Thus, it was decided to say with the 1/9ML coverage of $K^+$.

The (111) slab had 5 layers total when symmetrized with only the middle layer constrained. A unit cell of 3 x 3 Ag atoms was taken. With a lattice constant of 4.09 Å, this led to an overall unit cell dimensions of 8.65 Å x 8.65 Å x 60 Å. 60 Å of vacuum was taken so that there was at least 30 Å of space along the z-axis between the top of the slab and the bottom of the slab in the adjacent unit cell (Figure A18). This model was chosen as it reduced computational cost and to match our previous work.[8]

For the Ag(211) slab a 1/18 ML coverage of the $K^+$ and 1/18 ML coverage of all adsorbates was taken. This was done for 2 reasons. First when a 1/9 ML coverage was used, the size of the unit cell was too small to allow for ample space between adsorbates in adjacent unit cells.

Additionally, the most interesting part of the (211) is the step as this differentiates it from the (111). Therefore, it is ideal to place the step in the middle of the unit cell to accurately probe it without the possibility of adjacent unit cells altering its reactivity. Therefore, the (211) unit cell was 6x3 Ag atoms. With a lattice constant of 4.09 Å, this led to overall cell dimensions of 14.17 Å x 8.68 Å x 60 Å. Again, a vacuum of at least 30 Å vertically was established to allow for no interactions between adjacent vertical unit cells. As this surface has a slanted shape it is not trivial to describe its symmetric geometry. Figure 5 shows a symmetrized (211) slab.

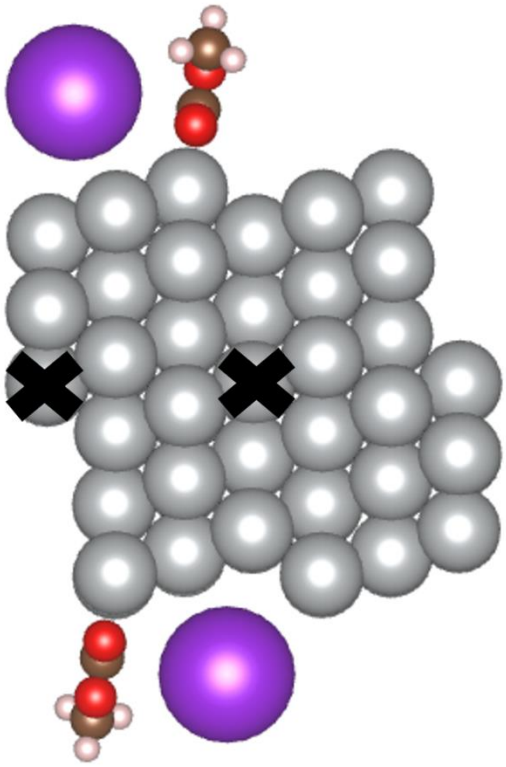

**Figure 5:** Example of a symmetrized Ag(211) with $KCH_3OCO_2$* adsorbate. The X refers to a constrained atom.

There are either 5 or 6 layers depending on what column described. Although strange, this model is able to eliminate the dipole moment and allow for reasonable calculations.

# Chapter 3: Mechanism

Figure 6 shows the overall mechanism used in this work.

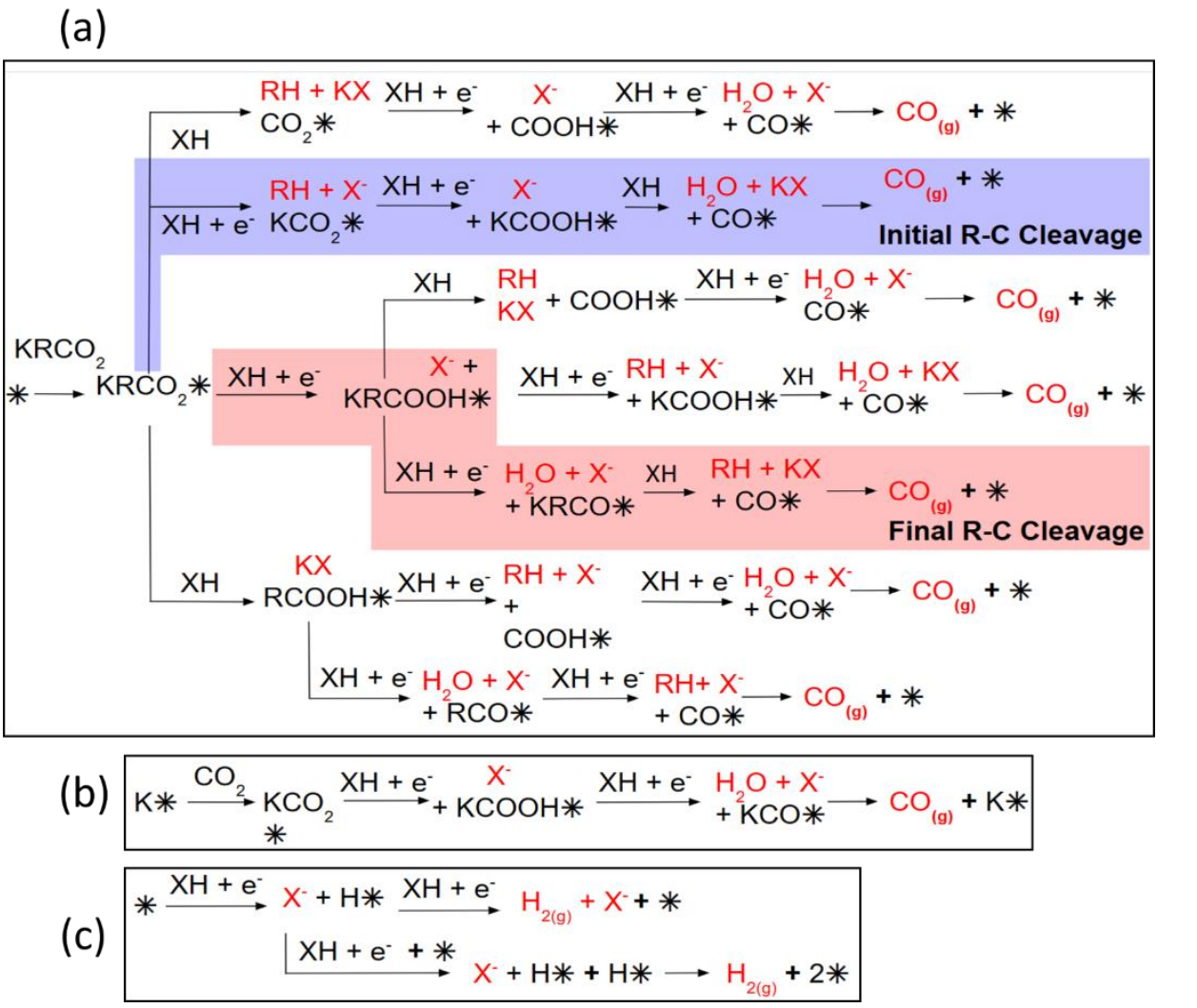


**Figure 6:** Overall reaction mechanism considered in this work for the (a) c-$CO_2$RR, (b) $CO_2$RR in the presence of $K^+$ cation, and (c) HER.

In the case of this work $KRCO_2$ is potassium methyl carbonate, potassium bicarbonate or potassium carbamate. Potassium is chosen as the counterion to the captured $CO_2$ anion because of its previous effectiveness.[11,63,64] It has been shown that larger alkali cations improve the activity of the $CO_2$RR.[63,64] The cation is important because the negatively charged carbonate or carbamate

must approach the negatively charged electrode to be reduced. Clearly this is not favorable so, the potassium cation assists in this process. In the $CO_2$RR, the potassium plays a similar role. When $CO_2$ adsorbs to Ag, it changes from a linear mode to a bent mode. The bent shape is desirable as this has a lower lowest unoccupied molecular orbital (LUMO) which assists in the electron transfer necessary to reduce $CO_2$.[65] This cation assists in the process by injecting some charge into the surface which helps to stabilize the $CO_2$.[66] Additionally, some possible carbamate reduction on Ag has been reported that when KCl electrolyte was used.[11] Therefore, in this work K is used as the cation. In this work K is assumed to be in its cationic state $K^+$ as the potentials are not made negative enough to reduce $K^+$ to metallic K.

Starting from the bare surface 3 possible compounds can adsorb: H, $CO_2$ or $KRCO_2$. H adsorbed electrochemically thought a PCET, and if this adsorption occurs, then the HER is assumed to undergo. After the H adsorbs, either the second PCET can occur to directly form $H_{2(g)}$ (Volmer-Heyrovsky Mechanism) or the second PCET can adsorb another H onto the surface. These two adsorbed Hs then combine to form $H_{2(g)}$ (Volmer-Tafel Mechanism).[28]

As this work if on Ag, if $CO_2$ adsorbs then it must undergo 2 PCETs to form CO. The adsorption is markedly endergonic and is typically taken as the potential limiting step (PLS). Once this adsorption occurs, a PCET follows to form COOH*. This COOH* is then reduced into CO* and $H_2O$. Finally, the CO* desorbed. In this work the $K^+$ is present in all steps of the $CO_2$RR.

For the c-$CO_2$RR the general form of the reaction was given in equation 6 (reprinted again for ease).

$$KRCO_2 + 3XH + 2e^- \rightarrow CO + H_2O + RH + KX + 2X^- \quad \text{(Eq 6)}$$

However, the $R^-$ and $X^-$ are placeholder compounds as the energetics will change depending on the capture agent and proton source combination used. In the case of $CH_3OH$, $KRCO_2$ is

$KCH_3OCO_2$, in the case of $H_2O$ capture agent $KRCO_2$ is $KHOCO_2$, and in the case of $NH_3$ capture agent, $KRCO_2$ is $KNH_2CO_2$. XH is the proton sources considered while KX is the corresponding potassium salt. The pairs considered are given in the format XH & KX: $CH_3OH$ & $KOCH_3$, $H_2O$ & KOH, $KHCO_3$ & $K_2CO_3$, and $NH_4ClO_4$ & $NH_3$ + $KClO_4$. Overall, 2 PCETs occur per cycle, but 3 protonation are required. This additional protonation, as compared to the $CO_2$RR, comes from releasing the capture agent. Therefore, 1 of these protonations is taken as chemical. From our calculations it is determined that the pathways that do the final protonation chemically are the most thermodynamically favorable. In this work 4 proton sources are considered: $CH_3OH$ which has a $pK_a$ of 15.5,[39,40] $H_2O$ which has a $pK_a$ of 14,[40] $KHCO_3$ which has a $pK_a$ of 10.3,[5] and $NH_4ClO_4$ (formally noted as $NH_4^+$) which has a $pK_a$ of 9.25.[36]

If $KRCO_2$ adsorbed, then there are four possibilities that can be broken in 2 groups: initial cleavage or direct reduction. Both these processes can have their first protonation and their last protonation as electrochemical or chemical. It was determined that the most thermodynamically stable pathways involve the final protonation done chemically. Therefore, these two pathways will be taken as initial R-C cleavage (blue highlight) and final R-C cleavage (red highlight).

If the initial R-C cleavage pathway is taken, then a PCET occurs to release the captured $CO_2$ from the capture agent. The $CO_2$ is taken to bind to the surface with the $K^+$ still present and the capture agent is removed into the solvent. Then a second PCET occurs to form KCOOH* and $X^-$. At this point both PCETs have been used. Therefore, a chemical protonation occurs to form CO*, $H_2O$ and a potassium salt. This CO* then desorbs from the surface.

If the final R-C cleavage pathway is taken, then a PCET will occur that forms KRCOOH* and $X^-$. A second PCET will occur to form KRCO*, $H_2O$ and $X^-$. As with the initial R-C cleavage

at this point both PCETs have been used so the final step is done chemically. This forms an adsorbed CO*, the capture agent, and KX. The cycle is completed by desorbing CO.

To start our analysis the overall reactions energies was considered.

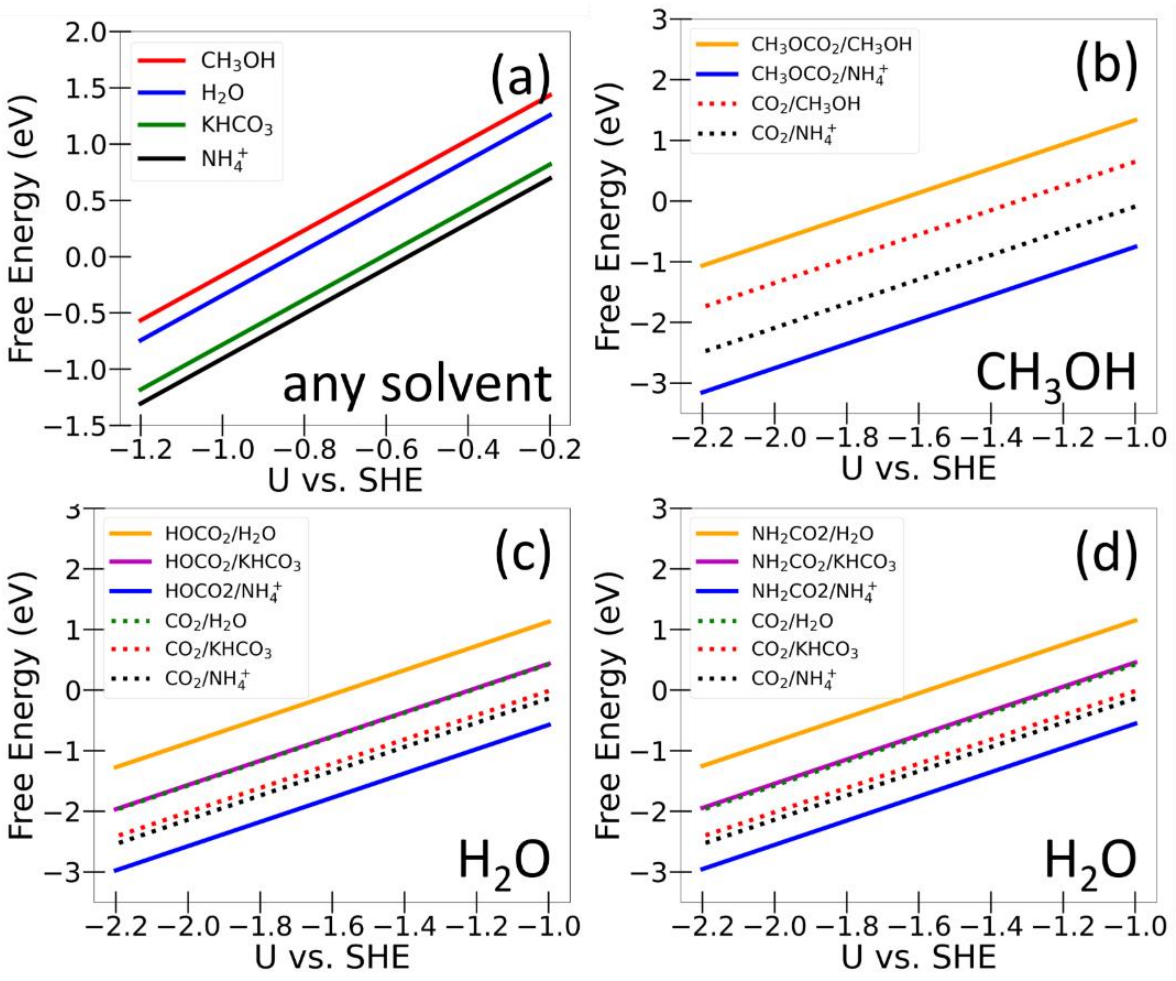


**Figure 7:** Overall reaction energetics for the (a) HER, (b) methanol c-$CO_2$RR (solid line) and $CO_2$RR (dotted line) in methanol solvent, (c) $H_2O$ c-$CO_2$RR (solid line) and $CO_2$RR (dotted line) in $H_2O$ solvent, and (c) $NH_3$ c-$CO_2$RR (solid line) and $CO_2$RR (dotted line) in $H_2O$ solvent.

From Figure 7, it is clear that overall, the HER is much more thermodynamically favorable than the $CO_2$ or c-$CO_2$RR. In our model the chemical potential of a coupled proton and electron is approximated by the computational hydrogen electrode (CHE) model (equation 5):

In the CHE, the chemical potential of a couple proton and electron are a function of the potential, the temperature, the pH, and the charge.[53] In our case the charge is always 1. The potential is determined by the SC method. The temperature is taken as room temperature (298.15K) and the pH is given by the $pK_a$ of the proton source. It was determined that the $pK_a$ of a buffer solution had the same effect on the equilibrium potential of the HER as changing the pH of the solution. In this work, we assume that all proton sources XH is in equilibrium with $X^- + H^+$. Therefore, this allows us to rewrite equation 4 as equation 9:

$$G_{H^+ + e^-} = \frac{1}{2} G_{H_{2(g)}} - eU - ln(10) * k_B * T * pK_a \quad \text{(Eq 9)}$$

Given that $H_2$ is taken in gas phase it is reasonable to assume that the solvent has little effects on its energetics. Therefore, the HER should be solvent insensitive and only dependent on the $pK_a$ of the proton source. Therefore, Figure 7a shows that as the $pK_a$ is decreased the reaction energy was made more exergonic, with $CH_3OH$ proton source leading to the least exergonic reaction and $NH_4^+$ proton source leading to the most.

For all capture agents involved the only proton source that leads to the c-$CO_2$RR being more exergonic than the $CO_2$RR is the $NH_4^+$. This comes from the final protonation. When $CH_3OH$, $H_2O$, and $KHCO_3$ are used in the chemical proton source, the $H^+$ is exchanged with the $K^+$. However, for $NH_4ClO_4$ the $NH_4^+$ is exchanged with $K^+$. The ionization potential is defined as the energy required to ionize a neutral atom to produce a cation and an electron. The ionization potential of H is 13.6 eV,[67] while the ionization potential of K and $NH_4$ are 4.34 eV[68,69] and 3.7 eV respectively.[70] As the ionization potentials of K and $NH_4$ are close, when they are exchanged this leads to a small reaction energy. However, when the $H^+$ and $K^+$ are exchanged this leads to a large reaction energy.

From Figure 7 the equilibrium potential for each of these reactions can be determined by finding the potential when the overall reaction energy is 0. This is plotted in Figure 8:

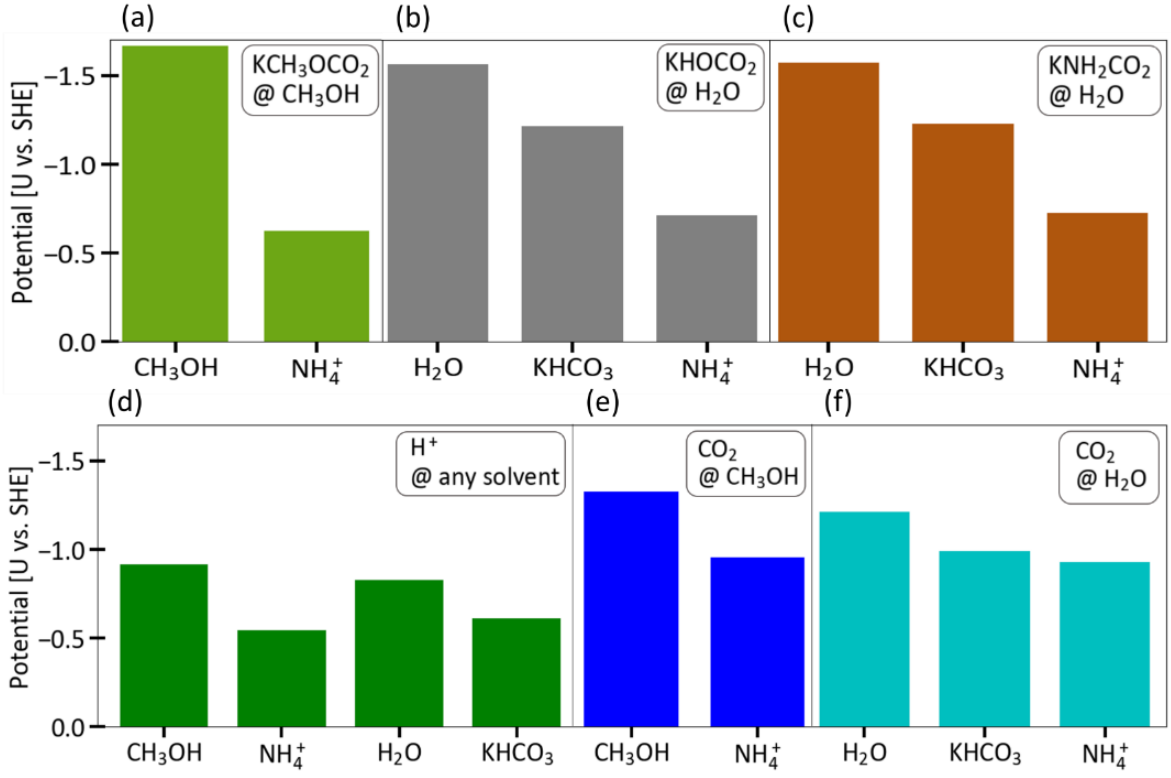


**Figure 8:** Equilibrium potentials for (a) methanol c-$CO_2$RR, (b) $H_2O$ c-$CO_2$RR, (c) $NH_3$ c-$CO_2$RR, (d) HER, (e) $CO_2$RR in methanol solvent, and (f) $CO_2$RR in water solvent. The proton source is given by the x-axis and the compound being reduced and the solvent are given in the top right corner by the notation compound @ solvent.

From Figure 8 it is proton source has a much larger effect on the equilibrium potentials than the capture agent. In all cases a proton source with a lower $pK_a$ leads to a less negative equilibrium potential. From Figure 8 only the c-$CO_2$RR using $NH_4^+$ proton source is more exergonic than the $CO_2$RR. Thus, this leads to the c-$CO_2$RR to have more negative equilibrium potential than the $CO_2$RR. However, for the $NH_4^+$ case the c-$CO_2$RR has a less negative equilibrium potential than the $CO_2$RR by about 0.25 V vs. SHE.

From Figure 8 we see that the HER is overall thermodynamically easier than the $CO_2$RR and c-$CO_2$RR. Thus, it is imperative to choose a catalyst that has a very endergonic elementary step for the HER. It is important to consider the full reaction pathway. An example using methanol capture agent in methanol solvent using methanol proton source is shown in Figures 9-11.

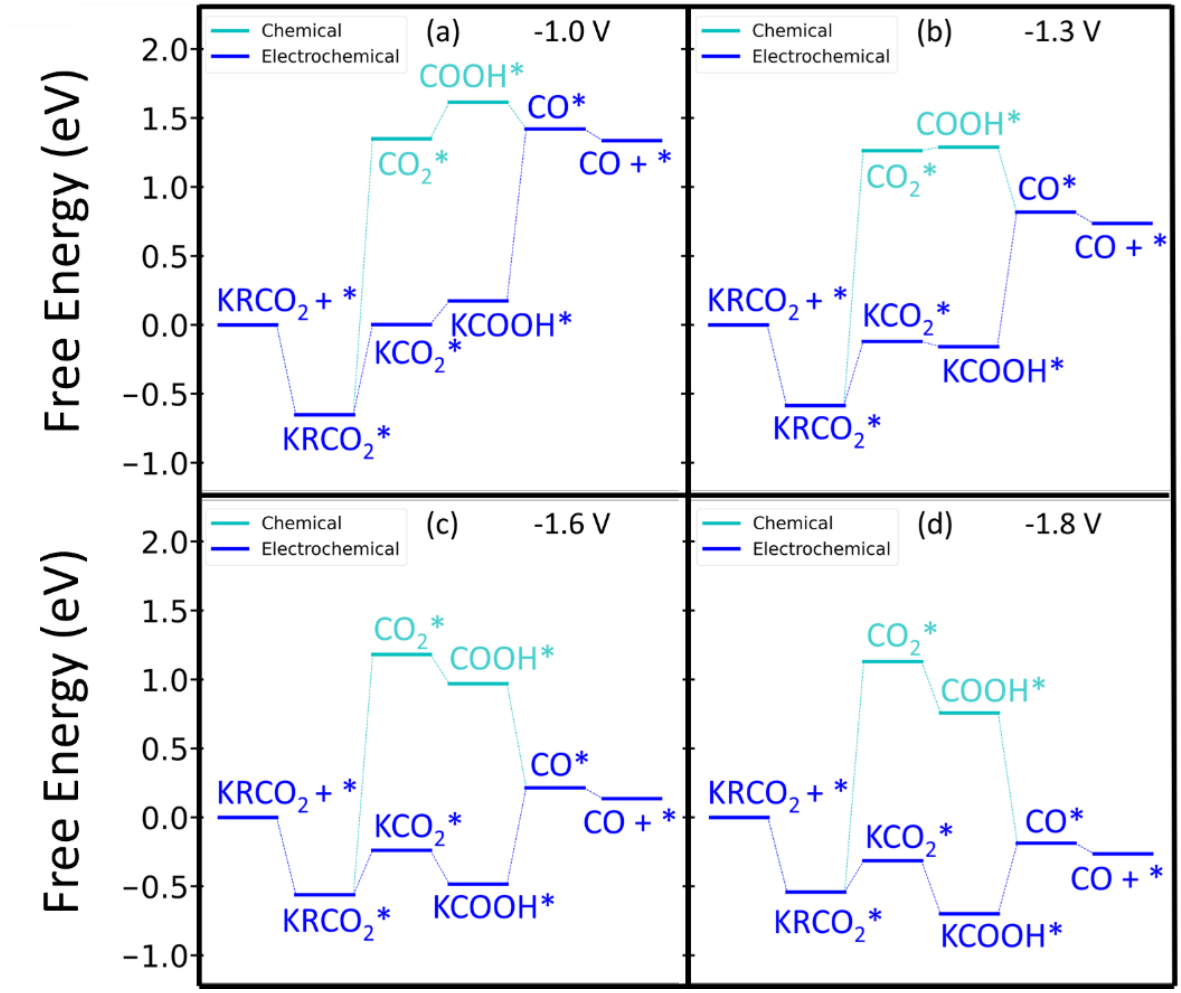


**Figure 9:** Part of the overall reaction pathway for methanol c-$CO_2$RR on Ag(111) as a function of potential. This path includes the initial R-C cleavage pathway if the first (light blue) and the final (dark blue) protonations are taken as the chemical step. (a) -1.0 V, (b) -1.3 V, (c) -1.6 V, and (d) -1.8 V all vs. SHE.

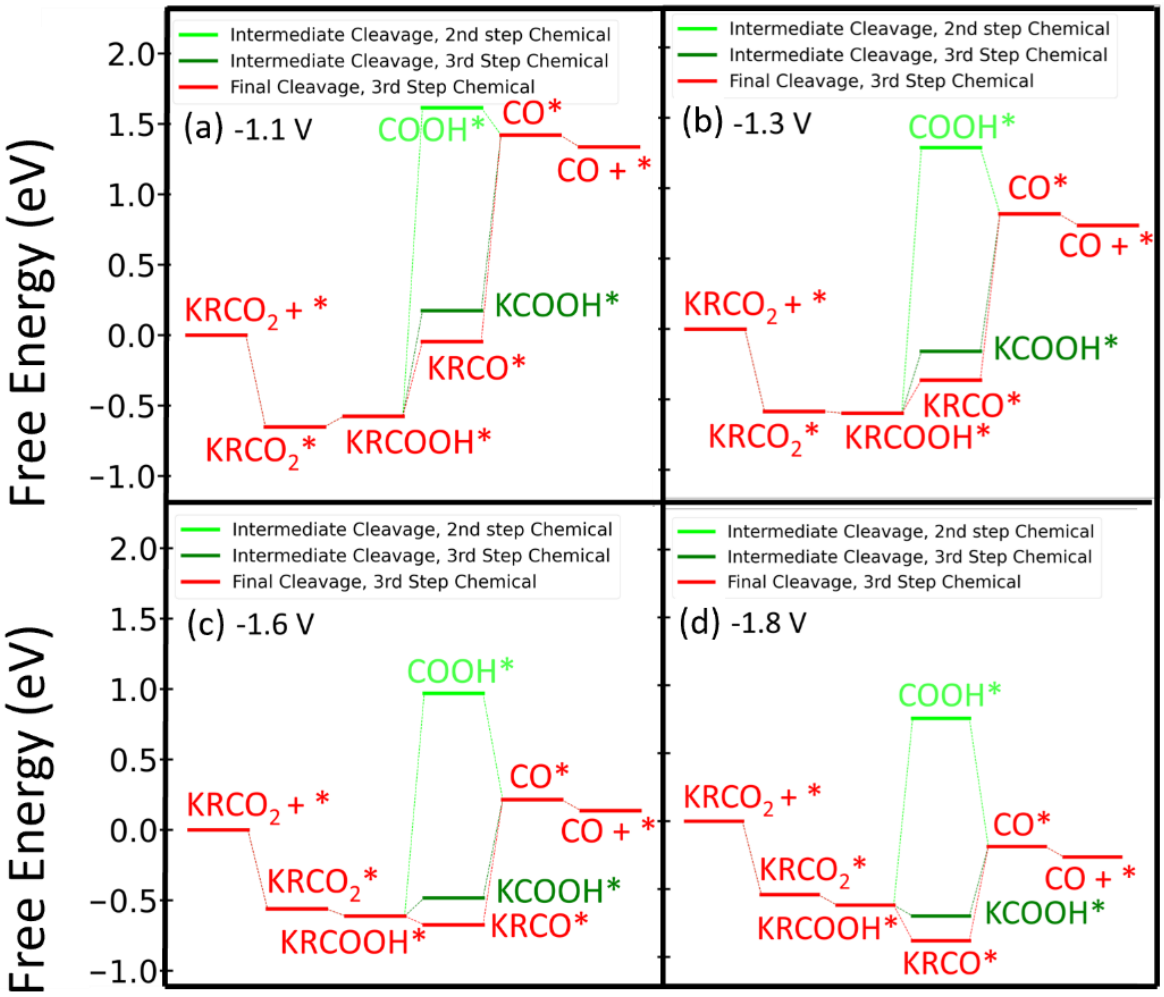


**Figure 10:** Part of the overall reaction pathway for methanol c-$CO_2$RR on Ag(111) as a function of potential. This path includes the intermediate R-C cleavage if the second protonation (light green) and the final (dark green) protonations are taken as the chemical step. The final R-C cleavage pathway when the final protonation is chemical is also shown (red) (a) -1.0 V, (b) -1.3 V, (c) -1.6 V, and (d) -1.8 V all vs. SHE.

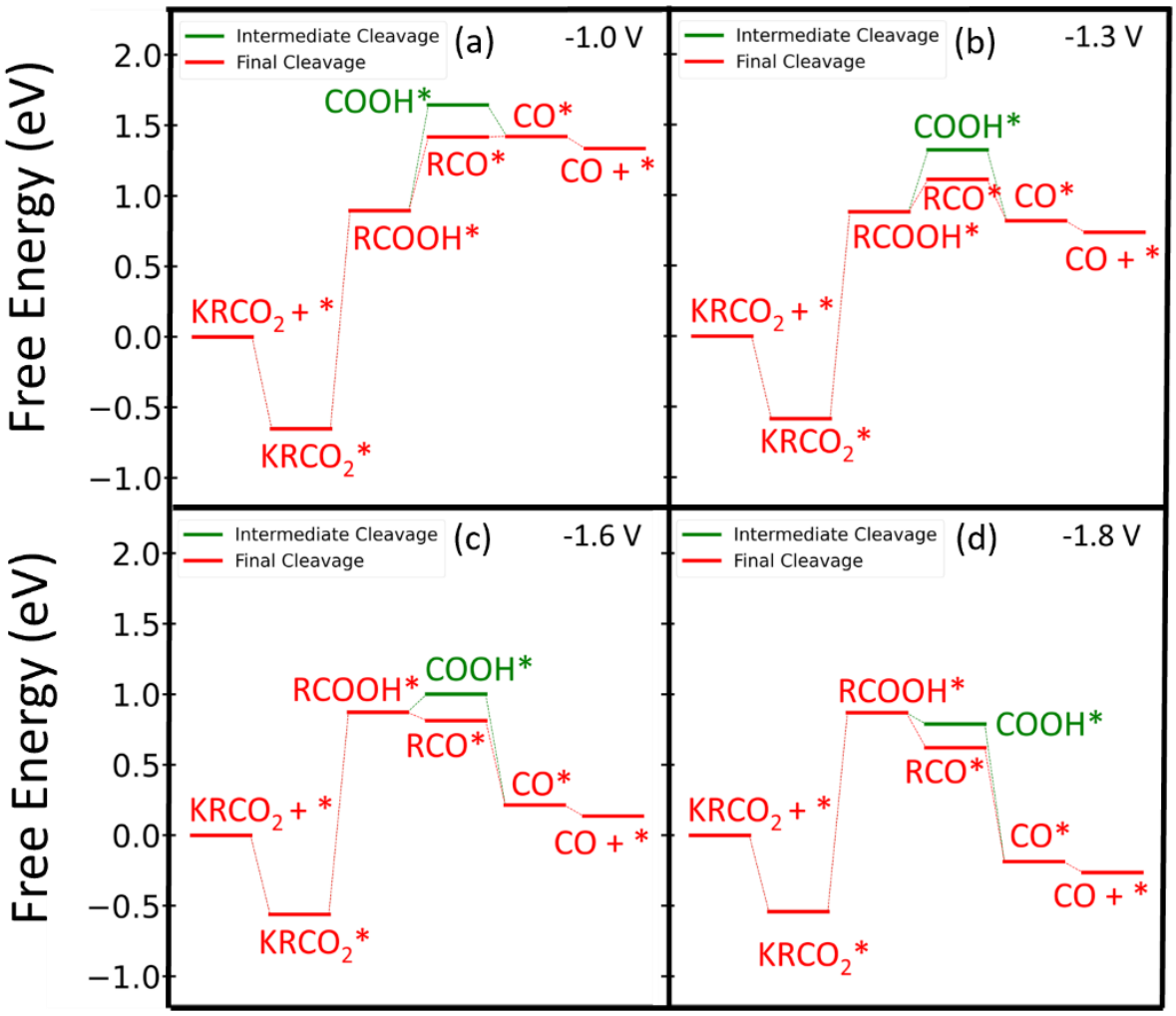


**Figure 11:** Part of the overall reaction pathway for methanol c-$CO_2$RR on Ag(111) as a function of potential. This path includes the intermediate (green line) and final (red) R-C cleavage if the first protonation is taken as the chemical step. (a) -1.0 V, (b) -1.3 V, (c) -1.6 V, and (d) -1.8 V all vs. SHE.

From Figures 9-11 it is clear that the overall reaction mechanism is complex and for reasonable analysis must be simplified. However, as seen in the Figures 9-11 is that 2 distinct pathways appear as the most thermodynamically favorable pathways. This trend holds true for all capture agents and proton sources tested. From Figure 9, it is clear that for the initial R-C cleavage, the first protonation must be electrochemical. However, it is interesting to note that at weakly

negative potential, these pathways have relatively similar energetics. However, as the potential is made more negative the energetics of the first step electrochemical pathway (dark blue) becomes much more favorable than the first step chemical (light blue). This is because of the nature of the chemical step. Typically, chemical steps are not potential dependent. From the SC method each intermediate is potential dependent,[54] but this trend of typical chemical steps having little potential dependence typically continues to appear when using the SC method.[55] Thus, the first chemical step stays very endergonic for the entire potential leading to an unusable pathway at all potentials. It is noted that the if the final step is chemical then there is a strange potential dependence. This will be elaborated further later in this work, but the reason is because of a shift in the PZC between the reactants and the products. From Figure 10, it is clear the if the second step is done chemically (light green), then the same potential independence is observed and thus, that pathway is not accessible at the window of interesting potential. Additionally, the final R-C cleavage (red) and the intermediate R-C cleavage (dark green) have similar reaction profiles. However, as will be explained in the section on energetic span, they would have the same energetic span, which means that the reactivity will be predicted to be the same. Thus, the red pathway is chosen since the reaction energy between KRCOOH* → KRCO* (red) is more exergonic than KRCOOH* → KCOOH* (dark green) at all potentials.

Finally, Figure 11 shows some interesting competition between doing the final R-C cleavage doing the last step chemically (Figure 10, red) and doing the first step chemically (Figure 11, red). However, it is important to remember that all these pathways are competing with each other. Between these two pathways, when the final step is done chemically, the most stable state (typically, KRCO*) is much most stable than any of the states when the first step is done chemically. Therefore, the final step would be done chemically.

We then consider the effect of the proton source on the overall reactivity (Figure 12).

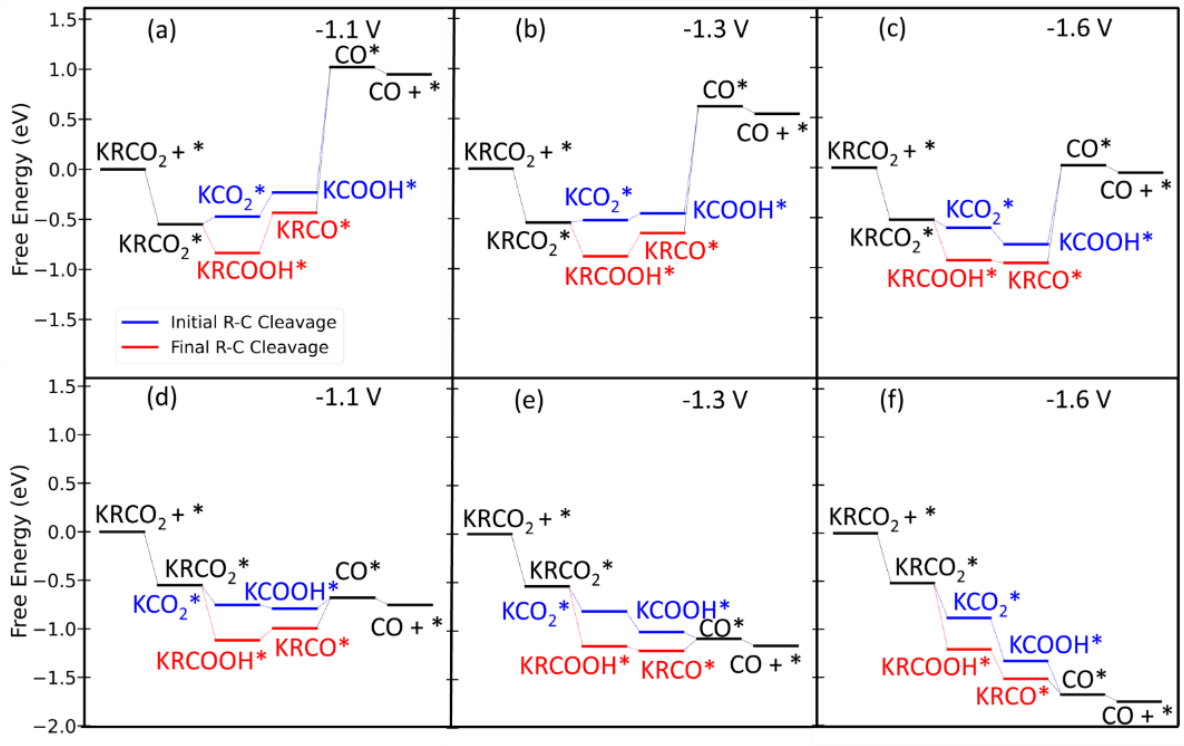


**Figure 12:** Reaction pathway for the reduction of potassium carbamate on Ag(111). (a-c) is using $H_2O$ and (d-f) is using $NH_4^+$ as the proton source. Potentials are as follows: (a,d) -1.1 V, (b,e) -1.3 V, and (c,f) -1.6 V all vs. SHE.

Figure 12 showcases how large the effect the proton source has on the elementary reaction steps. For Figures 12(a-c) shows using $H_2O$ as a proton source leads to a very endergonic reaction at -1.1 V and barely exergonic at -1.6 V. However, from Figures 12(d-f) using $NH_4^+$ as the proton source leads to an exergonic reaction at -1.1 V vs. SHE. However, the largest difference is in the chemical step, which is taken as the chemical step as this reaction can proceed the easiest without electrochemical assistance.

To gain a deeper insight into the electrochemical effect on the reaction energy it is necessary to consider the elementary reaction energies (Figures A19-A22)

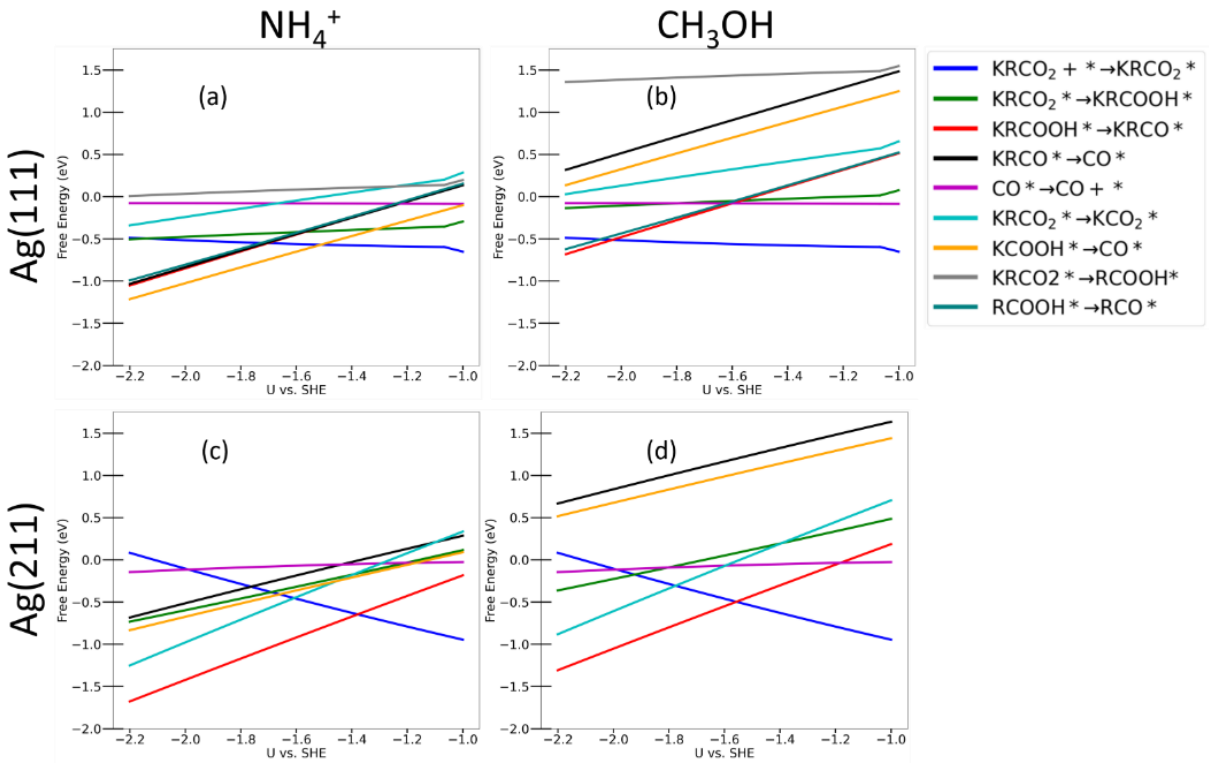


**Figure 13:** Elementary reaction energies for the c-$CO_2$RR using methanol capture agent in methanol solvent. The rows determine the facet top row (a,b) is uses Ag(111) and the bottom row uses Ag(211). The column determines the proton source first column (a,c) is $NH_4^+$ and the second column is $CH_3OH$.

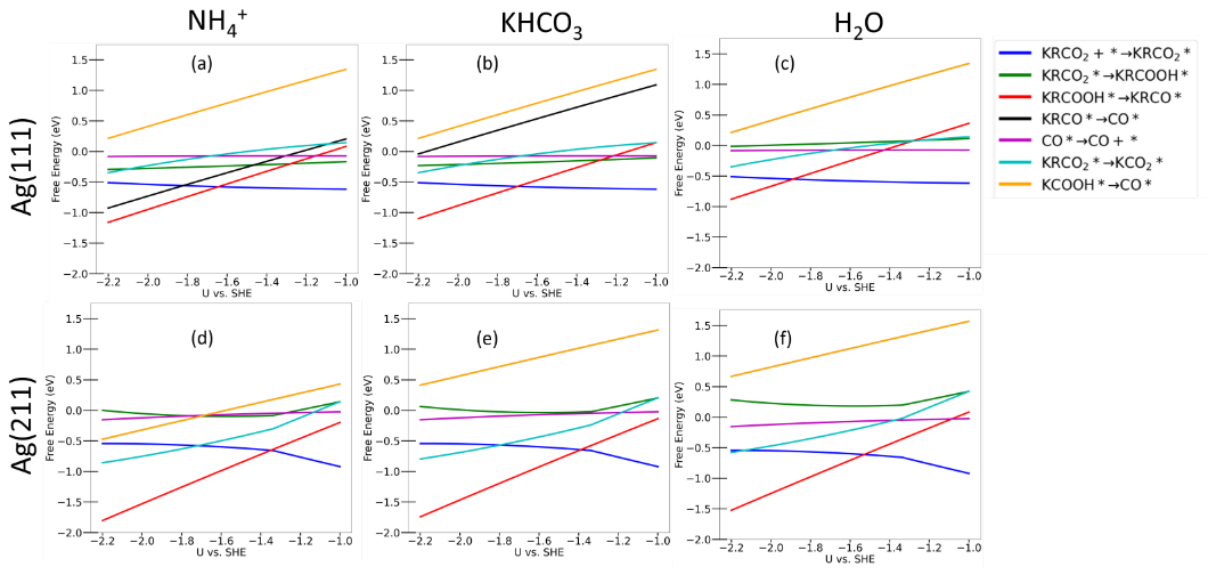


**Figure 14:** Elementary reaction energies for the c-$CO_2$RR using $H_2O$ capture agent in water solvent. The rows determine the facet top row (a,b) is uses Ag(111) and the bottom row uses Ag(211). The column determines the proton source. The first column (a,d) uses $NH_4^+$, the second column (b,e) uses $KHCO_3$ and the third column (c,f) uses $H_2O$.

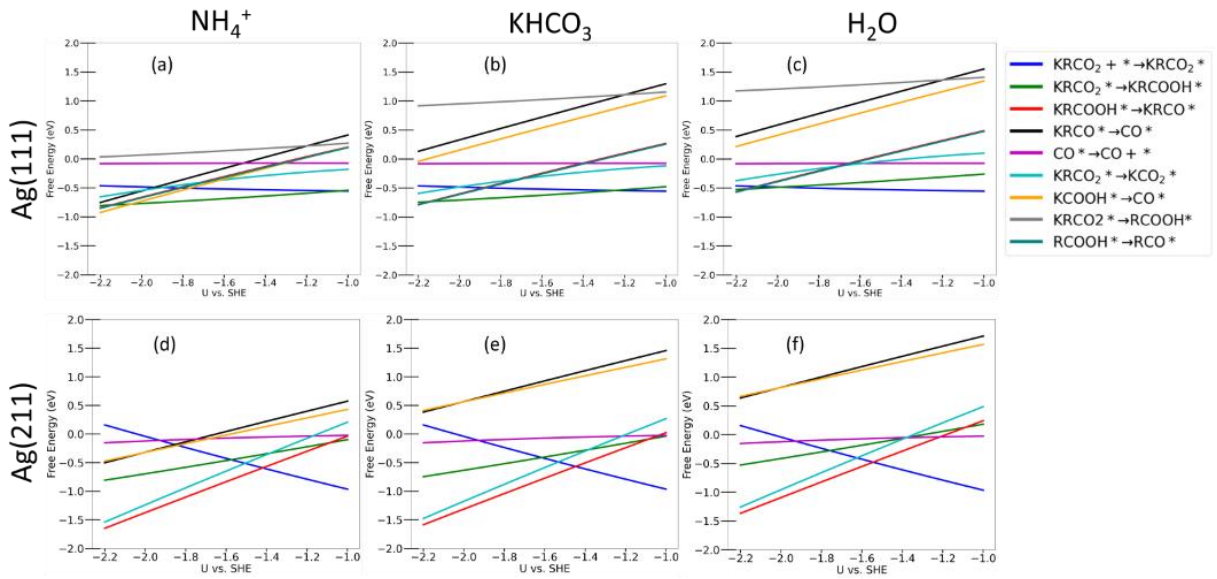


**Figure 15:** Elementary reaction energies for the c-$CO_2$RR using $NH_3$ capture agent in water solvent. The rows determine the facet top row (a,b) is uses Ag(111) and the bottom row uses Ag(211). The column determines the proton source. The first column (a,d) uses $NH_4^+$, the second column (b,e) uses $KHCO_3$ and the third column (c,f) uses $H_2O$.

From Figures 13-15 the adsorption of the complex on the (111) terrace is potential independent. This is logical as this step is non-electrochemical so the potential should have little effect. For the initial R-C cleavage the next step is a PCET to decompose the $KRCO_2$* into $KCO_2$*. This step is potential dependent, but not as potentially dependent as the other PCETs. Even more surprising is in the final R-C cleavage step. The first PCET is between $KRCO_2$* → KRCOOH*. However, on the (111) this step is seen to have little potential dependence despite being an electrochemical step. This occurs because of two simultaneous processes. The $KRCO_2^-$ is an anion so the $K^+$ interacts with it to stabilize it on the negatively charged cathode. However, $CO_2$* and KRCOOH* are neutral adsorbates. Therefore, the $K^+$ changes from sharing its electron with the adsorbate to with the surface. Therefore, two processes occur: a PCET and a charge injection that changes the potential of zero charge (PZC). This is shown in Figure 16.

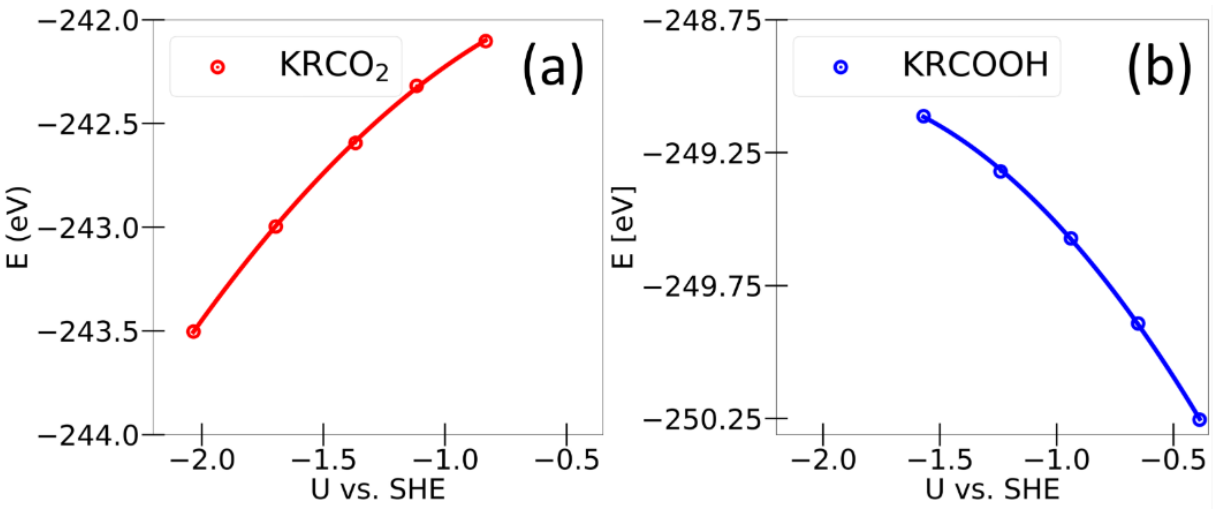


**Figure 16:** Electronic energy as a function of potential for (a) $KCH_3OCO_2$* and (b) $KCH_3OCOOH$* in methanol solvent.

As shown in Figure 16, the PZC shifts from about -1V vs. SHE to about -1.5 V vs. SHE. This was observed throughout the work that the $KRCO_2$* PZC would be about 0.5 – 1 V less negative than the KRCOOH* PZC. Therefore, this process counters the PCET process and leads to an overall thermal-neutral PCET for the final R-C cleavage.

For the initial R-C cleavage there is minor potential dependence even though there is a competition between the PCET and the $K^+$ changing where it is donating its electron. However, this comes from the change in dipole moment created from the adsorption of $CO_2$. This dipole moment is known as there have been reports of a large dipole moment change when $CO_2$ desorbs.[55] The $CO_2$ takes some charge from the surface which can be observed by an improvement in the $CO_2$ adsorption energy by injecting more charge. Therefore, when the processes are summed together there is some potential dependence.

After this step in the case of the initial R-C cleavage the $KCO_2$* undergoes a PCET to form KCOOH* and the in the case of the final R-C cleavage the KRCOOH* undergoes a PCET to form KRCO*. On the (111) this PCET shows the typical potential dependence.

Then the chemical step occurs. KCOOH* → CO* for the initial R-C cleavage and KRCO* → CO* for the final R-C cleavage. Typically, the chemical step should have limited potential dependence as no electron is transferred. However, it is observed that both steps have strong potential dependence on the (111). This is also from the shift in PZC of the KRCO* and the KCOOH* intermediate and the CO* intermediate as shown in Figure 17:

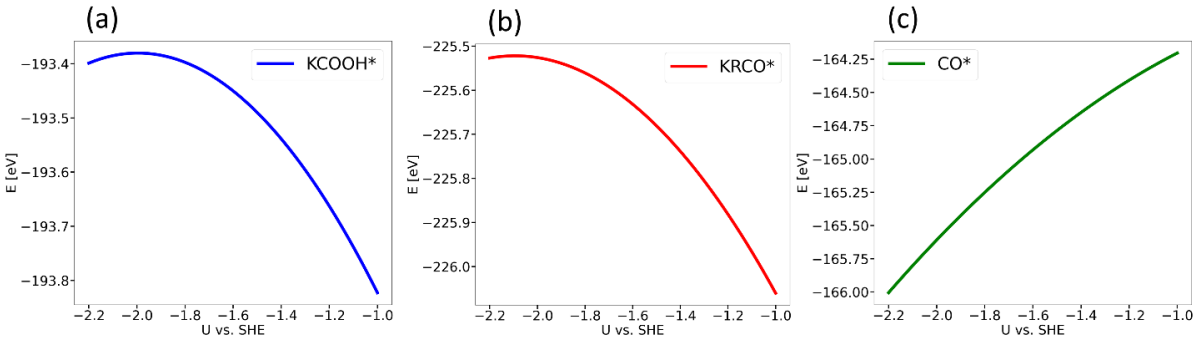


**Figure 17:** Electronic energy of (a) KCOOH*, (b) KRCO*, and (c) CO* as a function of potential in methanol solvent.

The PZC of the KRCO* and KCOOH* is at highly negative potential while the PZC of the CO* intermediate is at weakly negative potential. Therefore, when the reaction occurs there is a large shift in PZC that leads to a large potential dependence. This shows the importance of considering the reactions using the SC method as compared to the CHE model. Previous work has shown the SC method does have deviations from the CHE method, but the c-$CO_2$RR shows a stark difference between the methods leading to a requirement of using the SC method.

For the (211) there are differences in the reaction energy trends. The final chemical step has the same trend as the (111) where the chemical step is strongly potentially dependent. However, unlike the (111) the adsorption of $KRCO_2$ is inversely dependent on the potential. This is from the adsorption modes of the $KRCO_2$ shown in Figure 18.

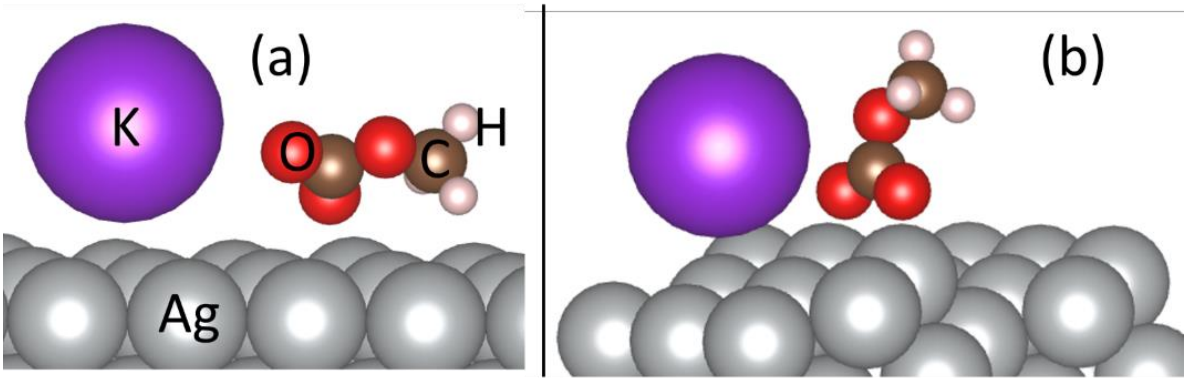


**Figure 18:** Typical carbonate and carbamate binding modes on (a) Ag(111) and (b) Ag(211). This figure shows $KCH_3OCO_2$*. All relevant structures can be found in the Figures A2-A17.

On the (111) the carbonate and carbamate adsorb in the mode shown in Figure 18a. However, on the (211) the carbonate and carbamate adsorb in the mode shown in Figure 18b. This occurs because of the undercoordination of the (211) atoms. As the (211) has steps it has undercoordinated atoms at the edge that are more reactive. This reactivity leads to better $CO_2$ adsorption, and this is why it is reported that steps and kinks improve the activity for $CO_2$RR.[71] Therefore, these sites want to chemosorb the $KRCO_2$ on the (211) as opposed to the physisorption of the $KRCO_2$ on the (111). However, as the surface is injected with more charge this stabilizes the bare surface, so the chemosorption mode becomes less stable.

This inverse potential dependence leads to a difference trend in the potential dependence of the first PCET. Unlike on the (111) where there are two coupled processes, on the (211) there are three: the PCET, the $K^+$ changing from donating its proton from the adsorbate to the slab, and the desorption of the adsorbate as the KRCOOH* is found to be physiosorbed on both the (111) and the (211). Therefore, this leads to some potential dependence on the (211). For the case of the $KRCO_2$ → $KCO_2$* there are the same two processes as on the (111) but the same methods that lead to more potential dependence of the $KRCO_2$* → $KCO_2$* than the potential dependence of the $KRCO_2$* → KRCOOH* are active on the (211) leading to a relatively normal PCET.

It is known that the concentration of cations affects the electric field effects near the surface of an electrode.[72] However, in this work the concentrations of cations were different by a factor of two when comparing the (111) terrace which had a cation coverage of 1/9 ML with the (211) facet which had a cation coverage of 1/18 ML. However, when the binding mode of the carbonate/carbamate was similar then the potential dependence of the elementary reactions was similar. For example, from Figure 18 the binding mode of methyl carbonate is different on the (111) and (211). As such the $KRCO_2$* → KRCOOH* has different potential dependence. However, from Figure A9, the binding mode of methyl carbonate on (111) is identical to the binding mode of methyl carbonate on (211) at potentials less negative than -1.06 V vs. SHE (ie. The complex is chemosorbed rather than physiosorbed). From Figure 13 in that small potential range the same potential dependence trends are seen on the (111) as the (211). Namely, the complex adsorption has an inverse stability relationship with the potential and the $KRCO_2$* → KRCOOH PCET is potential dependent.

This same trend can be observed when the $KRCO_2$* is physiosorbed on the (211). The bicarbonate does not chemisorb, but physiosorbed to the (211) (Figure A10). From Figure 14, the same potential dependence that is typically seen on the (111) is observed for bicarbonate on the (211).

To further confirm the that binding mode of the complex was the larger determining factor in the strange potential dependence it was necessary to consider the potential dependent KRCO* →CO* chemical step. From Figures 13-15 this chemical step is always highly potential dependent. From Figures A15-A17 the KRCO* and the CO* always binds chemically to the surface, regardless of the facet. Therefore, overall, it was determined that the larger driving force for this

interesting potential dependence was not the concentration of cation, but rather the mode at which the complex binds to the surface.

# Chapter 4: Reactivity Analysis

## 4.1 Energetic Span

Typically, the most robust method of studying kinetics is through a microkinetic model (MKM), which are commonly seen in thermocatalysis.[73–75] In this method all the transition state (TS) are calculated alongside the intermediate energies. Then the rates can be solved for typically using transition state theory.[76]

However, in the case of electrochemical systems finding the TS is challenging. This is because of the additional computational cost associated with the addition of solvation. In the c-$CO_2$RR and the $CO_2$RR this gets even more challenging because the intermediates react with the solvent. For example, to protonated adsorbed $CO_2$* to form COOH*, the proton comes from some solvated species, typically taken as water. This involves numerous complexities as the surface charging comes from both explicit and implicit methods.

In the c-$CO_2$RR the potential limiting step is typically seen as KRCO* → CO*, which involves the chemical removal of the capture agent. Thus, finding this TS is critical to understanding the activity of a catalyst. However, with capture agents with larger $pK_a$ values this reaction is quite endergonic, on the order of 1 eV for moderately negative potentials. Thus, calculating this TS with classical methods such as climbing image nudged elastic band (CI-NEB) is difficult.

Therefore, in this work kinetics are assumed to be related to the thermodynamics. What has been done is to assume that the TS is at 0.4 eV above the reaction energy. 0.4 eV was chosen

because it has been observed to be a reasonable barrier for the analogous processes in the $CO_2$RR.[77–79] Then the energetic span (ES) theory can be applied. In ES theory the reactivity is assumed to be linked to the largest difference between any intermediate (ES_I) and any stable TS (ES_TS). This method was first created by Kozuch *et al*.[80,81] It is to be noted that the intermediate and the TS need not to be on the same reaction pathway. The ES can then be calculated using equation 10 (if the intermediate is before the TS) and equation 11 (if the intermediate is after the TS).[80,81] Figure 19 shows the ES in the context of c-$CO_2$RR.

$$G_{TS} - G_{intermediate} \quad \text{(Eq 10)}$$

$$G_{TS} - G_{intermeidate} + G_{reaction} \quad \text{(Eq 11)}$$

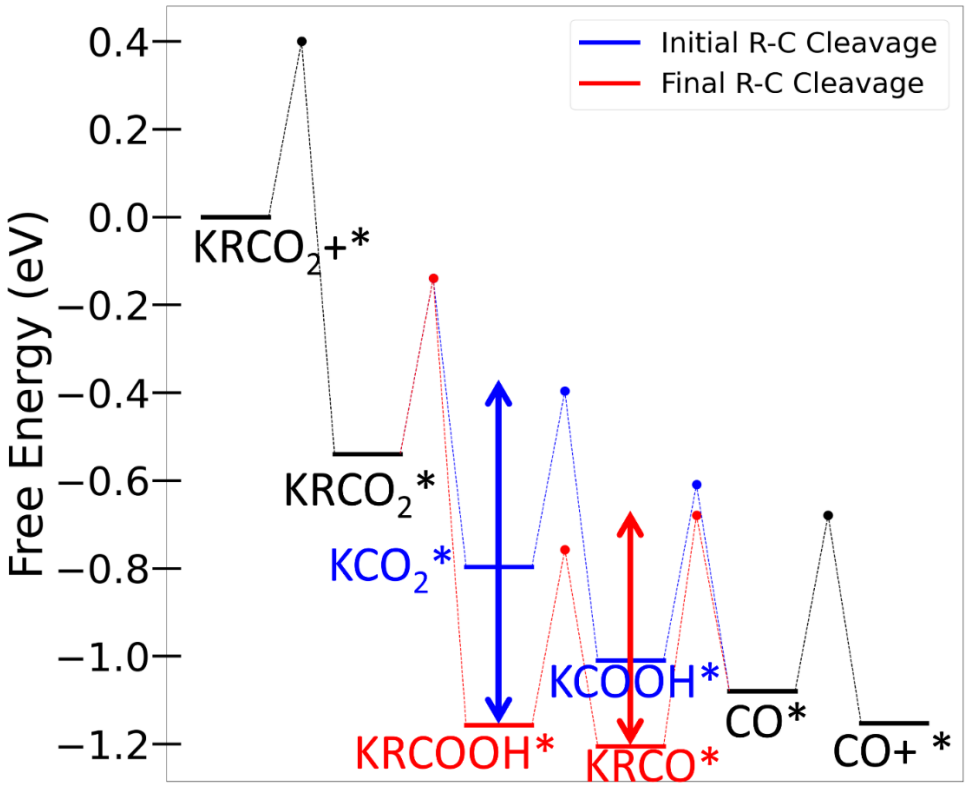


**Figure 19:** Energetic span (ES)[80,81] for the initial R-C cleavage (blue) and the final R-C cleavage (red) for potassium carbamate using $NH_4^+$ proton source in $H_2O$ solvent.

It is important to remember that the ES of a pathway is determined by the TS. The ES_I can be from any pathway. From Figure 19 it is clear that the most stable intermediate is the KRCO*. Thus, for the red pathway the ES ends up being the difference in energy from the KRCO* and the TS between KRCO* and CO*. It is noted that this TS occurs after KRCO* on the reaction pathway. Therefore, it is not necessary to include the reaction energy.

However, the blue pathway is not as clear. To explain the reason for the location of the ES it is first necessary to define what is meant by the ES_TS being before or after the ES_I. If the ES_TS lies on the same pathway as the ES_I, then it is trivial to determine if the ES_TS is before or after the ES_I. If they do not lie on the same pathway, then complications arise. What was done in this work was to consider types of reactions. In both the initial R-C cleavage and the final R-C cleavage pathways start with the adsorption of the complex. Then a 2 PCETs occur followed by a chemical protonation. This process is finished by a desorption. Therefore, what is assumed that if intermediates that have completed the same amount of a type of reaction are at the same point along their respective pathways. For example, to go from free $KRCO_2$ to KCOOH* the complex must first adsorb and undergo 2PCETs. Likewise for free $KRCO_2$ to become KRCO* an adsorption and 2PCETs must occur. Therefore, KCOOH* and KRCO* are consider analogous intermediates. This means that the TS between $KCO_2$* and KCOOH* would occur before KRCO* as $KCO_2$* occurs before KRCO*.

Using this knowledge make the calculation of the ES for the blue pathway non-trivial. Yes, the most stable intermediate globally is the KRCO*. However, when considering the TS that occur before the KRCO* an accounting the very negative overall reaction energy (~ -1.2 eV), it is possible to find that the span for the blue pathway is between the KRCOOH* and the $KCO_2$*.

## 4.2 Reactivity and Onset

Figure 20: plots the ES for all of the reaction pathways.

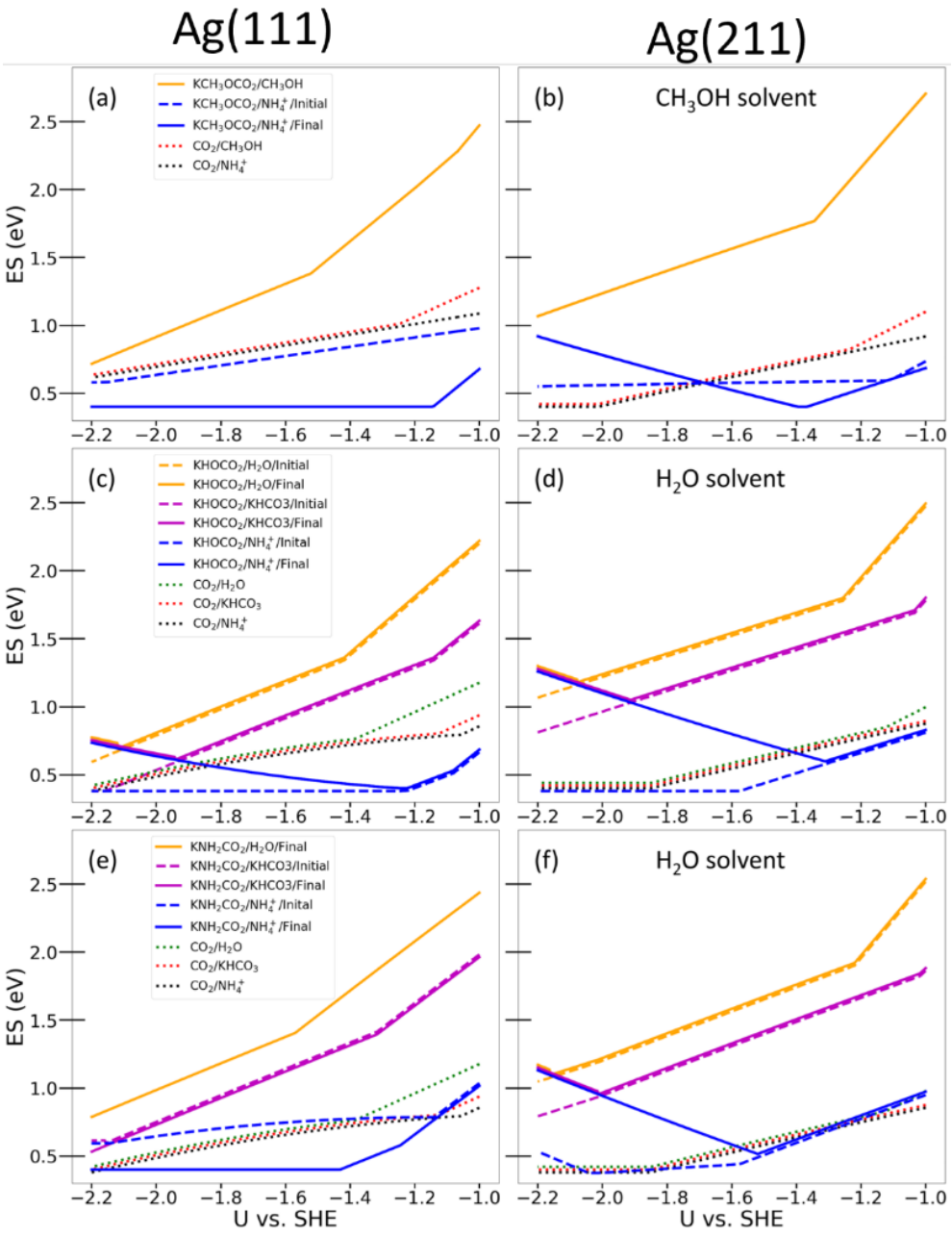


**Figure 20:** Energetic spans (ES) for all relevant systems. (a,b) is methanol c-$CO_2$RR in methanol solvent, (c,d) is $H_2O$ c-$CO_2$RR in $H_2O$ solvent, (e,f) is $NH_3$ c-$CO_2$RR in $H_2O$ solvent. (a,c,e) is on Ag(111) and (b,d,f) is on Ag(211).

From Figure 20 the $CH_3OH$, $H_2O$, and $KHCO_3$ proton sources lead to c-$CO_2$RR ES that are less than the $CO_2$RR ES. This is reasonable considering the same trend with the overall reaction energy occurred. However, it is observed that the $NH_4^+$ proton source leads to ES that are competitive or smaller than the $CO_2$RR, thus, showing that when $NH_4^+$ is used as the proton source c-$CO_2$RR could be conducted.

It is noted that for the $CH_3OH$ and the $NH_3$ capture agent on the (111) the final R-C cleavage is the most favorable pathway. However, typically the $H_2O$ capture agent and the (211) lead to the initial R-C cleavage as the most favorable pathway. The reason for this comes from the relative energy between the $KCO_2$* intermediate and the KRCOOH* intermediate. The KRCOOH* intermediate is methyl carbonic when $CH_3OH$ is the capture agent, carbonic acid when $H_2O$ is the capture agent, and carbamic acid when $NH_3$ is the capture agent. The $H_2O$ capture agent leads to a KRCOOH* intermediate of carbonic acid which is not stable because of its low $pK_a$,[4] as it wants to be deprotonated in its bicarbonate form. It is observed on the (111) that $CH_3OH$ and $NH_3$ capture agents have a KRCOOH* intermediate is more stable than the $KCO_2$*. However, for the $H_2O$ capture agent the $KCO_2$* intermediate is more stable. On the (211) the undercoordinated sites leads to stronger $CO_2$ adsorption. Thus, the $KCO_2$* intermediate is more stable than the KRCOOH intermediates. Therefore, the final R-C cleavage step is more favorable for the $CH_3OH$ and $NH_3$ capture agents on the (111) as the adsorbed $CO_2$* is unstable enough that the final R-C cleavage pathways has a smaller ES. However, once the $KCO_2$* is stabilized relative to the KRCOOH*, the initial R-C cleavage pathway dominates.

To truly compare the capture agents, it is necessary to consider the same proton source. $NH_4ClO_4$ is soluble in both $H_2O$ and $CH_3OH$. Therefore, it is used for comparison. From Figure 20 it can observed that the ES of the $CH_3OH$-captured $CO_2$ and the $NH_3$-captured $CO_2$ are similar

and lower than that of the $H_2O$ captured $CO_2$. Thus, it is determined that $CH_3OH$ capture agent is reasonable competitor to amine-based capture agents, provided that the proton source is similar.

To test the validity of 0.4 eV barrier we tested the effects of changing the barrier to 0.1 eV and 1.0 eV and plotted the ES in Figure 21.

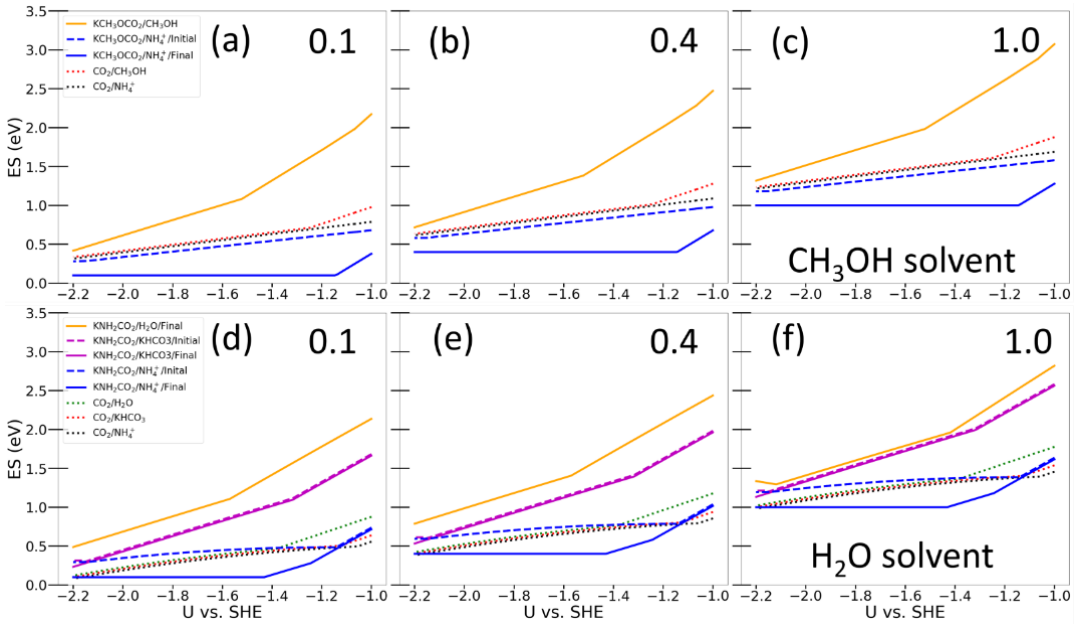


**Figure 21:** Testing the ES as a function of added barrier over the reaction energy. If a reaction energy as exergonic a flat barrier of (a,b) 0.1, (c,d) 0.4, (e,f) 1.0 eV is applied. (a-c) is methanol c-$CO_2$RR in methanol solvent on Ag(111) and (d-f) is $NH_3$ c-$CO_2$RR in $H_2O$ solvent on Ag(111).

From Figure 21 it is noted that the different barriers lead to the identical trend between the reaction systems but leads to different onset potentials. However, as the ES trend is identical the trend between the onset potentials between the reactions systems will be the same between all of the barriers. Therefore, absolute value of the onset potential may not be perfectly accurate by assuming all of the barriers are 0.4 eV, but as the trend will be the same for a wide range of potentials then it is assumed that choosing an 0.4 eV barrier is a reasonable method.

Importantly, it was necessary to consider the onset potentials of the different competing reactions to determined what reaction would be observed experimentally and if some CO was

being produced was it being produced from the $CO_2RR$ or the c-$CO_2RR$. It can be calculated that an energetic barrier of 0.75eV leads to a TOF of 1 $s^{-1}$ Therefore, the onset potential was determined as the potential necessary to make the ES equal to 0.75.

Figure 22 shows that onset and overpotential table of all reactions on the (111) terrace, and Figure 23 shows the onset potential and overpotential table of all reactions on the (211) facet.

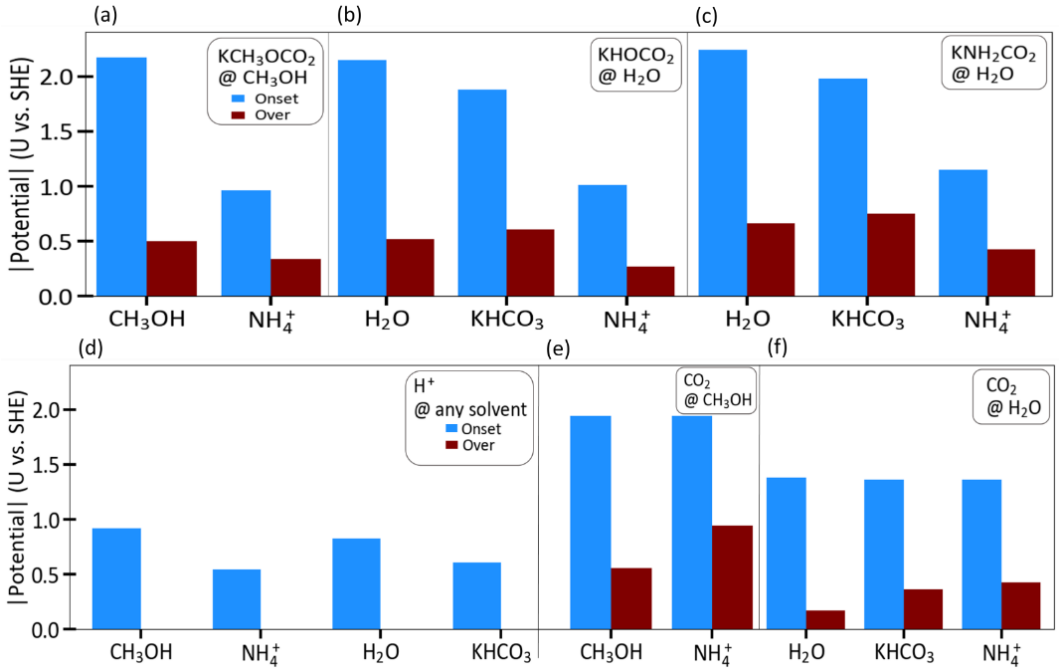


**Figure 22:** Onset (blue) and over (brown) potentials for the (a) methanol c-$CO_2RR$ in methanol, (b) $H_2O$ capture c-$CO_2RR$ in $H_2O$, (c) $NH_3$ capture c-$CO_2RR$ in $H_2O$, (d) HER, (e) $CO_2RR$ in methanol, and (f) $CO_2RR$ in $H_2O$ on Ag(111). Relevant proton sources are shown on the x-axis. The compound being reduced, and the relevant solvent are given in the right-hand corner with the notation compound @ solvent.

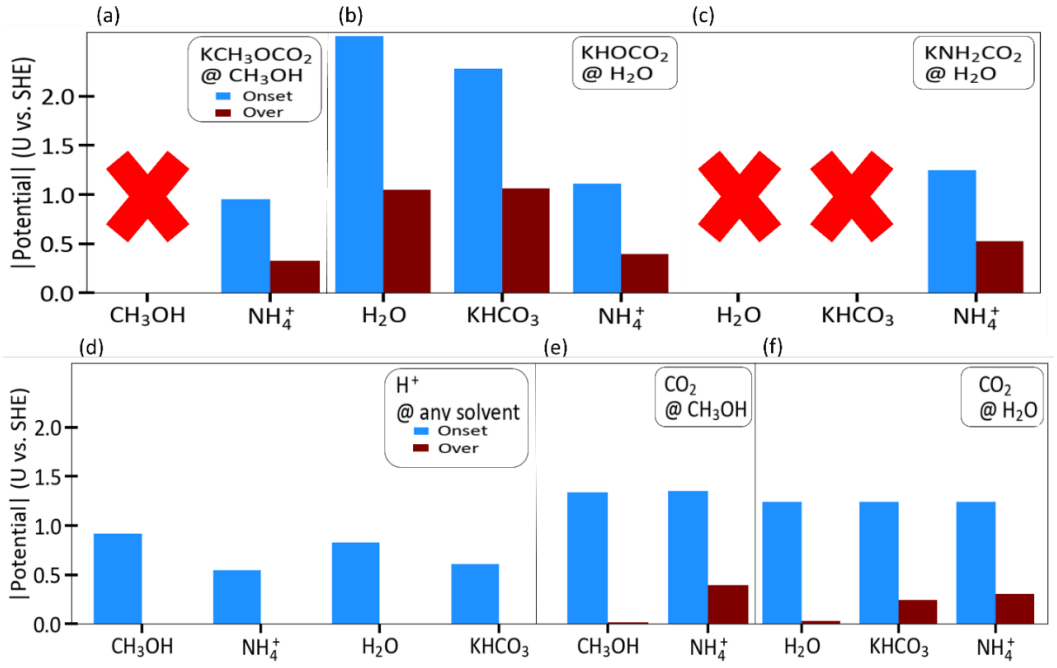


**Figure 23:** Onset (blue) and over (brown) potentials for the (a) methanol c-$CO_2$RR in methanol, (b) $H_2O$ capture c-$CO_2$RR in $H_2O$, (c) $NH_3$ capture c-$CO_2$RR in $H_2O$, (d) HER, (e) $CO_2$RR in methanol, and (f) $CO_2$RR in $H_2O$ on Ag(211). A red X means that the onset potential is never achieved. Relevant proton sources are shown on the x-axis. The compound being reduced, and the relevant solvent are given in the right-hand corner with the notation compound @ solvent.

From Figures 22 and 23 it is clear that the HER would dominate in these conditions, as the onset potential of the HER is much more negative than of the $CO_2$RR or the c-$CO_2$RR. Thus, we predict that experimentally, the F.E. of $H_2$ would be much larger than the F.E. for CO. However, because of the different proton source's $pK_a$ the onset potential of the HER is shifted, with $NH_4^+$ having the least negative onset potential, and $CH_3OH$ having the most negative onset potential. Thus, it is possible to suppress the HER intrinsically, by choosing a proton source with a larger $pK_a$. As Figure 20 showed this will also increase the ES of the $CO_2$RR and the c-$CO_2$RR. However, as shown from Figures 20 it is possible to use the proton source to change the activity of the chemical step from the ionization potentials of the cations being exchanged during the protonation.

Therefore, further optimization is possible to find proton sources with higher $pK_a$ values but has a chemical nature that provides a more thermodynamically favorable chemical step.

Interestingly, the onset potential of the $CO_2RR$ was only dependent on the solvent and not the proton source. This is because the ES span for the $CO_2RR$ is defined by the adsorption of $CO_2$. As this step is not a PCET the proton source plays no dependence on the onset potential. It is interesting to note that the adsorption of $CO_2$ is less favorable in methanol solvent over water. This trend is present on the (111) and the (211), but on the (211) the difference in onset potential between the solvents is much smaller than on the (111). This because of the undercoordinated sites on the (211) stabilizing the $CO_2$ adsorption. Even though the methanol solvent destabilize the $CO_2$ adsorption, the undercoordinated sites are able to assist in the $CO_2$ adsorption. However, it is to be noted that the $CO_2RR$ has a lower onset potential on the (211) facet than the (111) terrace. This has been shown in experiment,[71] so it gives further validation to our model.

When comparing Figures 22 and 23 the c-$CO_2RR$ is typically more favorable on the (111) surface as compared to the (211). This is interesting as the $CO_2RR$ has the opposite trend. Thus, this is important as trends that existed for the $CO_2RR$ may no longer be valid for the c-$CO_2RR$. Although out of the scope of this work, further investigation must be made on these similarities and differences. However, what is clear is that the onset potentials for the c-$CO_2RR$ on the (111) are less negative than on the (211). As expected, as the $pK_a$ of the proton source decreases then the onset potential is made more negative regardless of the capture agent. However, on the (211) some of the c-$CO_2RR$ reactions using proton sources with higher $pK_a$s never achieve onset. This is because for these systems as the potential is made negative enough the adsorption of the $KRCO_2$ becomes endergonic. Thus, the span becomes defined by the adsorbed $KCO_2$* and the TS of the complex adsorption. As the reaction becomes more endergonic with potential, this TS grew larger

by our definition of how to approximate the TS. For the $NH_4^+$ proton source the proton source is strong enough that it can achieve onset at potentials less negative than the potential at which the adsorption becomes endergonic. However, for the other proton sources this onset potential would be too negative, and as such onset is never achieved. Interestingly the adsorption of $KHOCO_2$ never becomes endergonic on the (211). Thus, the process becomes completely exergonic which is assumed to have achieved onset.

From the (111) interestingly, the capture agent seems to have little effect on the onset potential, but the proton source seems to have the greater effect. From Figure 20, the mechanism with which the c-$CO_2$RR is conducted is different for the $H_2O$ capture agent as compared to the $CH_3OH$ and the $NH_3$. However, all pathways can become completely exergonic by moderate potentials when $NH_4^+$ is used as the proton source. Therefore, for optimization purposes this shows that the capture agent seems to have a minor effect on the reactivity and can be selected depending on the necessary catalyst and solvent constraints. However, the only reasonable c-$CO_2$RR onset potentials were found by using the $NH_4^+$ proton source, which lead to the HER dominating. Therefore, this shows that there is interest to explore further proton sources.

The calculations also help to predict the source of any CO. All proton sources except for $NH_4^+$ the $CO_2$RR has a less negative onset potential and less negative ES for most of the range of potentials tested, regardless of c-$CO_2$RR capture agent. Thus, in the case of reaction systems where these proton sources are the strongest proton donors, it is predicted that the majority of CO produced will be from the $CO_2$RR. Additionally, most of the CO produced will be from the step and kink sites as the onset potential for the $CO_2$RR is less negative on the (211). When the potential is made negative enough then it may be possible that (111) terrace could be used for $CO_2$RR and if the potentials are made even more negative, then the c-$CO_2$RR could be conducted. However,

for the case of the c-$CO_2$RR is conducted in the presence of $NH_4^+$ then the onset potential and ES for c-$CO_2$RR is less negative than the $CO_2$RR. Thus, it is likely that the majority of CO would be produced from the c-$CO_2$RR. It is to be noted that the onset potential and ES for the $CO_2$RR using $NH_4^+$ as a proton source is close to the onset potential and ES for the c-$CO_2$RR on both the facets, but especially close on the (211) facet. Thus, likely the CO produced will be a mixture of c-$CO_2$RR and $CO_2$RR.

However, unfortunately experimentally what will likely be observed is a complete dominance by the HER, as the onset potentials for the HER as significantly less negative than that of the $CO_2$RR and c-$CO_2$RR. The F.E. of $H_2$ will likely get larger as the proton source is made less negative as the HER is able to achieve onset at even less negative potentials. Thus, although this work proves that there is a chance for c-$CO_2$RR to produce CO and that there are number of c-$CO_2$RR parameters to optimize that are different than the parameters needed to optimize the $CO_2$RR, the ultimate winner on Ag catalyst is the HER. However, this means that further work needs to be done on optimizing the catalyst, proton source, and reaction conditions.

# Chapter 5: Conclusions

In this work VASP and VASPSol were used to elucidate the effect of capture agent and proton sources on the c-$CO_2$RR when Ag is used as the catalyst. Ag was chosen because of its large binding energy of H. The first goal of this work was to elucidate the reaction mechanism when the c-$CO_2$RR produces CO. As there are 3 required protonations and only 2 electrons per cycle it was necessary to figure out the most thermodynamically stable reaction to do thermally. Overall, it was determined that only 2 pathways were necessary to fully describe the c-$CO_2$RR reaction network. Both did the final protonation chemically, but the difference was if the first

protonation was used to cleavage the $CO_2$ from the capture agent (initial R-C cleavage) or if this cleavage was done from the final protonation (final R-C cleavage). Thus, work was done on elucidating which pathways were the most thermodynamically stable depending on the capture agent used and catalyst facet. For some capture agent, proton source, catalyst fact combinations the initial R-C cleavage and the final R-C cleavage had an identical ES. This was typically the case for proton sources with higher $pK_a$ as the chemical step was highly endergonic. As the product of this chemical step, CO*, was shared by both pathways then the ES was the same for both pathways. However, for case when differences in the pathways existed, the $CH_3OH$ and $NH_3$ capture agents on Ag(111) it was determined that typically, the final R-C cleavage was the most favorable pathway, but the $H_2O$ capture agent on Ag(111) and all of the processes on the (211) typically the initial R-C cleavage was the most favorable.

Overall, it was determined that the capture agent had little effect on the onset potential and ES, but the proton source was more important. Thus, this provides 2 interesting optimization challenges: the proton source and the relationship between capture agent and catalyst.

It was shown that when the proton source was taken as $NH_4^+$ then the c-$CO_2$RR had a reasonable competition with the $CO_2$RR. Unfortunately, it was determined that the onset potentials required for the c-$CO_2$RR and the $CO_2$RR were negative enough that the HER was spontaneous throughout the whole process. Therefore, on Ag it is predicted that the HER will dominate, and little CO will be produced. However, this work provides a proof of concept that the c-$CO_2$RR has much potential to be optimized.

# Appendix

```
calc=Vasp(
gga='PE',
ivdw=11,
lsol=True,
tau=0.0,
lambda_d_k=1.382,
eb_k=32.42,
#nelect = 572,
lreal='Auto',
nsw = 500,
algo = 'Fast',
isym=2,
prec='Accurate',
ismear=2,
sigma=0.2,
nelmin=6,
npar=4,
encut=400,
ediff=1e-6,
ediffg=-0.02,
kpts=[4,4,1],
gamma=True,
ibrion = 2,
potim = 0.5,
ispin = 1,
nelm = 300,
lrhoion = False,
lrhob = False,
lcharg = False,
lwave = False,
setups={'base': 'recommended'}
```

**Figure A1:** Example ASE script to be interfaced with VASP to automatically generate the INCAR, KPOINTS, and POTCAR.

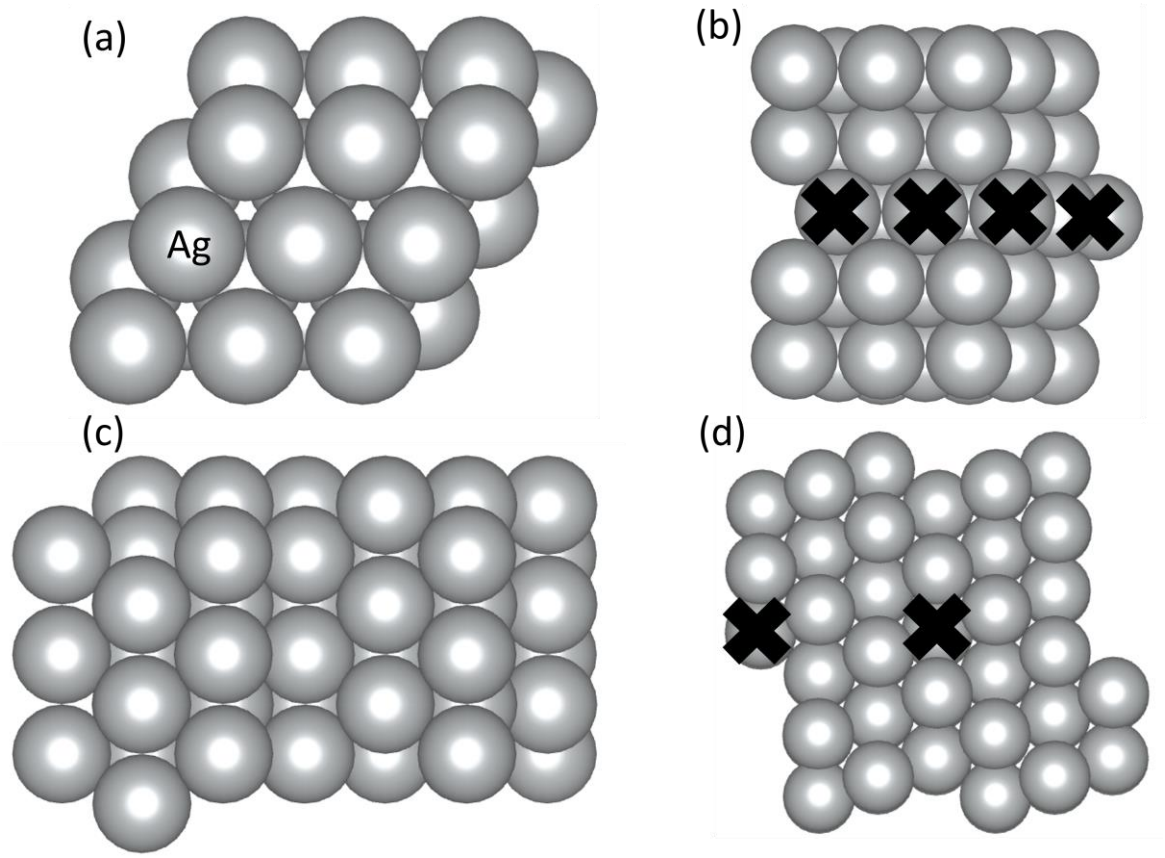


**Figure A2: Bare slab configurations** (a,b) are the Ag(111) and (c,d) are the Ag(211). A black X refers to a constrained atom in optimization. The most stable configuration is shown. This is configurations with the notation * in Figure 6. All Ag(111) slabs had the same number of atoms and cell parameters as in (a,b) and all Ag(211) slabs had the same number of atoms and cell parameters as in (c,d).

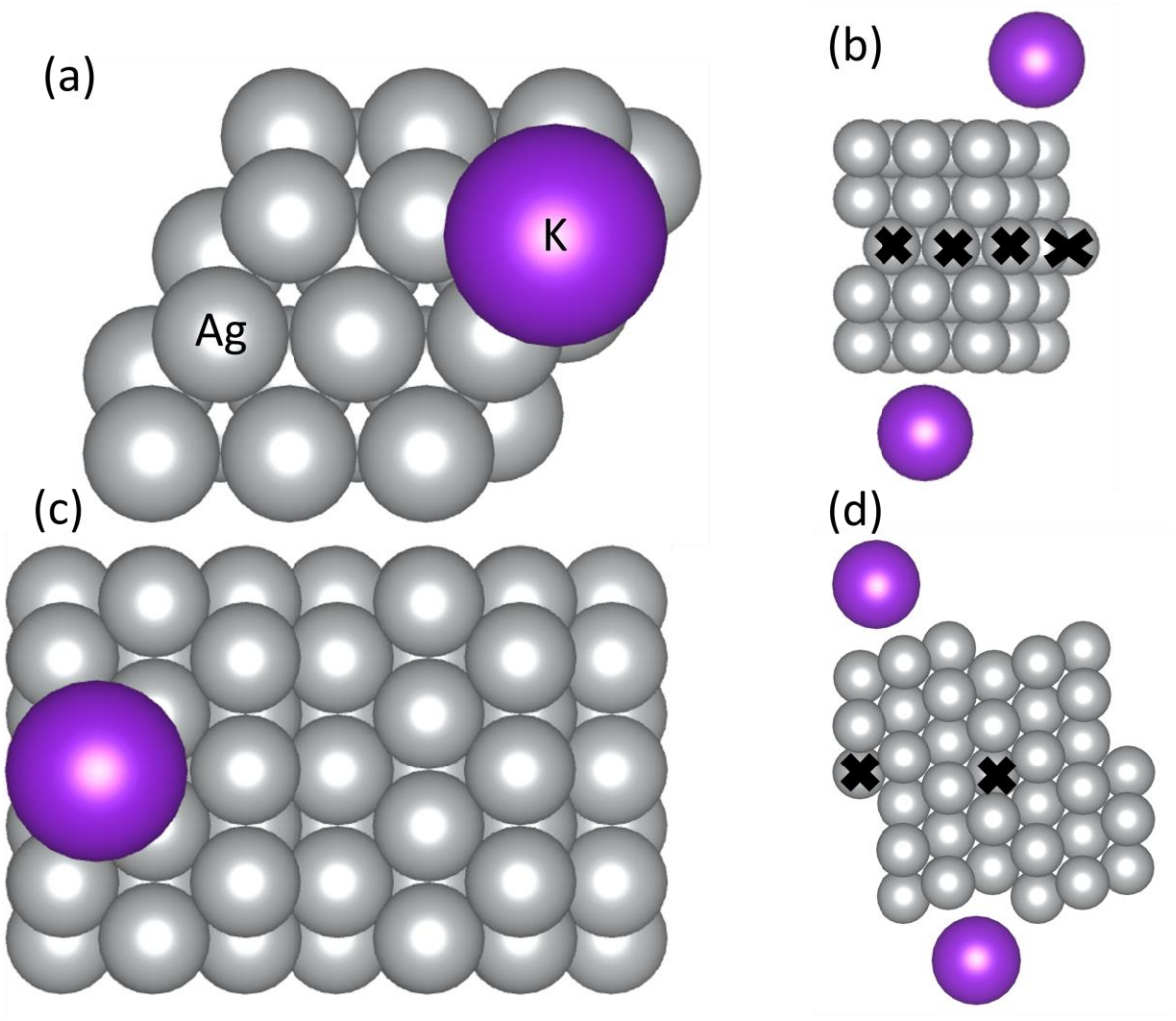


**Figure A3: $K^+$ adsorbed on slab configurations** (a,b) are the Ag(111) and (c,d) are the Ag(211). A black X refers to a constrained atom in optimization. The most stable configuration is shown. This is configurations with the notation K* in Figure 6. All Ag(111) slabs had the same number of atoms and cell parameters as in (a,b) and all Ag(211) slabs had the same number of atoms and cell parameters as in (c,d). All slabs were symmetrized in this same manner.

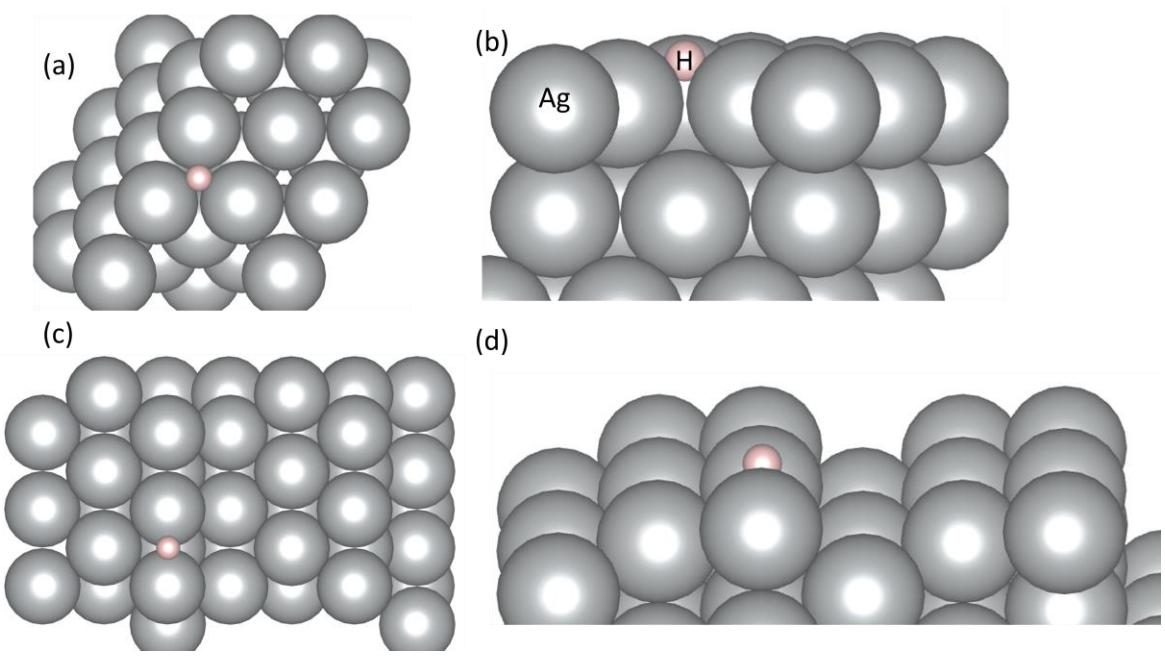


**Figure A4: H adsorbed configurations** (a,b) are the Ag(111) and (c,d) are the Ag(211). The most stable configuration is shown. This is configurations with the notation H* in Figure 6.

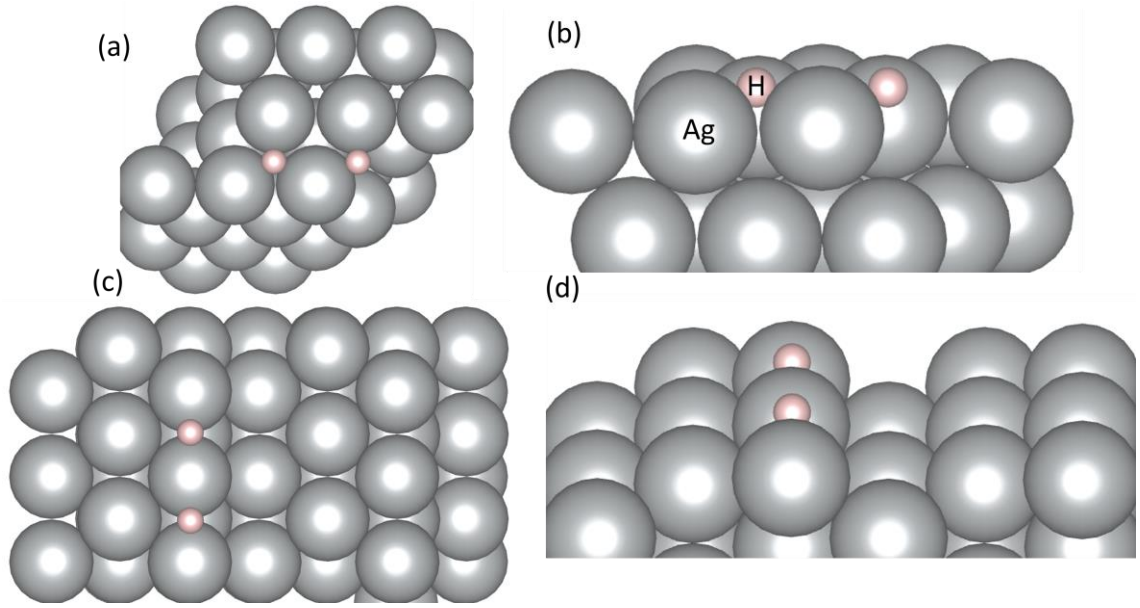


**Figure A5: 2H adsorbed configurations** (a,b) are the Ag(111) and (c,d) are the Ag(211). The most stable configuration is shown. This is configurations with the notation H* + H* in Figure 6.

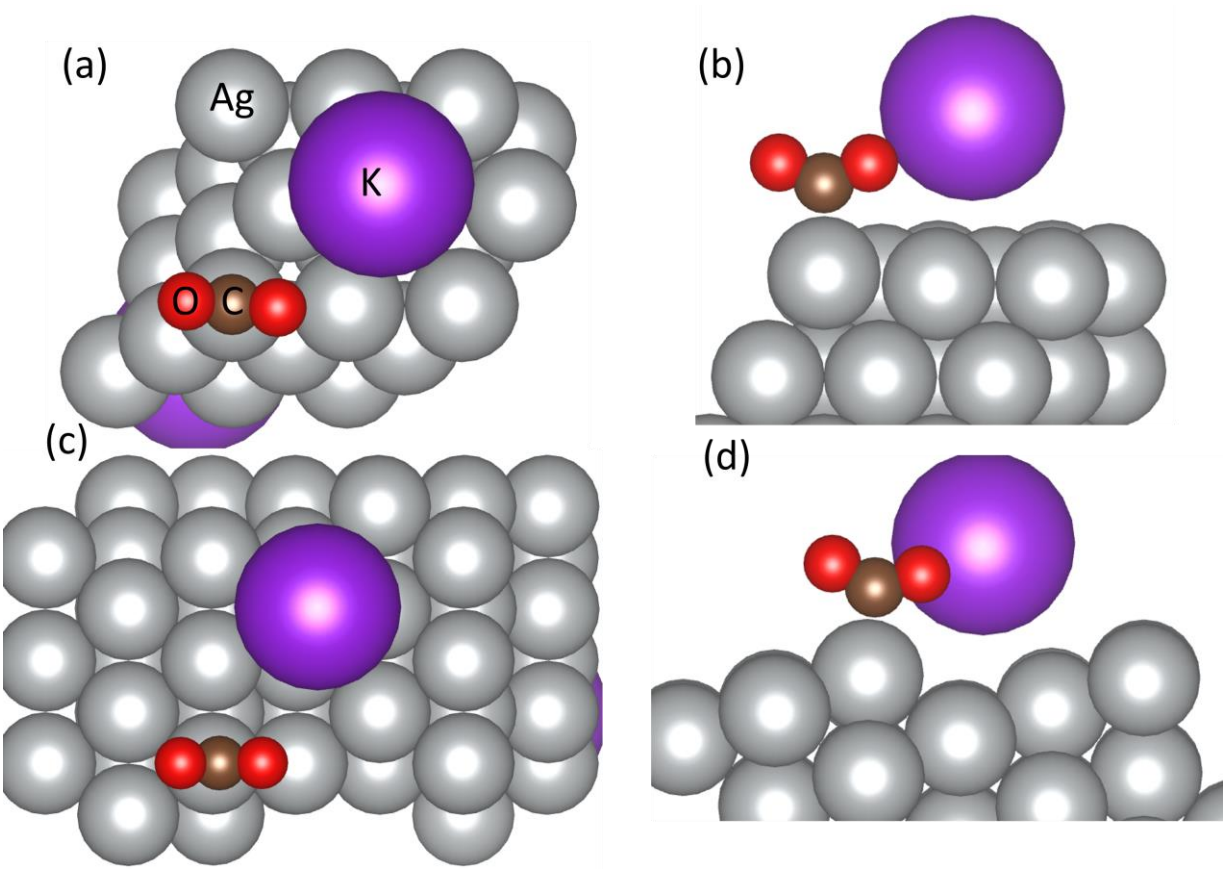


**Figure A6: $K^+ + CO_2$* adsorbed configurations** (a,b) are the Ag(111) and (c,d) are the Ag(211). The most stable configuration is shown. This is the configuration with the notation $KCO_2$* in Figures 6 and 12.

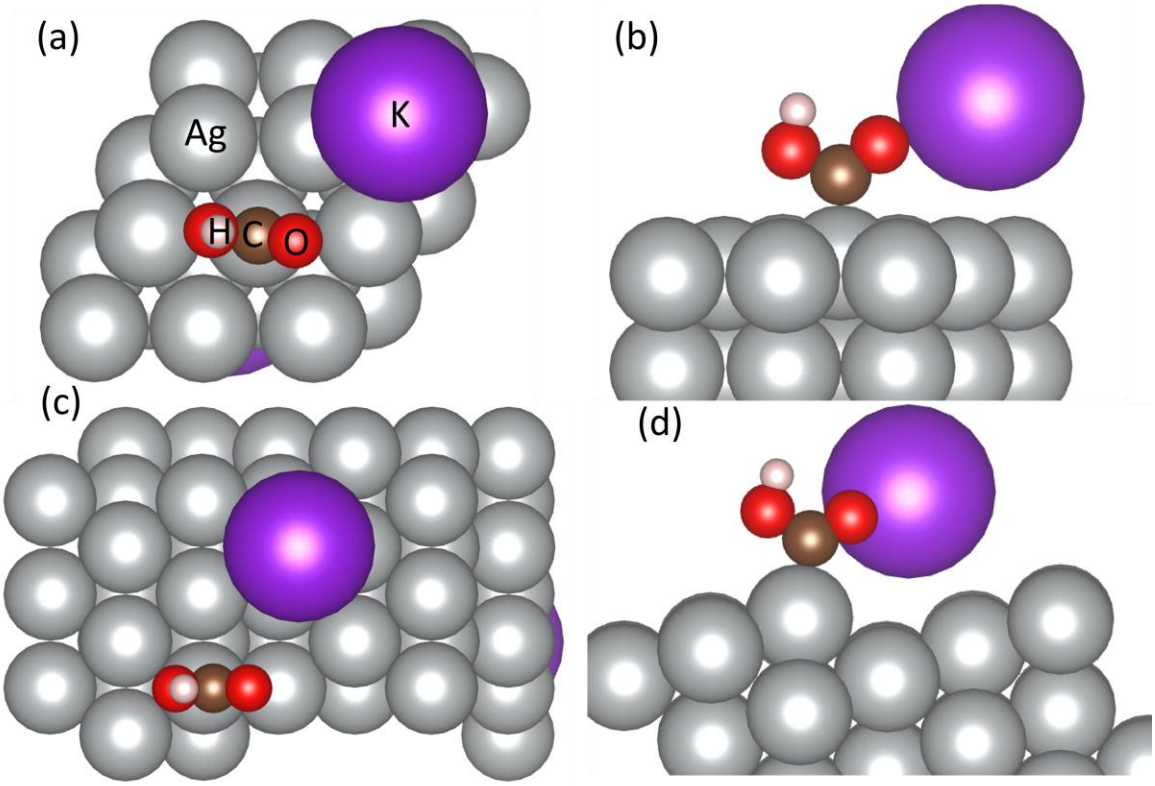


**Figure A7: $K^+$ + COOH* adsorbed configurations** (a,b) are the Ag(111) and (c,d) are the Ag(211). The most stable configuration is shown. This is the configuration with the notation KCOOH* in Figures 6 and 12.

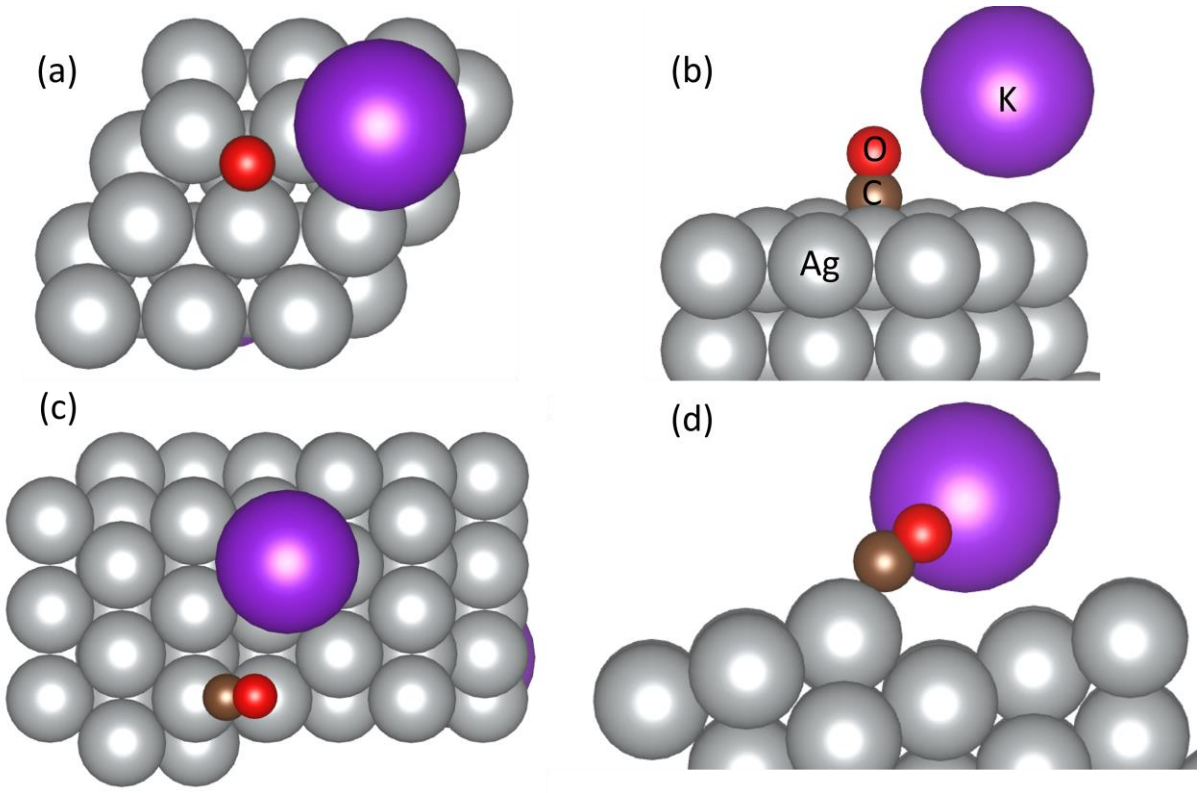


**Figure A8: $K^+$ + CO* adsorbed configurations** (a,b) are the Ag(111) and (c,d) are the Ag(211). The most stable configuration is shown. This is the configuration with the notation KCO* in Figures 6 and 12.

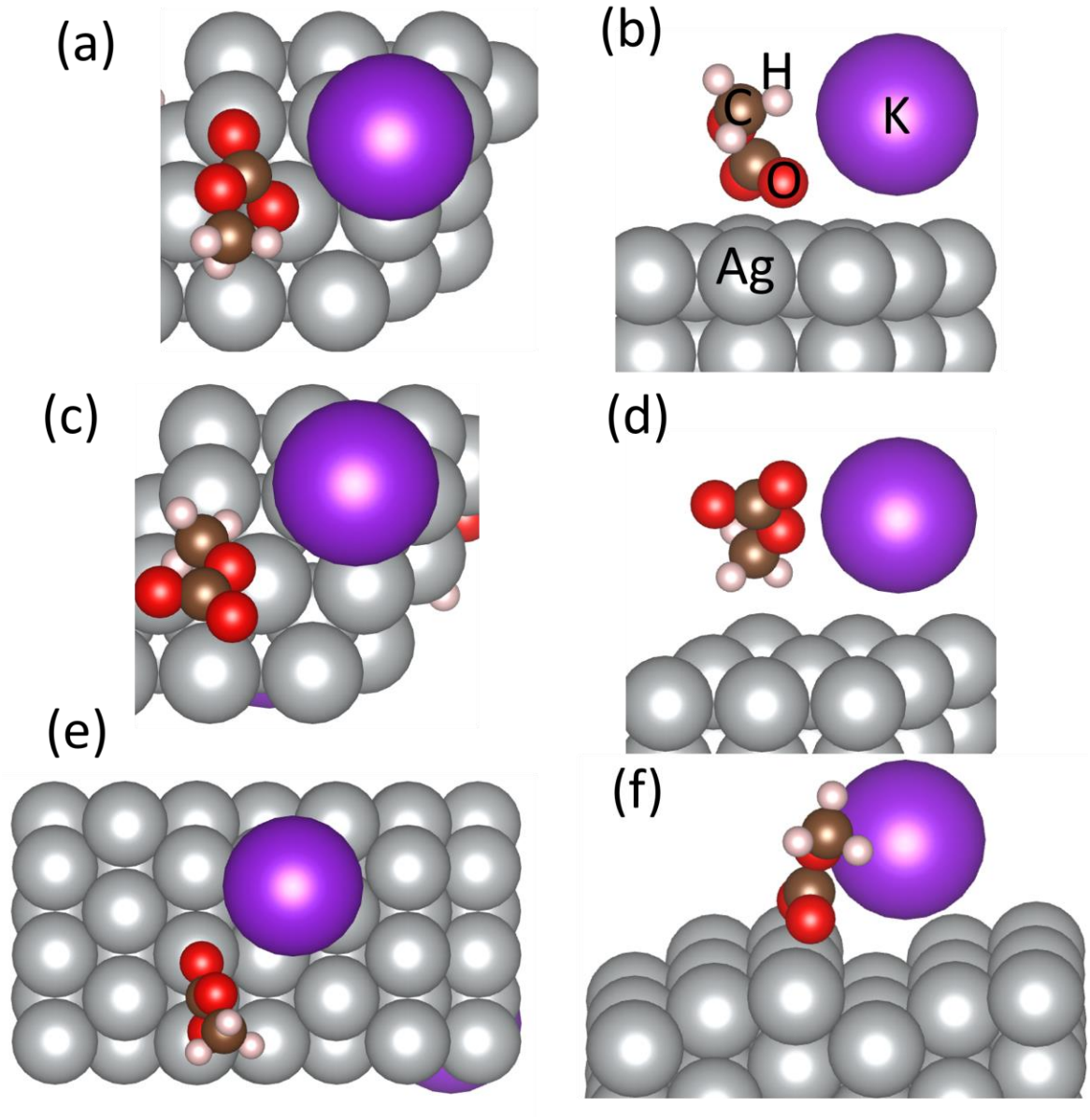


**Figure A9: $K^+RCO_2^-$* adsorbed configurations with $CH_3OH$ capture agent** (a-d) are the Ag(111) and (e,f) are the Ag(211). The most stable configuration is shown. (a,b) is the most stable configuration for potential less negative than -1.06 V vs. SHE, and (c,d) is the most stable configuration for potentials more negative than -1.06 V vs. SHE. This is the configuration with the notation $KCO_2$* for the $CH_3OH$ in Figure 6.

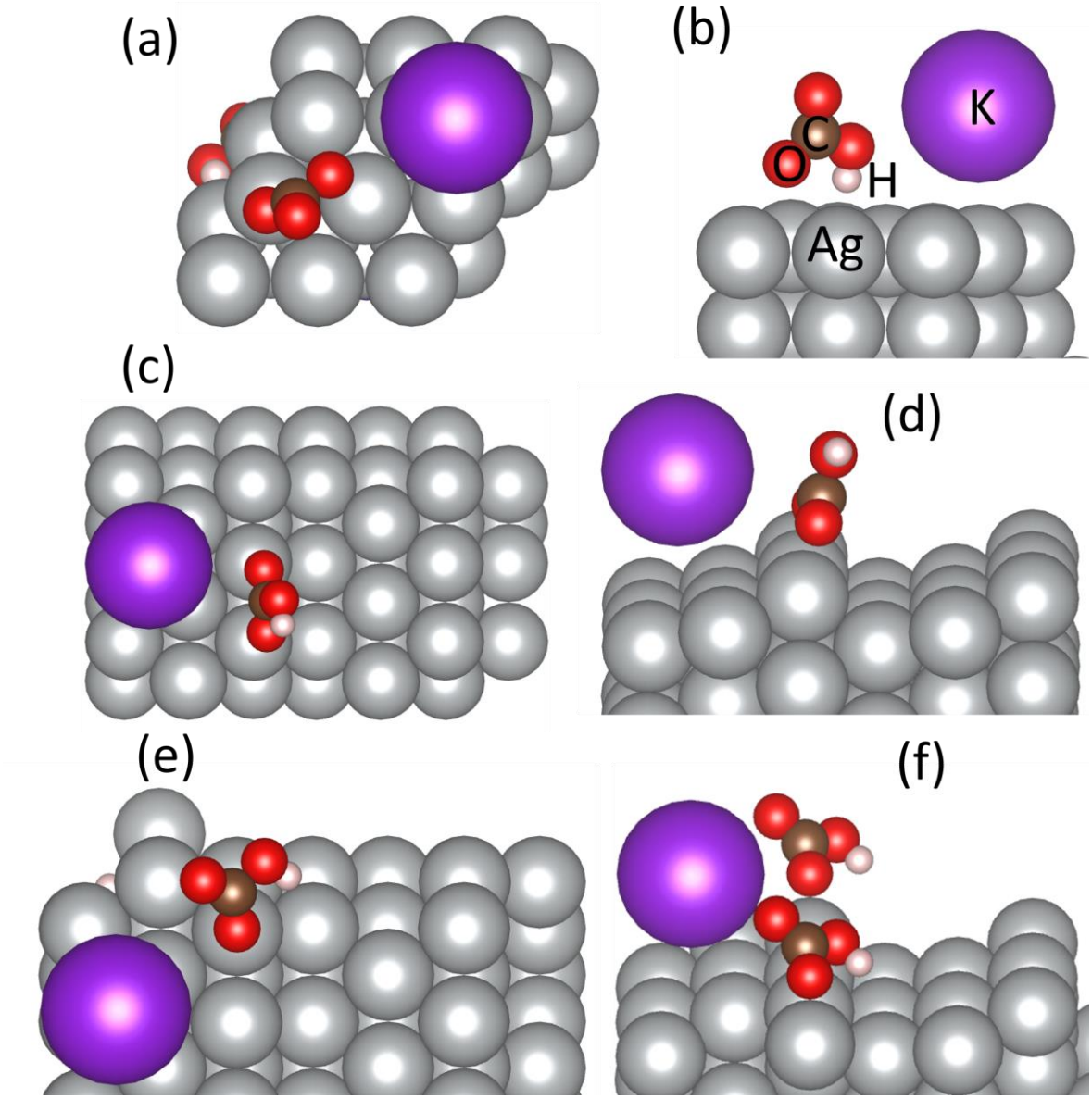


**Figure A10: $K^+RCO_2^-$* adsorbed configurations with $H_2O$ capture agent** (a,b) are the Ag(111) and (c-f) are the Ag(211). The most stable configuration is shown. (c,d) is the most stable configuration for potential less negative than -1.33 V vs. SHE, and (e,f) is the most stable configuration for potentials more negative than -1.33 V vs. SHE. This is the configuration with the notation $KRCO_2$* for the $H_2O$ capture agent in Figure 6. The coverage is 1/9 ML on Ag(111) and 1/18 on Ag(211). If duplicate atoms appear they are in adjacent unit cells.

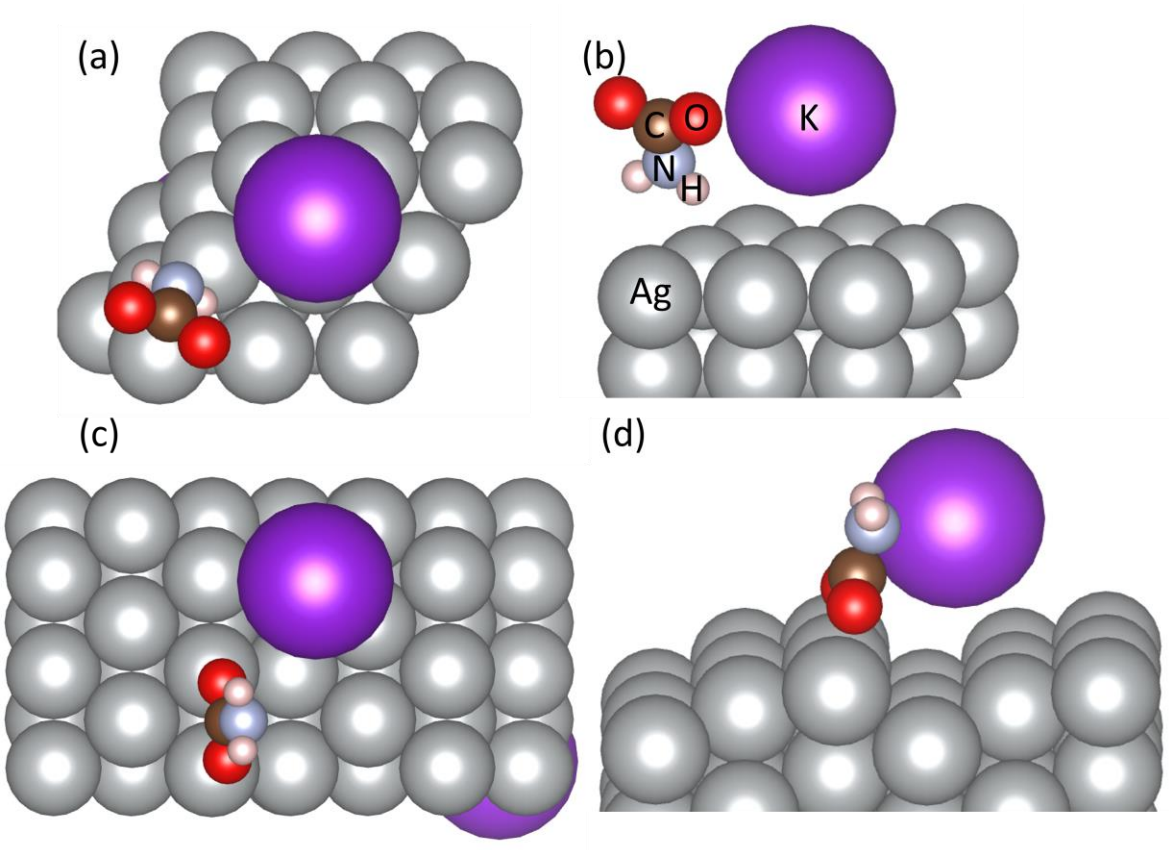


**Figure A11: $K^+RCO_2^-$* adsorbed configurations with $NH_3$ capture agent** (a,b) are the Ag(111) and (c,d) are the Ag(211). The most stable configuration is shown. This is the configuration with the notation $KRCO_2$* for the $NH_3$ capture agent in Figures 6 and 12.

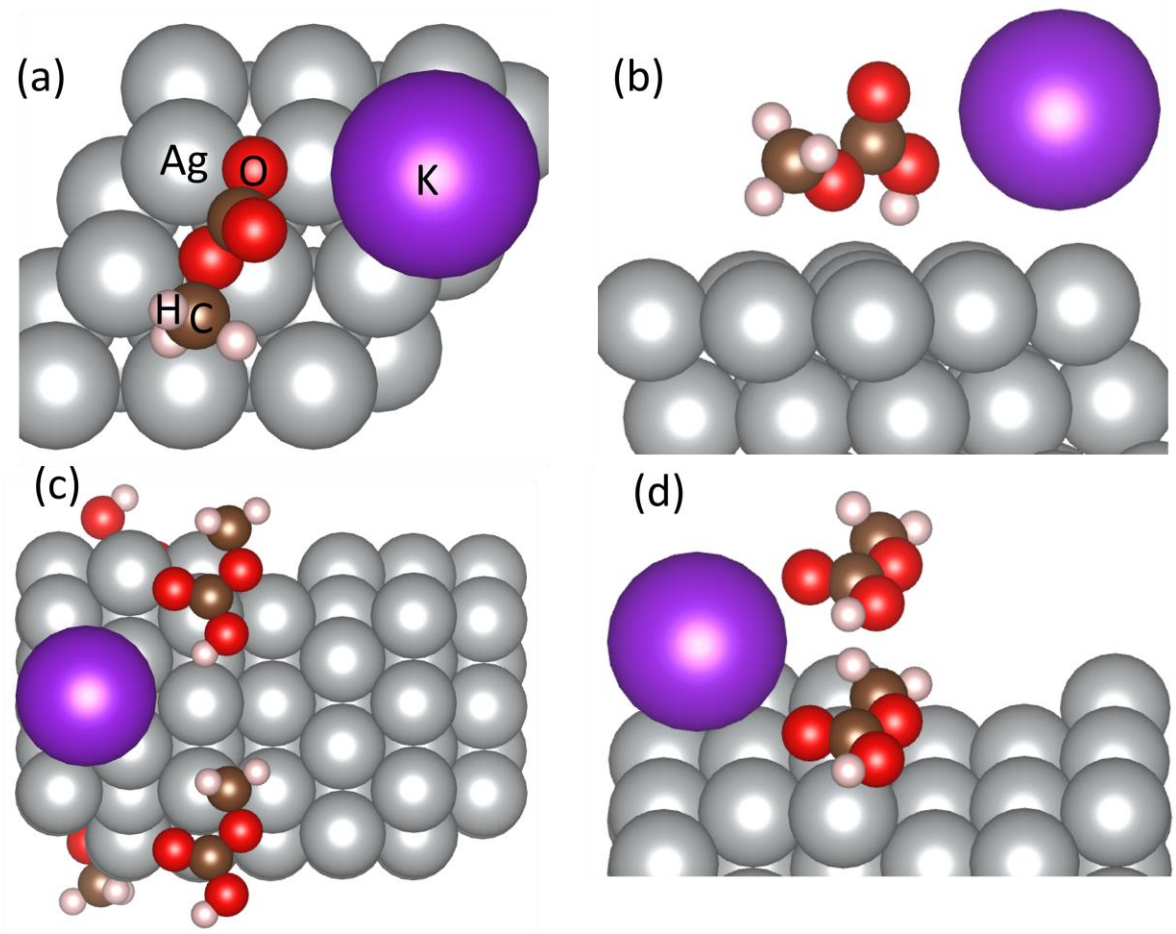


**Figure A12: $K^+$ + RCOOH* adsorbed configurations with $CH_3OH$ capture agent** (a,b) are the Ag(111) and (c,d) are the Ag(211). The most stable configuration is shown. This is the configuration with the notation KRCOOH* for the $CH_3OH$ capture agent in Figure 6. The coverage is 1/9 ML on Ag(111) and 1/18 on Ag(211). If duplicate atoms appear they are in adjacent unit cells.

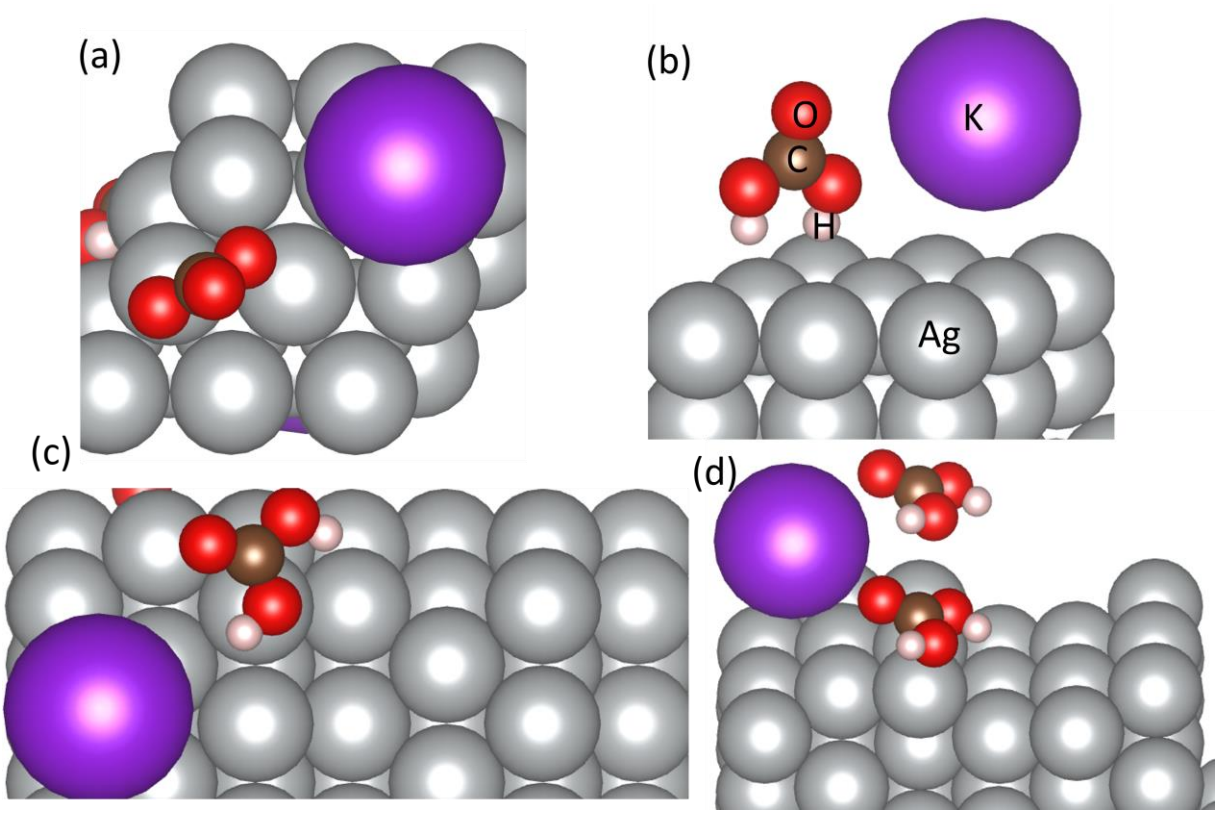


**Figure A13: $K^+$ + RCOOH* adsorbed configurations with $H_2O$ capture agent** (a,b) are the Ag(111) and (c,d) are the Ag(211). The most stable configuration is shown. This is the configuration with the notation KRCOOH* for the $H_2O$ capture agent in Figure 6. The coverage is 1/9 ML on Ag(111) and 1/18 on Ag(211). If duplicate atoms appear they are in adjacent unit cells.

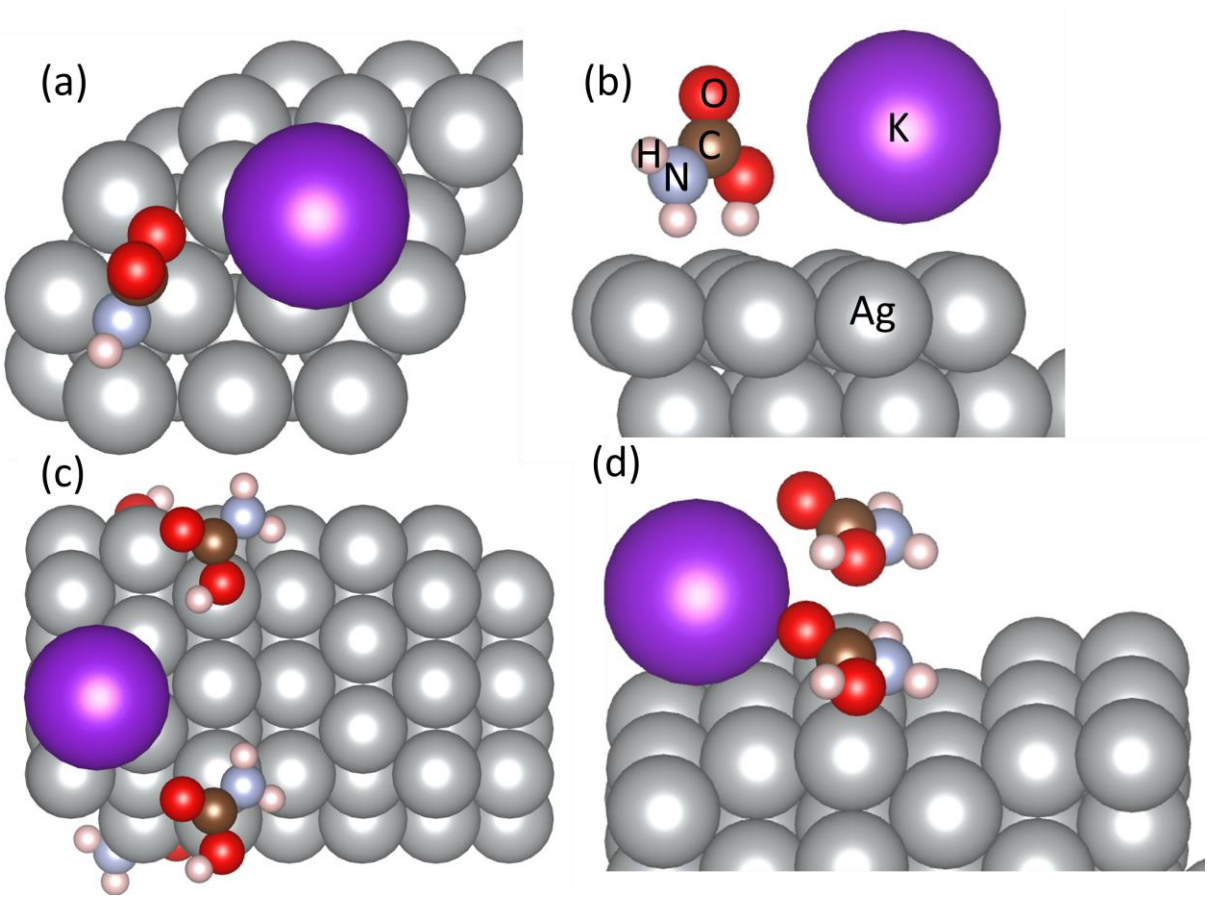


**Figure A14: $K^+$ + RCOOH* adsorbed configurations with $NH_3$ capture agent** (a,b) are the Ag(111) and (c,d) are the Ag(211). The most stable configuration is shown. This is the configuration with the notation KRCOOH* for the $NH_3$ capture agent in Figures 6 and 12. The coverage is 1/9 ML on Ag(111) and 1/18 on Ag(211). If duplicate atoms appear they are in adjacent unit cells.

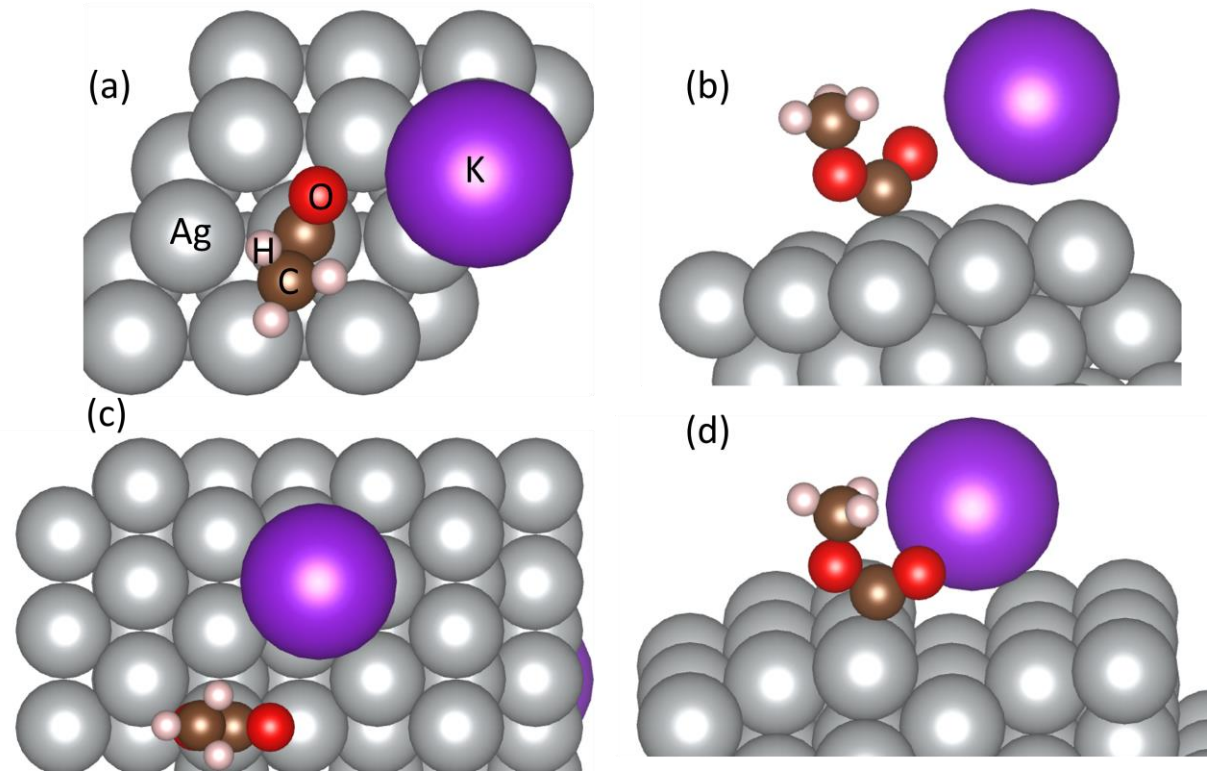


**Figure A15: $K^+$ + RCO* adsorbed configurations with $CH_3OH$ capture agent** (a,b) are the Ag(111) and (c,d) are the Ag(211). The most stable configuration is shown. This is the configuration with the notation KRCO* for the $CH_3OH$ capture agent in Figure 6.

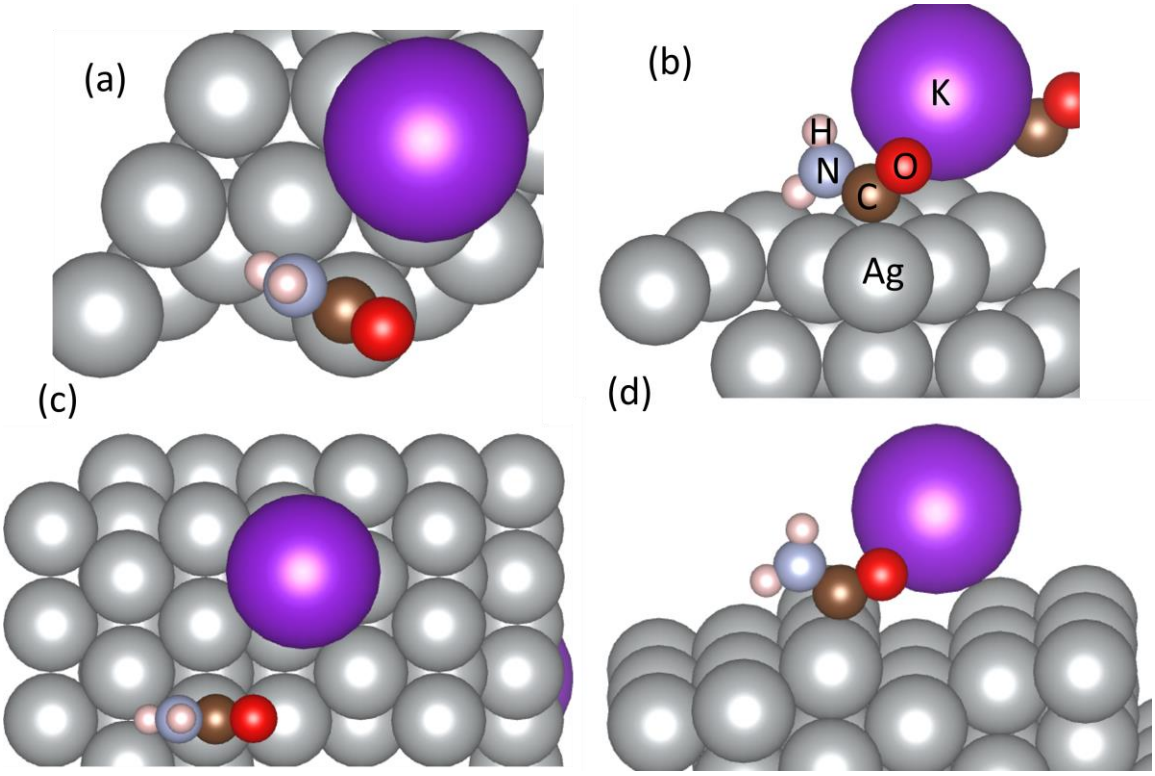


**Figure A16: $K^+$ + RCO* adsorbed configurations with $NH_3$ capture agent** (a,b) are the Ag(111) and (c,d) are the Ag(211). The most stable configuration is shown. This is the configuration with the notation KRCO* for the $NH_3$ capture agent in Figures 6 and 12.

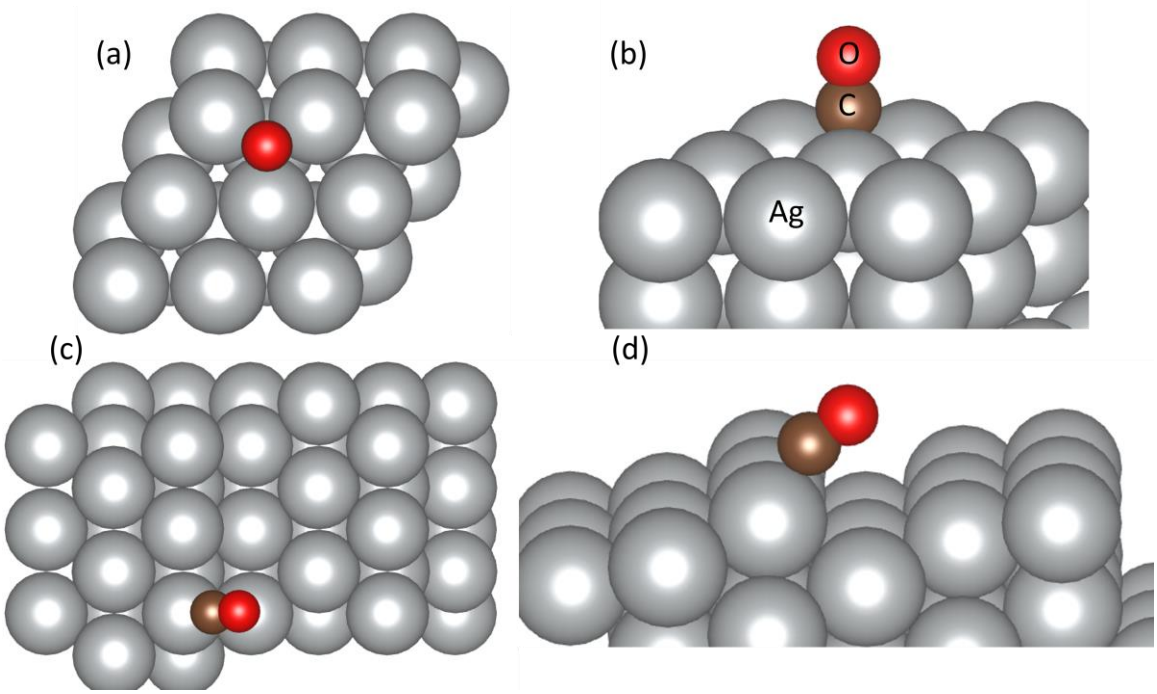


**Figure A17: CO* adsorbed configurations with $NH_3$ capture agent** (a,b) are the Ag(111) and (c,d) are the Ag(211). The most stable configuration is shown. This is the configuration with the notation CO* in Figures 6 and 12.

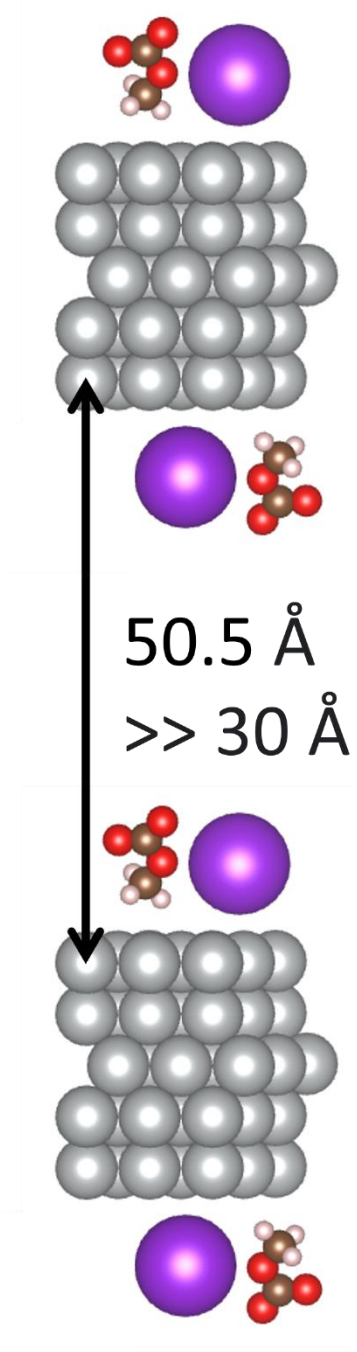


**Figure A18:** Schematic of two units adjacent with respect to the z axis. At least 30 Å of space is between the cells.

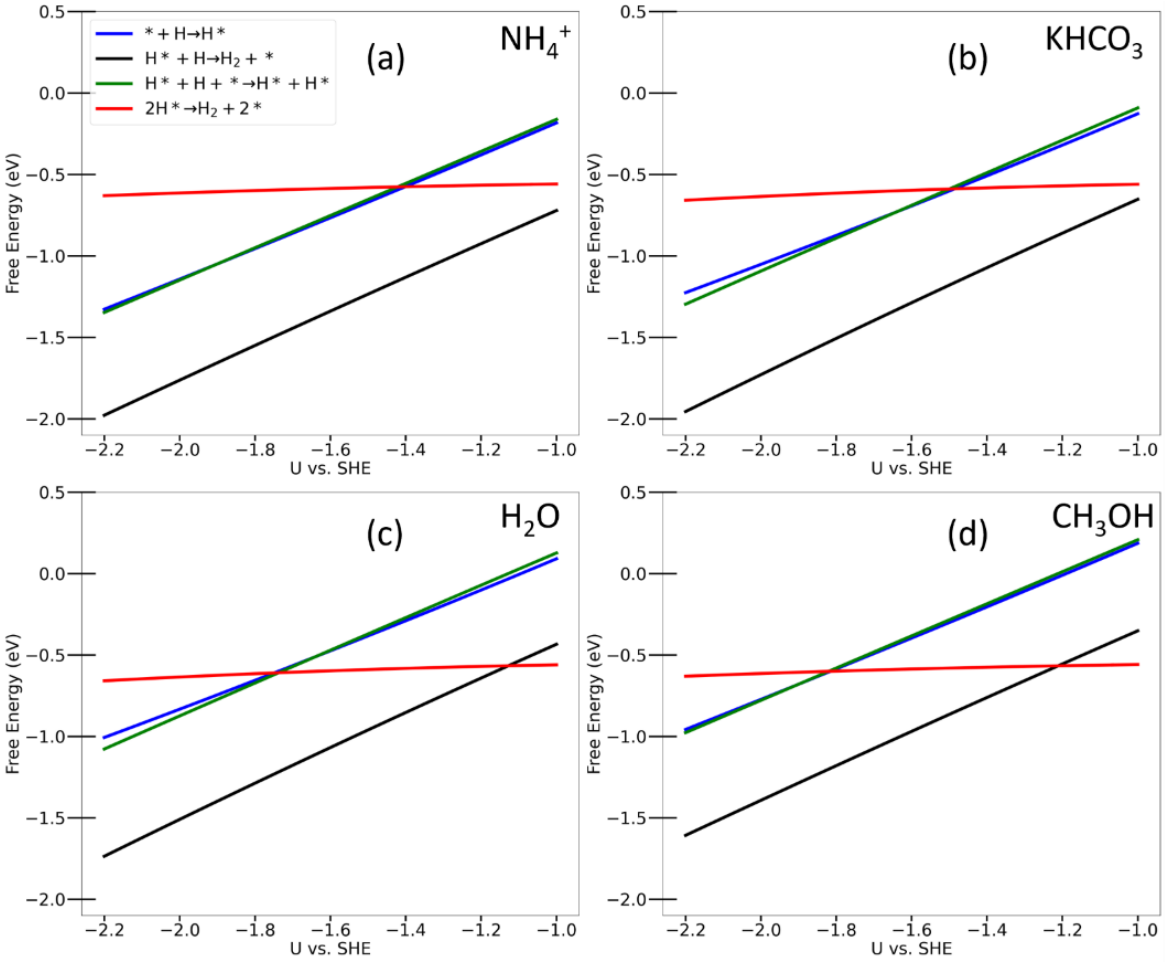


**Figure A19:** Elementary reaction energies for the HER on Ag(111). The proton source is listed in the top right corner of each panel. (a) $NH_4^+$, (b) $KHCO_3$, (c) $H_2O$, and (d) $CH_3OH$. The solvent does not affect the reaction energetics.

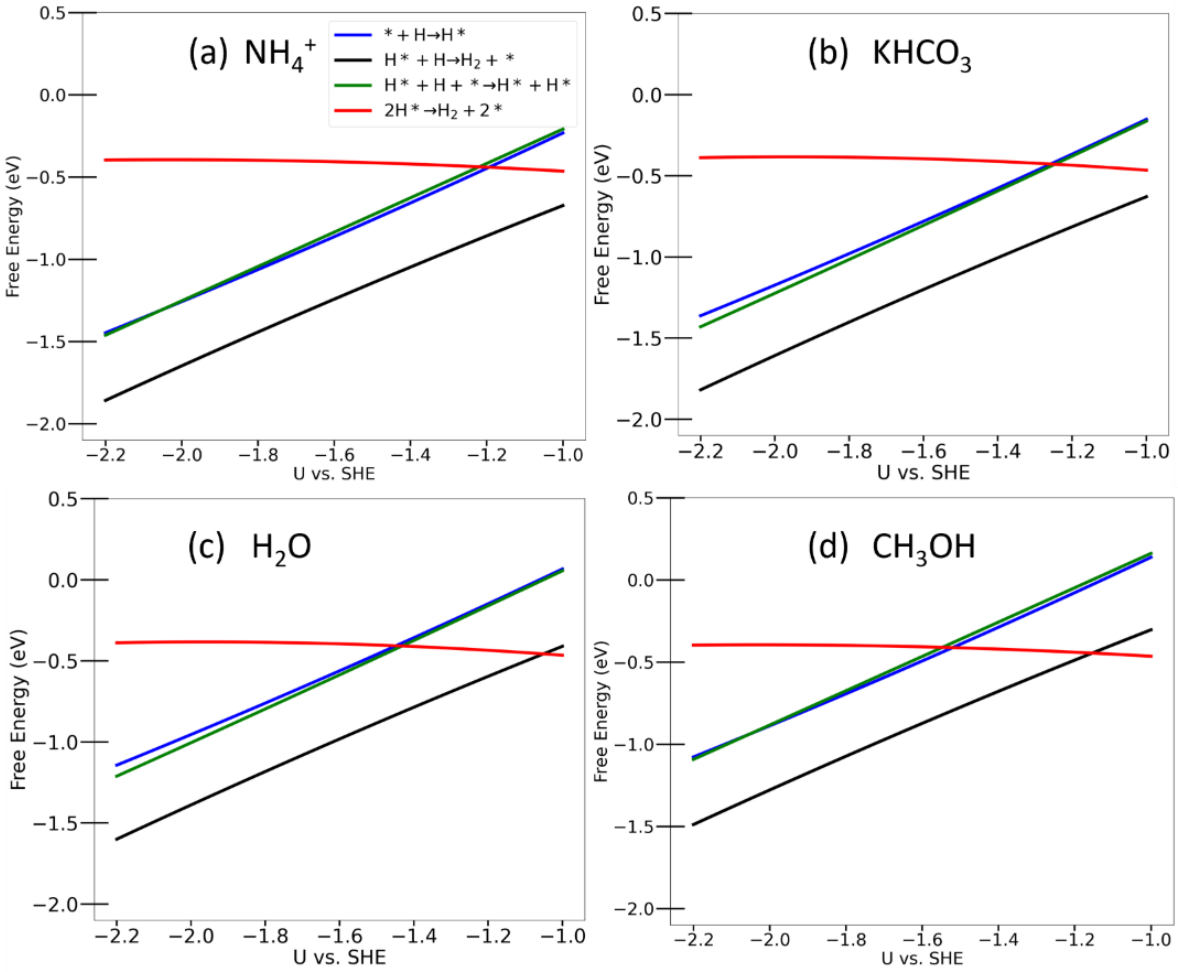


**Figure A20:** Elementary reaction energies for the HER on Ag(211). The proton source is listed in the top right corner of each panel. (a) $NH_4^+$, (b) $KHCO_3$, (c) $H_2O$, and (d) $CH_3OH$. The solvent does not affect the reaction energetics.

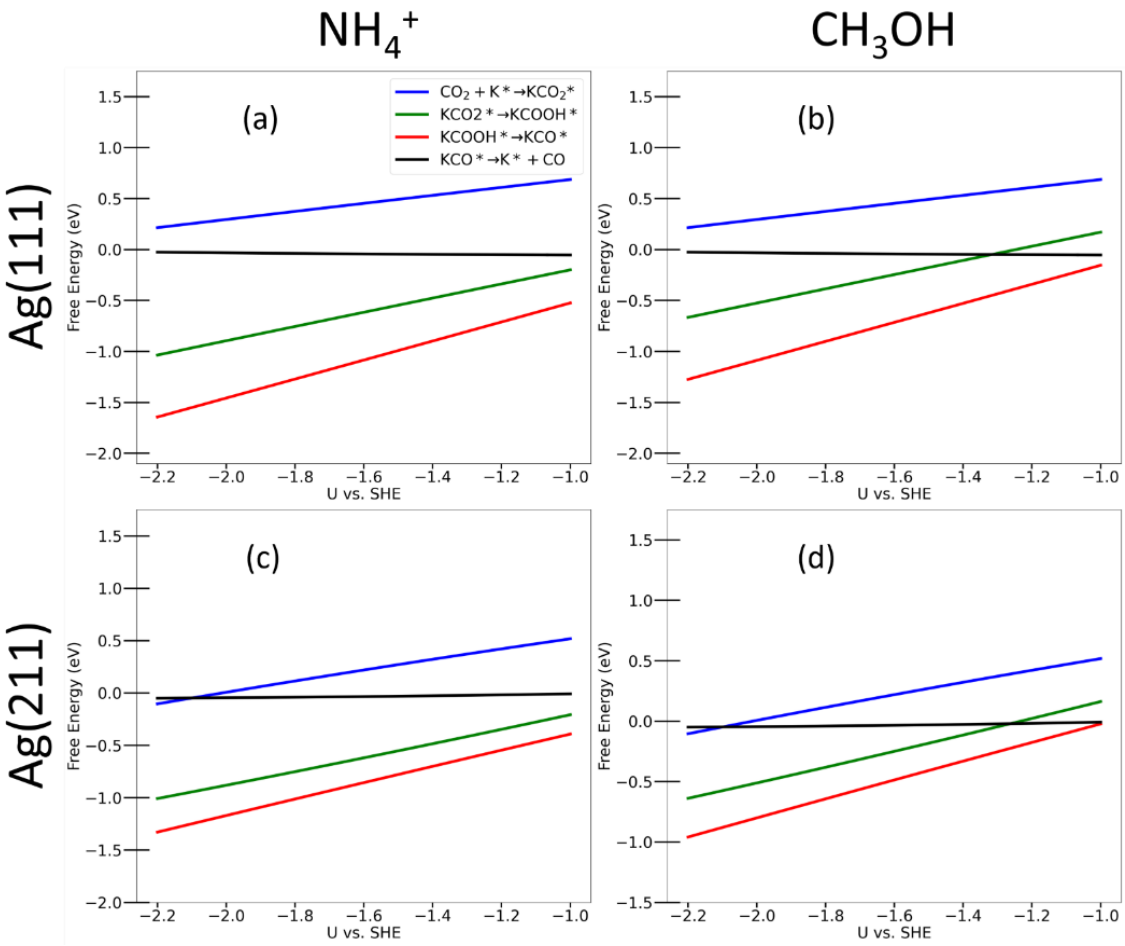


**Figure A21:** Elementary reaction energies for the $CO_2$RR in methanol solvent. (a,c) is using $NH_4^+$ proton source and (b,d) is using methanol proton source. (a,b) is on Ag(111) while (c,d) is on Ag(211).

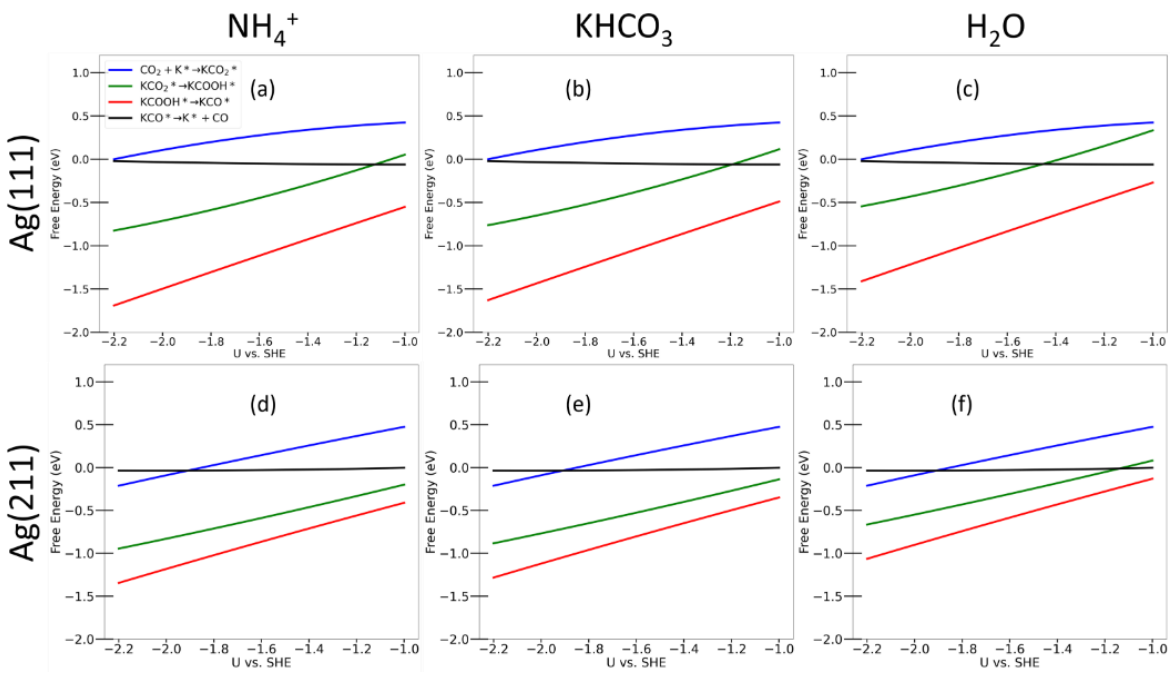


**Figure A22:** Elementary reaction energies for the $CO_2$RR in $H_2O$ solvent. (a,d) is using $NH_4^+$ proton source, (b,e) is using $KHCO_3$ proton source, and (c,f) is using $H_2O$ proton source. (a-c) is on Ag(111) while (d-f) is on Ag(211).

# References


(1) Cheng, W.; Dan, L.; Deng, X.; Feng, J.; Wang, Y.; Peng, J.; Tian, J.; Qi, W.; Liu, Z.; Zheng, X.; Zhou, D.; Jiang, S.; Zhao, H.; Wang, X. Global Monthly Gridded Atmospheric Carbon Dioxide Concentrations under the Historical and Future Scenarios. *Sci Data* **2022**, *9* (1). https://doi.org/10.1038/s41597-022-01196-7.

(2) Ballantyne, A. P.; Alden, C. B.; Miller, J. B.; Trans, P. P.; White, J. W. C. A Newtonian Approach to Extraordinarily Strong Negative Refraction. *Nature* **2012**, *488* (7409), 70–73. https://doi.org/10.1038/nature11299.

(3) Ledley, T. S.; Sundquist, E. T.; Schwartz, S. E.; Hall, D. K.; Fellows, J. D.; Killeen, T. L. Climate Change and Greenhouse Gases. *Eos (Washington DC)* **1999**, *80* (39). https://doi.org/10.1029/99EO00325.

(4) Pines, D.; Ditkovich, J.; Mukra, T.; Miller, Y.; Kiefer, P. M.; Daschakraborty, S.; Hynes, J. T.; Pines, E. How Acidic Is Carbonic Acid? *Journal of Physical Chemistry B* **2016**, *120* (9), 2440–2451. https://doi.org/10.1021/acs.jpcb.5b12428.

(5) Leverick, G.; Bernhardt, E. M.; Ismail, A. I.; Law, J. H.; Arifutzzaman, A.; Aroua, M. K.; Gallant, B. M. Uncovering the Active Species in Amine-Mediated $CO_2$ Reduction to CO on Ag. *ACS Catal* **2023**, *13* (18), 12322–12337. https://doi.org/10.1021/acscatal.3c02500.

(6) Kroeker, K. J.; Kordas, R. L.; Crim, R. N.; Singh, G. G. Meta-Analysis Reveals Negative yet Variable Effects of Ocean Acidification on Marine Organisms. *Ecology Letters*. **2010**, *13*, 1419–1434. https://doi.org/10.1111/j.1461-0248.2010.01518.x.

(7) Lucile, F.; Cézac, P.; Contamine, F.; Serin, J. P.; Houssin, D.; Arpentinier, P. Solubility of Carbon Dioxide in Water and Aqueous Solution Containing Sodium Hydroxide at Temperatures from (293.15 to 393.15) K and Pressure up to 5 MPa: Experimental

Measurements. *J Chem Eng Data* **2012**, *57* (3), 784–789. https://doi.org/10.1021/je200991x.

(8) Shen, K.; Cheng, D.; Reyes-Lopez, E.; Jang, J.; Sautet, P.; Morales-Guio, C. G. On the Origin of Carbon Sources in the Electrochemical Upgrade of $CO_2$ from Carbon Capture Solutions. *Joule* **2023**, *7* (6), 1260–1276. https://doi.org/10.1016/j.joule.2023.05.010.

(9) Al-Mamoori, A.; Krishnamurthy, A.; Rownaghi, A. A.; Rezaei, F. Carbon Capture and Utilization Update. *Energy Technology*. **2017**, *5*, 834–849. https://doi.org/10.1002/ente.201600747.

(10) Siegel, R. E.; Pattanayak, S.; Berben, L. A. Reactive Capture of CO2: Opportunities and Challenges. *ACS Catal* **2023**, *13* (1), 766–784. https://doi.org/10.1021/acscatal.2c05019.

(11) Lee, G.; Li, Y. C.; Kim, J. Y.; Peng, T.; Nam, D. H.; Sedighian Rasouli, A.; Li, F.; Luo, M.; Ip, A. H.; Joo, Y. C.; Sargent, E. H. Electrochemical Upgrade of CO2 from Amine Capture Solution. *Nat Energy* **2021**, *6* (1), 46–53. https://doi.org/10.1038/s41560-020-00735-z.

(12) Cheng, D.; Wei, Z.; Zhang, Z.; Broekmann, P.; Alexandrova, A. N.; Sautet, P. Restructuring and Activation of Cu(111) under Electrocatalytic Reduction Conditions. *Angewandte Chemie - International Edition* **2023**, *62* (20). https://doi.org/10.1002/anie.202218575.

(13) Cheng, D.; Zhang, G.; Li, L.; Shi, X.; Zhen, S.; Zhao, Z. J.; Gong, J. Guiding Catalytic $CO_2$ Reduction to Ethanol with Copper Grain Boundaries. *Chem Sci* **2023**, *14* (29), 7966–7972. https://doi.org/10.1039/d3sc02647g.

(14) Varela, A. S.; Ju, W.; Bagger, A.; Franco, P.; Rossmeisl, J.; Strasser, P. Electrochemical Reduction of CO2 on Metal-Nitrogen-Doped Carbon Catalysts. *ACS Catal*. **2019**, *9,* (8), 7270–7284. https://doi.org/10.1021/acscatal.9b01405.

(15) Nitopi, S.; Bertheussen, E.; Scott, S. B.; Liu, X.; Engstfeld, A. K.; Horch, S.; Seger, B.; Stephens, I. E. L.; Chan, K.; Hahn, C.; Nørskov, J. K.; Jaramillo, T. F.; Chorkendorff, I. Progress and Perspectives of Electrochemical $CO_2$ Reduction on Copper in Aqueous Electrolyte. *Chemical Reviews* **2019**, *119* (12), 7610–7672. https://doi.org/10.1021/acs.chemrev.8b00705.

(16) Kuhl, K. P.; Hatsukade, T.; Cave, E. R.; Abram, D. N.; Kibsgaard, J.; Jaramillo, T. F. Electrocatalytic Conversion of Carbon Dioxide to Methane and Methanol on Transition Metal Surfaces. *J Am Chem Soc* **2014**, *136* (40), 14107–14113. https://doi.org/10.1021/ja505791r.

(17) Kumari, S.; Alexandrova, A. N.; Sautet, P. Nature of Zirconia on a Copper Inverse Catalyst Under $CO_2$ Hydrogenation Conditions. *J Am Chem Soc* **2023**, *145* (48), 26350–26362. https://doi.org/10.1021/jacs.3c09947.

(18) Fauzi, A.; Chen, X.; Zhao, H.; Cao, S.; Kong, L.; Huang, S.; Zhang, S.; Ma, X. Recent Progress of M-N-C Single Atom Electrocatalysts for Carbon Dioxide Reduction Reaction. *Next Energy* **2023**, *1* (4), 100045. https://doi.org/10.1016/j.nxener.2023.100045.

(19) Choi, J.; Chiu, S.; Banerjee, A.; Sacci, R. L.; Veith, G. M.; Stieber, C.; Hahn, C.; Alexandrova, A. N.; Morales-Guio, C. G. Direct Electrochemical Reduction of Ammonium Carbamate on Transition Metal Surfaces: Finding Activity and Stability Descriptors beyond Those for CO 2 Reduction. https://doi.org/10.26434/chemrxiv-2024-5xsp5.

(20) Banerjee, S.; Gerke, C. S.; Thoi, V. S. Guiding CO2RR Selectivity by Compositional Tuning in the Electrochemical Double Layer. *Acc Chem Res* **2022**, *55* (4), 504–515. https://doi.org/10.1021/acs.accounts.1c00680.

(21) Su, D. J.; Xiang, S. Q.; Gao, S. T.; Jiang, Y.; Liu, X.; Zhang, W.; Zhao, L. Bin; Tian, Z. Q. Kinetic Understanding of Catalytic Selectivity and Product Distribution of Electrochemical Carbon Dioxide Reduction Reaction. *JACS Au* **2023**, *3* (3), 905–918. https://doi.org/10.1021/jacsau.3c00002.

(22) Ma, H.; Ibáñez-Alé, E.; Ganganahalli, R.; Pérez-Ramírez, J.; López, N.; Yeo, B. S. Direct Electroreduction of Carbonate to Formate. *J Am Chem Soc* **2023**. *145*, (45) https://doi.org/10.1021/jacs.3c08079.

(23) Cheng, Q.; Huang, M.; Ye, Q.; Deng, B.; Dong, F. Indium-Based Electrocatalysts for CO2 Reduction to C1 Products. *Chinese Chemical Letters* **2023**, 109112. https://doi.org/10.1016/j.cclet.2023.109112.

(24) Ni, B.; Wang, X. Face the Edges: Catalytic Active Sites of Nanomaterials. *Advanced Science*. **2015**, *2*, 1500085, https://doi.org/10.1002/advs.201500085.

(25) Peterson, A. A.; Nørskov, J. K. Activity Descriptors for CO 2 Electroreduction to Methane on Transition-Metal Catalysts. *Journal of Physical Chemistry Letters* **2012**, *3* (2), 251–258. https://doi.org/10.1021/jz201461p.

(26) Mahyoub, S. A.; Qaraah, F. A.; Chen, C.; Zhang, F.; Yan, S.; Cheng, Z. An Overview on the Recent Developments of Ag-Based Electrodes in the Electrochemical Reduction of $CO_2$ to CO. *Sustainable Energy and Fuels* **2019**, *4*, 50–67. https://doi.org/10.1039/c9se00594c.

(27) Han, W.; Li, M.; Ma, Y.; Yang, J. Cobalt-Based Metal-Organic Frameworks and Their Derivatives for Hydrogen Evolution Reaction. *Frontiers in Chemistry* **2020**. *8*, 592915 https://doi.org/10.3389/fchem.2020.592915.

(28) Bao, F.; Kemppainen, E.; Dorbandt, I.; Bors, R.; Xi, F.; Schlatmann, R.; van de Krol, R.; Calnan, S. Understanding the Hydrogen Evolution Reaction Kinetics of Electrodeposited

Nickel-Molybdenum in Acidic, Near-Neutral, and Alkaline Conditions. *ChemElectroChem* **2021**, *8* (1), 195–208. https://doi.org/10.1002/celc.202001436.

(29) Trasatti, S. Work function, electronegativity, and electrochemical behaviour of metals: III. Electrolytic hydrogen evolution in acid solutions. Journal of Electroanalytic Chemistry and Interfacial Electrochemistry. 1972, 39 (1), 163-184. https://doi.org/10.1016/S0022 0728(72)80485-6.

(30) Thevenon, A.; Rosas-Hernández, A.; Fontani Herreros, A. M.; Agapie, T.; Peters, J. C. Dramatic HER Suppression on Ag Electrodes via Molecular Films for Highly Selective $CO_2$ to CO Reduction. *ACS Catal* **2021**, *11* (8), 4530–4537. https://doi.org/10.1021/acscatal.1c00338.

(31) Akbashev, A. R. Electrocatalysis on Oxide Surfaces: Fundamental Challenges and Opportunities. Current Opinion in Electrochemistry. 2022, 35, 101095. https://doi.org/10.1016/j.coelec.2022.101095.

(32) Quaino, P.; Juarez, F.; Santos, E.; Schmickler, W. Volcano Plots in Hydrogen Electrocatalysis-Uses and Abuses. *Beilstein Journal of Nanotechnology* **2014**, *5* (1), 846–854. https://doi.org/10.3762/bjnano.5.96.

(33) Dziejarski, B.; Serafin, J.; Andersson, K.; Krzyżyńska, R. CO2 Capture Materials: A Review of Current Trends and Future Challenges. Materials Today Sustainability 2023, 24, 100483 https://doi.org/10.1016/j.mtsust.2023.100483.

(34) Davran-Candan, T. DFT Modeling of $CO_2$ Interaction with Various Aqueous Amine Structures. *Journal of Physical Chemistry A* **2014**, *118* (25), 4582–4590. https://doi.org/10.1021/jp503929g.

(35) Appel, A. M.; Yang, J. Y. Maximum and Comparative Efficiency Calculations for Integrated Capture and Electrochemical Conversion of CO2. ACS Energy Letters 2024, 9 (2), 768–770. https://doi.org/10.1021/acsenergylett.3c02489.

(36) Khoo, K. H.; Culberson, C. H.; Bates, R. G. Thermodynamics of the Dissociation of Ammonium Ion in Seawater from 5 to 40OC. Journal of Solution Chemistry, 1977, 6, 281 290. https://doi.org/10.1007/BF00645459.

(37) Safipour, J.; Weber, A. Z.; Bell, A. T. Detrimental Effects of Monoethanolamine and Other Amine-Based Capture Agents on the Electrochemical Reduction of $CO_2$. *ACS Energy Lett* **2023**, *8* (12), 5012–5017. https://doi.org/10.1021/acsenergylett.3c01953.

(38) Zhang, Z.; Kummeth, A. L.; Yang, J. Y.; Alexandrova, A. N. Inverse Molecular Design of Alkoxides and Phenoxides for Aqueous Direct Air Capture of $CO_2$ Proc Natl Acad Sci, 2022, 119 (25), https://doi.org/10.1073/pnas.2123496119.

(39) Ballinger, P; Long, F. A. Acid Ionization Constants of Alcohols. II. Acidities of Some Substituted Methanols and Related Compounds. J. Am. Chem. Soc., 1960, 82 (4), 795 798.

(40) Silverstein, T. P.; Heller, S. T. PKa Values in the Undergraduate Curriculum: What Is the Real pKa of Water? *J Chem Educ* **2017**, *94* (6), 690–695. https://doi.org/10.1021/acs.jchemed.6b00623.

(41) Kresse, G.; Furthmüller, J. Efficient Iterative Schemes for Ab Initio Total-Energy Calculations Using a Plane-Wave Basis Set. Phys. Rev. B. 1996, 54 (16). https://doi.org/10.1103/PhysRevB.54.11169.

(42) Kresse, G.; Furthmüller, J. Efficiency of Ab-Initio Total Energy Calculations for Metals and Semiconductors Using a Plane-Wave Basis Set. Comp. Mater. Sci. 1996, 6 (1). https://doi.org/10.1016/0927-0256(96)00008-0.

(43) Grimme, S.; Antony, J.; Ehrlich, S.; Krieg, H. A Consistent and Accurate Ab Initio Parametrization of Density Functional Dispersion Correction (DFT-D) for the 94 Elements H-Pu. *Journal of Chemical Physics* **2010**, *132* (15). https://doi.org/10.1063/1.3382344.

(44) Larsen, A. H.; Mortensen, J.J.; Blomqvist J.; Castelli I. E.; Christensen R.; Dułak M.; Friis J.; Groves M. N.; Hammer B.; Hargus C.; Hermes E. D.; Jennings P. C.; Jensen P. B.; Kermode J.' Kitchin J. R.; Kolsbjerg E. L.; Kubal J.; Kaasbjerg K.; Lysgaard S.; Maronsson J. B.; Maxson T.; Olsen T.; Pastewka L.; Peterson A.; Rostgaard C.; Schiøtz J.; Schütt O.; Strange M.; Thygesen K. S.; Vegge T.; Vilhelmsen L.; Walter M.; Zeng Z.; and Jacobsen K. W. The atomic simulation environment - A Python library for working with atoms. Journal of Physics Condensed Matter 2017, 29, 273002. https://doi.org/10.1088/1361-648X/aa680e.

(45) Chen, H.; Yang, X.; Sun, L.; Yu, P.; Zhang, X.; Luo, L. Effects of Ag on the Magnetic and Mechanical Properties of Sintered NdFeB Permanent Magnets. *J Magn Magn Mater* **2019**, *485*, 49–53. https://doi.org/10.1016/j.jmmm.2019.04.071.

(46) Ringe, S.; Morales-Guio, C. G.; Chen, L. D.; Fields, M.; Jaramillo, T. F.; Hahn, C.; Chan, K. Double Layer Charging Driven Carbon Dioxide Adsorption Limits the Rate of Electrochemical Carbon Dioxide Reduction on Gold. *Nat Commun* **2020**, *11* (1). https://doi.org/10.1038/s41467-019-13777-z.

(47) Zhang, Z.; Li, H.; Shao, Y.; Gan, L.; Kang, F.; Duan, W.; Hansen, H. A.; Li, J. Molecular Understanding of the Critical Role of Alkali Metal Cations in Initiating $CO_2$ Electroreduction on Cu(100) Surface. *Nat Commun* **2024**, *15* (1). https://doi.org/10.1038/s41467-024-44896-x.

(48) Mathew, K.; Sundararaman, R.; Letchworth-Weaver, K.; Arias, T. A.; Hennig, R. G. Implicit Solvation Model for Density-Functional Study of Nanocrystal Surfaces and Reaction Pathways. *Journal of Chemical Physics* **2014**, *140* (8). https://doi.org/10.1063/1.4865107.

(49) Mathew, K.; Kolluru, V. S. C.; Mula, S.; Steinmann, S. N.; Hennig, R. G. Implicit Self-Consistent Electrolyte Model in Plane-Wave Density-Functional Theory. *Journal of Chemical Physics* **2019**, *151* (23). https://doi.org/10.1063/1.5132354.

(50) Kumari, S.; Sautet, P. Elucidation of the Active Site for the Oxygen Evolution Reaction on a Single Pt Atom Supported on Indium Tin Oxide. *Journal of Physical Chemistry Letters* **2023**, *14* (10), 2635–2643. https://doi.org/10.1021/acs.jpclett.3c00160.

(51) Gauthier, J. A.; Ringe, S.; Dickens, C. F.; Garza, A. J.; Bell, A. T.; Head-Gordon, M.; Nørskov, J. K.; Chan, K. Challenges in Modeling Electrochemical Reaction Energetics with Polarizable Continuum Models. *ACS Catal* **2019**, *9* (2), 920–931. https://doi.org/10.1021/acscatal.8b02793.

(52) Gauthier, J. A.; Dickens, C. F.; Heenen, H. H.; Vijay, S.; Ringe, S.; Chan, K. Unified Approach to Implicit and Explicit Solvent Simulations of Electrochemical Reaction Energetics. *J Chem Theory Comput* **2019**, *15* (12), 6895–6906. https://doi.org/10.1021/acs.jctc.9b00717.

(53) Nørskov, J. K.; Rossmeisl, J.; Logadottir, A.; Lindqvist, L.; Kitchin, J. R.; Bligaard, T.; Jónsson, H. Origin of the Overpotential for Oxygen Reduction at a Fuel-Cell Cathode. *Journal of Physical Chemistry B* **2004**, *108* (46), 17886–17892. https://doi.org/10.1021/jp047349j.

(54) Steinmann, S. N.; Michel, C.; Schwiedernoch, R.; Sautet, P. Impacts of Electrode Potentials and Solvents on the Electroreduction of CO2: A Comparison of Theoretical Approaches. *Physical Chemistry Chemical Physics* **2015**, *17* (21), 13949–13963. https://doi.org/10.1039/c5cp00946d.

(55) Steinmann, S. N.; Michel, C.; Schwiedernoch, R.; Filhol, J. S.; Sautet, P. Modeling the HCOOH/CO2 Electrocatalytic Reaction: When Details Are Key. *ChemPhysChem* **2015**, *16* (11), 2307–2311. https://doi.org/10.1002/cphc.201500187.

(56) Mohsen-Nia, M.; Amiri, H.; Jazi, B. Dielectric Constants of Water, Methanol, Ethanol, Butanol and Acetone: Measurement and Computational Study. *J Solution Chem* **2010**, *39* (5), 701–708. https://doi.org/10.1007/s10953-010-9538-5.

(57) Fernández, D. P.; Mulev, Y.; Goodwin, A. R. H.; Sengers, J. M. H. L. A Database for the Static Dielectric Constant of Water and Steam. *J Phys Chem Ref Data* **1995**, *24* (1), 33–70. https://doi.org/10.1063/1.555977.

(58) Ikada, E.; Hida, Y.; Okamoto, H.; Hagino, J.; Koizumi, N. *Dielectric Properties of Ethanolaanines*; 1968; Vol. 46.

(59) Steinmann, S. N.; Sautet, P. Assessing a First-Principles Model of an Electrochemical Interface by Comparison with Experiment. *Journal of Physical Chemistry C* **2016**, *120* (10), 5619–5623. https://doi.org/10.1021/acs.jpcc.6b01938.

(60) Ye, C.; Dattila, F.; Chen, X.; López, N.; Koper, M. T. M. Influence of Cations on HCOOH and CO Formation during CO2 Reduction on a PdMLPt(111) Electrode. *J Am Chem Soc* **2023**, *145* (36), 19601–19610. https://doi.org/10.1021/jacs.3c03786.

(61) Monteiro, M. C. O.; Dattila, F.; López, N.; Koper, M. T. M. The Role of Cation Acidity on the Competition between Hydrogen Evolution and $CO_2$ Reduction on Gold Electrodes. *J Am Chem Soc* **2022**, *144* (4), 1589–1602. https://doi.org/10.1021/jacs.1c10171.

(62) Gao, D.; McCrum, I. T.; Deo, S.; Choi, Y. W.; Scholten, F.; Wan, W.; Chen, J. G.; Janik, M. J.; Roldan Cuenya, B. Activity and Selectivity Control in $CO_2$ Electroreduction to Multicarbon Products over CuOx Catalysts via Electrolyte Design. *ACS Catal* **2018**, *8* (11), 10012–10020. https://doi.org/10.1021/acscatal.8b02587.

(63) Shin, S. J.; Choi, H.; Ringe, S.; Won, D. H.; Oh, H. S.; Kim, D. H.; Lee, T.; Nam, D. H.; Kim, H.; Choi, C. H. A Unifying Mechanism for Cation Effect Modulating C1 and C2 Productions from CO2 Electroreduction. *Nat Commun* **2022**, *13* (1). https://doi.org/10.1038/s41467-022-33199-8.

(64) Pan, B.; Wang, Y.; Li, Y. Understanding and Leveraging the Effect of Cations in the Electrical Double Layer for Electrochemical CO2 Reduction. *Chem Catalysis*. Cell Press June 16, 2022, pp 1267–1276. https://doi.org/10.1016/j.checat.2022.03.012.

(65) Sandoval, M. G.; Walia, J.; Houache, M. S. E.; Abu-Lebdeh, Y.; Berini, P.; Faccio, R.; Weck, A. CO2 Adsorption and Activation on Ag(1 1 1) Surfaces in the Presence of Surface Charge Density: A Static Gas Phase DFT Study. *Appl Surf Sci* **2023**, *610*. https://doi.org/10.1016/j.apsusc.2022.155498.

(66) Wu, J.; Li, W.; Liu, K.; Kucernak, A.; Liu, H.; Chai, L.; Liu, M. Cation Effects on Electrochemical CO2 Reduction Reaction. *Next Energy* **2023**, *1* (3), 100032. https://doi.org/10.1016/j.nxener.2023.100032.

(67) Garcia, J. D.; Mace, J. E. Energy Level and Line Tables for One-Electron Atomic Spectra. J. Opt. Soc. Am., 1965, 55 (6), 654–685. https://doi.org/10.1364/JOSA.55.000654.

(68) Foster, P. J.; Leckenby, R. E.; Robbins, E. J. The ionization potentials of clustered alkali metal atoms. J. Phys. B: Atomic and Molecular Physics, 1969, 2, 478, https://doi.org/10.1088/0022-3700/2/4/307.

(69) Herrmann, A.; Schumacher, E.; Wöste, L. Preparation and Photoionization Potentials of Molecules of Sodium, Potassium, and Mixed Atoms. *J Chem Phys* **1978**, *68* (5), 2327–2336. https://doi.org/10.1063/1.436003.

(70) Wight, G. R.; Brion, C. E. Estimation of the excitation and ionization energies of NH4, H3O and H2F radicals using core analogies applied to K-shell electron energy loss spectra. Chem. Phys. Letters 1974, 26 (4), 607–609. https://doi.org/10.1016/0009-2614(74)80427-6

(71) Jin, W.; Wang, Y.; Liu, T.; Ding, C.; Guo, H. CO2 Chemisorption and Dissociation on Flat and Stepped Transition Metal Surfaces. *Appl Surf Sci* **2022**, *599*, 154024 *https*://doi.org/10.1016/j.apsusc.2022.154024.

(72) Yu, J.; Yin, J.; Li, R.; Ma, Y.; Fan, Z. Interfacial Electric Field Effect on Electrochemical Carbon Dioxide Reduction Reaction. Chem Catalysis. 2022, 2 (9), 2229–2252. https://doi.org/10.1016/j.checat.2022.07.024.

(73) Ngan, H. T.; Sautet, P. Tuning the Hydrogenation Selectivity of an Unsaturated Aldehyde via Single-Atom Alloy Catalysts. *J Am Chem Soc* **2024**, *146* (4), 2556–2567. https://doi.org/10.1021/jacs.3c10994.

(74) Ngan, H. T.; Yan, G.; Van Der Hoeven, J. E. S.; Madix, R. J.; Friend, C. M.; Sautet, P. Hydrogen Dissociation Controls 1-Hexyne Selective Hydrogenation on Dilute Pd-in-Au Catalysts. *ACS Catal* **2022**, *12* (21), 13321–13333. https://doi.org/10.1021/acscatal.2c03560.

(75) Almisbaa, Z.; Aljama, H. A.; Almajnouni, K.; Cavallo, L.; Sautet, P. Acetylene Semi-Hydrogenation on Intermetallic Ni-In Catalysts: Ni Ensemble and Acetylene Coverage Effects from a Theoretical Analysis. *ACS Catal* **2023**, *13* (11), 7358–7370. https://doi.org/10.1021/acscatal.3c01175.

(76) Laidler, K. J.; King, M. C. The Development of Transition-State Theory, J. Phys. Chem. 1983, 87 (15), 2657-2664, https://doi.org/10.1021/j100238a002

(77) Chen, L. D.; Urushihara, M.; Chan, K.; Nørskov, J. K. Electric Field Effects in Electrochemical CO2 Reduction. *ACS Catal* **2016**, *6* (10), 7133–7139. https://doi.org/10.1021/acscatal.6b02299.

(78) Liu, X.; Xiao, J.; Peng, H.; Hong, X.; Chan, K.; Nørskov, J. K. Understanding Trends in Electrochemical Carbon Dioxide Reduction Rates. *Nat Commun* **2017**, *8*. https://doi.org/10.1038/ncomms15438.

(79) Shi, C.; Chan, K.; Yoo, J. S.; Nørskov, J. K. Barriers of Electrochemical CO2 Reduction on Transition Metals. *Org Process Res Dev* **2016**, *20* (8), 1424–1430. https://doi.org/10.1021/acs.oprd.6b00103.

(80) Kozuch, S.; Shaik, S. A Combined Kinetic-Quantum Mechanical Model for Assessment of Catalytic Cycles: Application to Cross-Coupling and Heck Reactions. *J Am Chem Soc* **2006**, *128* (10), 3355–3365. https://doi.org/10.1021/ja0559146.

(81) Kozuch, S.; Shaik, S. How to Conceptualize Catalytic Cycles? The Energetic Span Model. *Acc Chem Res* **2011**, *44* (2), 101–110. https://doi.org/10.1021/ar1000956.